Biologically Inspired Design of Protein-Silica Hybrid Nanoparticles for Drug Delivery Applications

by

Wei Han

Department of Biomedical Engineering
Duke University

Date:_____

Approved:

_____
William M. Reichert, Chair

_____
Gabriel P. López, Supervisor

_____
Nichlaus J. Carroll

_____
Ashutosh Chilkoti

_____
Stefan Zauscher

Dissertation submitted in partial fulfillment of
the requirements for the degree of Doctor of Philosophy in the
Department of Biomedical Engineering
in the Graduate School of Duke University

2016

ABSTRACT

Biologically Inspired Design of Protein-Silica Hybrid Nanoparticles for Drug Delivery Applications

by

Wei Han

Department of Biomedical Engineering
Duke University

Date:_____

Approved:

_____
William M. Reichert, Chair

_____
Gabriel P. López, Supervisor

_____
Nichlaus J. Carroll

_____
Ashutosh Chilkoti

_____
Stefan Zauscher

An abstract of a dissertation submitted in partial fulfillment of
the requirements for the degree of Doctor of Philosophy in the
Department of Biomedical Engnieering
in the Graduate School of Duke University

2016

Abstract

The design and application of effective drug carriers is a fundamental concern in the delivery of therapeutics for the treatment of cancer and other vexing health problems. Traditionally utilized chemotherapeutics are limited in efficacy due to poor bioavailability as a result of their size and solubility as well as significant deleterious effects to healthy tissue through their inability to preferentially target pathological cells and tissues, especially in treatment of cancer. Thus, a major effort in the development of nanoscopic drug delivery vehicles for cancer treatment has focused on exploiting the inherent differences in tumor physiology and limiting the exposure of drugs to non-tumorous tissue, which is commonly achieved by encapsulation of chemotherapeutics within macromolecular or supramolecular carriers that incorporate targeting ligands and that enable controlled release. The overall aim of this work is to engineer a hybrid nanomaterial system comprised of protein and silica and to characterize its potential as an encapsulating drug carrier. The synthesis of silica, an attractive nanomaterial component because it is both biocompatible as well as structurally and chemically stable, within this system is catalyzed by self-assembled elastin-like polypeptide (ELP) micelles that incorporate of a class of biologically-inspired, silica-promoting peptides, silaffins. Furthermore, this methodology produces near-monodisperse, hybrid inorganic/micellar materials under mild reaction conditions such as temperature, pH

and solvent. This work studies this material system along three avenues: 1) proof-of-concept silicification (i.e. the formation and deposition of silica upon organic materials) of ELP micellar templates, 2) encapsulation and pH-triggered release of small, hydrophobic chemotherapeutics, and 3) selective silicification of templates to potentiate retention of peptide targeting ability.

We first designed diblock ELP constructs that self-assemble into spherical micelles between the intrinsic phase transition temperatures of the two blocks and incorporated silaffin peptides to decorate the micelles. We performed systematic characterization of the silicification process using these micelle constructs and found that both the presence of the silaffin peptide as well as assembly are required to synthesize monodisperse hybrid silica-protein nanoparticles. In addition, we found that size of the particles closely aligns with that of the underlying template and was largely independent of peptide and silica precursor concentration. We next developed a relatively hydrophilic ELP construct containing a silaffin peptide sequence at the N-terminus which self-assembles into micelles upon conjugation with hydrophobic molecules at the C-terminus. We performed similar silicification experiments using two hydrophobes, including one chemotherapeutic (doxorubicin) linked to the ELP through a pH-labile linker, and found that pH controlled release of the drug from hybrid ELP and silica nanoparticles was possible over a 36 hour window. Lastly, we sought to explore the tunability of silicification as well as the potential to create a shell of silica

while retaining exposure of targeting ligands appended to the ELP sequences. We designed a series of modified silaffin-ELP sequences and found that encoding the silaffin sequence proximal to the hydrophobic (C-terminal) core of a micelle results in an enhanced availability of N-terminal sequence amines beyond the periphery of the formed silica nanoparticles. Altogether, this work provides a direct design strategy for a versatile protein-silica hybrid nanoparticle system that may offer a powerful approach toward a nanomedicine platform for the efficient targeted delivery of drugs.

Dedication

To my mother and father, Ling and Dehua, for their unwavering love and support in all my pursuits.

Contents

List of Tables

List of Figures

Acknowledgements

I would first and foremost like to thank Prof. Gabriel P. López for giving me an opportunity to join his lab and work toward my Ph.D. In doing so and mentoring me throughout the course of graduate school, he has imprinted upon me a motivation, critical thinking tendency and problem solving mindset that will help me succeed wherever my career takes me. When I look back upon my time spent in the López lab – one that essentially started when Nicky, Phani and I joined the lab as the first class of graduate students – I will always remember walking into the lab during orientation with them, and finding a space with the just the research essentials. Gabriel allowed us to fill the lab – our physical toolbox – in the same way we expanded our intellectual toolbox, by granting us utmost freedom to explore research directions that we found interesting and to progress in experimental directions we identified, all the while providing guidance and feedback as needed. I would like to thank Profs. Ashutosh Chilkoti, Stefan Zauscher, Nick Carroll and Fan Yuan for their valuable guidance and feedback in research. In addition, I would like to express my gratitude toward Prof. Monty Reichert for his enduring support both in the lab environment as well as in extracurricular pursuits toward professional development and enrichment of the graduate experience. To all the members of my committee, thank you for your time and effort in allowing me to pursue and defend my dissertation. I would also like to acknowledge my funding

sources, the Triangle MRSEC, Duke CBTE and the department of Biomedical Engineering at Duke for their generous support.

My pursuit of a Ph.D. would not have been a success without the tremendous amount of support that I received from my lab mates, friends and family that have always been there to discuss research, the highs and lows of graduate school and the ins and outs of life. I would like to first thank my compadres, the aforementioned Nicky Virdone and Phanindhar Shivapooja. We entered graduate school together, and I would not have been able to get through my first year without you two. In addition, I would like to thank Drs. Leah Johnson and Getachew Tizazu, the intrepid postdoctoral fellows who brought to the lab scientific knowledge, safety from biohazards and OSHA alike, and endless humor. I want to express gratitude to all the members past and present of the López for sharing the experience and contributing to my learning, including Drs. Lu Gao, Qian Yu (experimentalist extraordinaire), James Morgan Harris, Ali Ghoorchian, Pearlson Prashanth, Lizzy Mayorga Szott, the newly minted Drs. C. Wyatt Shields IV, Vrad Levering, and fellow graduate students Alice (Linying) Li, Joseph Simon, Dalton Sycks, Mark Gonzalez and Romel Menacho-Melgar. I would also like to thank Drs. Weiping Gao, Miriam Amiram, Sarah MacEwan and Felipe Quiroz, who collectively taught me about ELPs during my time as a Pratt Fellow and into graduate school. I would especially like to acknowledge Lei Tang and Isaac Weitzhandler, my companions in our adventure to Eindhoven, The Netherlands to learn cryogenic electron microscopy;

I will always treasure those evenings spent in that hotel conference room trying to figure out what where those electrons are going and with how much energy. Since our return, I would like to further thank Lei for her help in QCM and Isaac for his help in DLS/SLS characterization techniques. I would also be senseless not to acknowledge Elaine Fulton, Katie Krieger and Carla Sturdivant, the dedicated, meticulous and, most importantly, caring administrators who work diligently behind the scenes and ensure the MRSEC and departments are what they are.

Most importantly, I would like to thank my loving parents, Ling Ma and Dehua Han for their amazing support and eternal love; my extended family and especially my aunt, Jian Ma, for their love and encouragement from around the world; and finally my love, Pratiksha Thakore, for her intellectual and emotional support throughout graduate school. I will always be thankful to Duke for bringing us to the same place at the same time, and I look forward to sharing our lives together.

1. Introduction

1.1 Silica nanoparticles and biotechnological applications

1.1.1 Formation and properties

Silica, also known as silicon dioxide and consisting of the chemical formula SiO_2, in its various forms is one of the most utilized materials in both the research and commercial spaces, owing to its natural abundance as well as wide range of physiochemical properties [1]. In particular, one subclass of silica materials that is of significant interest in biotechnological applications are amorphous silica nanoparticles. Since the seminal report by Stöber *et al.* [2] with regards to the facile fabrication of monodisperse silica from approximately 50 nm to greater than 2 μm in size, research into the applications for nanoscale silica have increased dramatically and especially in the biotechnology and biomedical research areas due primarily to the known biocompatibility of silica *in vivo*. In fact, the U.S. Food and Drug Administration (FDA) has classified amorphous, *i.e.* non-crystalline, silica as "generally regarded as safe" with regards to its potential applications in the human body because it is not known to cause an immunogenic effect, is nontoxic and also degrades over time [3]. In addition to its biocompatibility, silica is mechanically robust, offering high environmental and temporal stability, and the well-characterized, tight control over its synthesis and composition make it an attractive component of many material systems [4-6].

Silica nanoparticles are primarily fabricated through the hydrolysis and condensation of silicon alkoxide precursors in the presence of ammonia or other catalysts, as first laid out by the Stöber method; however, since that development, numerous other groups have adapted the methodology to generate even smaller monodisperse silica particles down to approximately 5 – 10 nm in size [7,8]. Another widely utilized methodology for producing silica nanoparticles is through water/oil reverse microemulsions highlighted by Arriagada and Osseo-Asare in which highly monodisperse, sub-100 nm silica can be generated [9-11]. In addition, the versatility of the polycondensation reaction can be employed to drive the formation of anisotropic silica nanorods [12,13], nanotubes [14,15] or other morphologies [16] by templated condensation, which are inherently useful for biomedical applications. The vast space of sol-gel chemistries, stemming from the availability of organosilane precursors to the ease of modification of surface silanol groups, also lends to the attractiveness of silica materials as they can be easily augmented with active targeting moieties [17,18]. This collective and relatively simple control of the formation and properties of silica nanoparticles has contributed to its use in various applications such as encapsulation, controlled release and medical imaging diagnostics.

1.1.2 Biotechnological applications

The appealing physiochemical features of silica materials have made them an attractive encapsulation tool to both protect and stabilize precious cargo as well as to enhance the biocompatibility of other materials. Silica encapsulation has been proven useful on many length scales, from small molecule therapeutics and imaging probes to enzymes, highlighted by work by Wang *et al.* [19-22], as well as even bacterial and mammalian cells [23,24]. For instance in the field of medical imaging, Wiesner *et al.* demonstrated that the sol-gel encapsulation of a variety of dyes within core-shell silica nanoparticles not only stabilized and significantly reduced photo-bleaching by limiting exposure to dissolved oxygen, they also enhanced the fluorescence intensity up to twenty-fold, potentiating their use in optical imaging and disease detection [25-28]. In addition, silica nanoparticles have also been used in the encapsulation of magnetic resonance imaging contrast agents, such as gadolinium, which serves to enhance the biocompatibility and stability of the underlying diagnostic tools [29,30]. Lastly, the ease of fabrication as well as control of nucleation, growth and encapsulation has enabled one-pot synthesis techniques to develop multimodal diagnostic imaging tools. Tang *et al.* recently encapsulated both a silane-modified near-infrared fluorescence dyes and a silane-modified chelating agent for positron emission tomography imaging, as well as surface-functionalized the resulting silica nanoparticles with an aptamer to target a specific surface membrane receptor [4,31].

In addition to imaging agents, another application of silica nanoparticles in biotechnology has been the encapsulation and sustained release of therapeutics. Chen *et al.* demonstrated the use of porous and hollow silica nanoparticles, templated from $CaCO_3$, to entrap the antibiotic cefradine and showed that release of the drug occurred in two stages: 1) initial release within a window of 20 minutes of cefradine adsorbed to the surface of the nanoparticles accounting for 74% of release and 2) delayed release of entrapped drug from the porous matrix after 10 hours, totaling 82% cumulative release [32]. Multi-component silica materials have also been used to encapsulate and release drugs. For instance, Huo *et al.* used ethylene oxide/propylene oxide micelles with a silica crosslinked core-shell morphology to load and show a two to five fold increase in sustained release time of a collection of small molecule anti-inflammatory drugs compared to surfactant F127 micelle delivery systems [33]. In addition, Tan *et al.* demonstrated the encapsulation of celecoxib, a small hydrophobic anti-inflammatory drug, using oil/water emulsion synthesis of lipid-silica hybrid microcapsules that resulted in similar sustained release kinetics [34]. The ability to load small hydrophobic molecules for sustained release and to incorporate surface targeting modifications also make silica nanoparticles an attractive material for the delivery of cancer therapeutics, which is discussed in the next section.

1.2 Cancer

1.2.1 Cancer as a disease

Cancer, in its various forms and originating from a host of cells and tissues, is a disease family that has plagued human health throughout history and remains a leading cause of death in the United States today. Approximately 1.6 million men and women per year will develop the disease, and over 590,000 will succumb to cancer in the United States alone; more than 8 million deaths are reported worldwide per year in addition to the 5.5 million disability-adjusted life years lost [35-38]. While the costs of cancer care have increased dramatically, accounting for greater than $140 billion in direct care in the U.S. alone, the five-year survival rate for all cancers has only improved from 55% to 69% in the last 30 years [35,39]. Broadly characterized as the uncontrolled proliferation and spread of abnormal cells, cancer may arise due to a number of inherited or environmental conditions that result in the irrevocable mutation of the cell genome [36,37]. It is this unregulated persistence of the cell cycle in combination with an inherent ability to evade the body's natural corrective machinery, insidious invasion of neighboring tissues, rapid angiogenesis, and eventual systemic metastasis that have prevented the development of effective cancer treatments to date. In addition, the variations between disparate cancer types as well as the intrinsic cellular heterogeneity within a single tumor compound the difficulty in discovery of effective therapeutics [36]. Traditionally, the treatment of solid tumors, accounting for most cancers, has involved

direct surgical extrication if possible in addition to treatment by radiation and chemotherapeutics, both of which cannot distinguish between healthy and cancerous tissues and therefore result in severe and toxic side effects [37]. Specifically, chemotherapeutic agents are generally effective in ceasing cell proliferation by affecting different stages within the cell cycle [40]. For instance, gemcitabine and other antimetabolites hinder DNA synthesis within the S-phase while taxanes such as paclitaxel and docetaxel prevent prophase to metaphase advancement by stabilizing microtubule organization within the centrosome, both resulting in cell death; however, since these drugs have a mechanism of action by affecting rapidly-dividing cells and are not prejudiced toward tumor cells, their use and dose are limited by systemic side effects on the body. One avenue of research that aims to target the diseased cells while limiting exposure and damage to healthy cells is the encapsulation of chemotherapeutics within nanoscale carriers and preferential delivery to tumor microenvironments.

1.2.2 Nanoparticle delivery of cancer therapeutics

The nanoparticle delivery of cancer therapeutics has been widely researched within the past thirty years, and an abundance of novel and adapted, simple and advanced materials have been brought to bear toward the treatment of cancer [36,41-43]. The application of nanoscale delivery vehicles is attractive as a general platform for the delivery of many therapeutics because it is able to overcome many of the limitations of

previously discovered chemotherapeutics; the advantages that nanocarriers are able to imbue upon a drug delivery system include protection of the drug from affecting healthy tissues, the enhancement of the pharmacokinetic profile of the drug, as well as increasing the solubility of some therapeutics [41].

Selection of the drug carrier material itself is also an important feature. A good carrier should be biocompatible *in vivo* as well as be able to be degraded as the drug is released or shortly thereafter [41,44]. In addition, one of the most important aspects of nanoparticle delivery of drugs is passive and active targeting these systems can provide. Due to the hurried and imperfect angiogenesis to support rapid tumor growth and invasion of healthy tissue, the vasculature within the tumor microenvironment is incomplete and flawed. Yuan *et al.* performed size dependent vascular permeability studies on tumor xenografts and found that liposomes of up to approximately 400 nm were able to permeate through pores within the tumor vasculature [45]. In a similar study, Hobbs *et al.* characterized the pore cutoff size of tumor vasculature by modulating the location of implantation as well as inducing tumor regression; they found that tumors in non-cranial locations exhibited pore sizes of up to 1.2 μm, while tumors planted cranially as well as those undergoing vascular regression exhibited only 200 nm pore size cutoffs [46]. The rapid development of tumor microenvironments also manifests in another beneficial facet in the delivery of therapeutics – poor lymphatic drainage, which limits the removal of accumulated material within tumors [41]. Given

the relative size of these pores and the ability of molecules to freely transport out of the vasculature directly into the tumor interstitium in addition to enhanced retention, this presented an attractive basis for the development of passive targeting nanoparticle delivery systems. Passive targeting takes advantage of both the leaky vasculature and poor lymphatic drainage of the tumor microenvironment, collectively known as the enhanced permeability and retention (EPR) effect, to deliver drugs preferentially to their target locale [47]. Based on this understanding, sub-200 nm carriers using a variety of materials have been developed and employed in the passive targeting of drugs in numerous studies and have resulted in several clinical successes [43,48].

In addition to the passive targeting benefits of nanoparticle drug carriers, the utilization of macromolecular assemblies also affords the ability to incorporate site-specific targeting through various biorecognition pathways. Active targeting of drug carriers requires a way to bind the drug delivery vehicle to specific targets preferentially expressed on tumor cells and has included numerous biological and biosynthetic materials including antibodies and antibody fragments [49,50], aptamers [51,52], peptides [53-55] and other ligands [56,57]. Lastly, the benefits from passive and active targeting can be collectively realized using nanoparticle carriers by localization and retention of the therapeutic from systemic delivery to the tumor microenvironment through the EPR effect and subsequently release of cargo near or within tumor cells by active ligand-receptor interactions.

In summarizing the most desirable traits of a nanocarrier material and system, Peer *et al.* asserted that the vehicle should 1) exhibit the size to take advantage of the EPR effect and extend circulating half-life, 2) remain soluble and stable in aqueous solution over time and 3) comprise of well-characterized, biocompatible materials that can be easily augmented to adopt targeting functionalities [41]. One such material that fits these qualifications and has thus been extensively researched as a drug carrier material is silica.

1.2.3 Silica nanoparticles as drug carriers for cancer

Silica nanoparticles have been studied extensively as a valuable carrier of chemotherapeutic drugs [18,58-61]. One type of silica materials, mesoporous silica nanoparticles (MSNPs), has likely received the most attention to date due to their favorable porosity and functionalization. MSNPs are formed using surfactants as the foundation and subsequent polycondensation of silicates to form nano- and micro-particles of various sizes. Grun *et al.* first demonstrated the formation of nanoscale, spherical and highly ordered mesoporous silica (MCM-41) using modified a Stöber process, which has served as a base material for the encapsulation of delivery of drugs in numerous studies [58,60-62]. After MSNPs are fabricated and processed (a disadvantage of this methodology to be discussed later), drugs are loaded into the pores of the nanoparticles through adsorption or chemical conjugation; the nanoparticles are then

capped mechanically or chemically and delivered – frequently functionalized with additional active targeting moieties [63]. Recent examples of MSNP delivery have included co-delivery of doxocubicin and siRNA to treat multi-drug resistant (MDR) breast cancer that is effective in killing tumor cells *in vivo* by Meng *et al*. [64]. In another clever application of MSNPs, nanoparticles were capped with both pH and esterase sensitive polymers such that delivery (of doxorubicin) only occurred in a specified tumor environment [65]. However, MSNPs are not without their disadvantages. MSNPs are generally synthesized using high temperature and extreme pH conditions as well as necessitating a calcination step to formulate; this is due to the incorporation of surfactants to drive the formation of the particles, which need to subsequently be removed prior to drug loading [6,18]. This requires a multistep procedure to first manufacture MSNPs, followed by their loading and functionalization [6]. In parallel to research in the purely synthetic methods to manufacture amorphous silica, there has also been a significant amount of progress in co-opting biomineralization strategies for silica generation to drive the discovery of new materials.

1.3 Silica biomineralization and biologically-inspired silicification

In the historical overview of siliceous nanomaterial research and knowledge, one of the most important sources of exploration and advancement has been through the study of biomineralization from living organisms. Through natural and evolutionary

forces, numerous species of life on different orders of complexity have developed simple, rapid and elegant techniques to synthesize silica from abundantly available precursors [66-70]. In sea diatoms, one of the best characterized sources of biosilica, nanoscopically-ornate silica deposits are produced through processes under biological conditions, including aqueous solvents, low temperatures and neutral pH and leading to high interest and extensive research in the mechanisms for biosilica generation for the past decade [66,67,71-74]. Indeed, the discovery of biological entities and the biomimetic and biologically-inspired synthetic molecules that have additionally come as a result of these studies have allowed for the development of new materials with controllable composition, size, porosity and formation rate with various applications.[69] For instance, biologically-inspired methodologies for the synthesis of silica have been reported extensively within just the last decade [21,75-77]. The application of peptides [71,73,78], proteins [79,80], and polymers [81] that facilitate the polymerization of silica under physiologically relevant conditions at controllable rates has expanded the utility of silica-based materials as well as silica-stabilized organic materials. While the corpus of this dissertation will focus on a specific family of peptides that template the formation of silica – silaffins – it is also important to note the other major biomineralization components that have been characterized and utilized towards the development of silica materials in research.

1.3.1 Silicateins

Silicateins, as the name suggests, are a class of proteins that have able to catalyze the formation of silica from silicic acid precursors first discovered in the spicules of the sea sponge *Tethya aurantia* [66,68,69,72,82]. The first isolation of the major fraction of the silicatein subunits, silicatein α, performed by Shimizu *et al.*[72], was obtained from *Tethya aurantia* and naturally forms silica morphologies through silicatein-mediated processes. This work was followed directly by the *in vitro* work of Cha *et al.*[82], who proposed an active site of serine, histadine and asparagine to catalyze silica formation. In addition, it was proposed that the mechanism for the catalyzed reaction occurs through a nucleophilic attack of precursors such as tetraethoxysilane (TEOS) through the serine hydroxyl and histadine imidazole groups in which the asparagine acts to support and stabilize the intermediate products [68,82]. In addition, silicateins have also been isolated in other sponges, *Lubromirskia baicalensis and Suberites somuncula*, and show a large degree of homology, especially with respect to the active site and proposed enzymatic mechanism [83]. Due to the enzymatic nature of silicateins, many applications for this protein have stemmed from the ability to control the silica-precipitating activity and rate through concentration and activity of the enzyme. For instance, Rai and Perry showed that silica film properties such as thickness, roughness, and contact angle are determined by silicatein pre-adsorption onto surfaces and can be controlled by degree of adsorption as well as reaction time [84]. The coverage of

silicatein on the surface was controlled by silicatein immobilization to a gold surface adsorbed with by either cystamine or cysteamine and through the crosslinking agent glutardialdehyde (GDA). While silicatein adsorbed nonspecifically and minimally to the gold surface or gold with either cystamine or cysteamine, the addition of glutardialdehyde provided a high level of surface coverage with silicateins. In addition, more silicatein was able to be loaded onto the gold-cystamine-glutardialdehyde surface. By ramping the concentration of adsorbed silicateins, ranging from 10 to 30 ng/cm^2, it was possible to linearly increase the thickness of silica film formed from 20 to over 90 nm, respectively, and also increase the average roughness from approximately 1 to greater than 5 nm, respectively.

This work showed how silicateins can effect changes in silica film properties. In addition, silicateins have also been attributed to imbuing self-healing capabilities to silica materials [85]. As previously mentioned, silica encapsulation of enzymes retains enzymatic activity while providing stabilizing and protective forces for the encapsulated entity. Because silicatein itself is an enzyme, when entrapped in silica such as in sponge spicules or within applications, the ability for silicatein to catalyze the formation of silica is prolonged significantly. These properties have silicatein an attractive potential partner for the formation of silica through biomineralization.

1.3.2 Long chain and cyclic polyamines

Within both sea diatoms and sponges and in addition to the various protein components that drive biosilicification, one class of molecules that has similarly been implicated as crucial to an organisms ability to for biosilica has been polyamines [77,78,81]. Kröger *et al.* first characterized the presence of polyamines through isolation from the cell walls of six different diatom species [81]. Interestingly, they found that almost all species shared the same fundamental polymer subunit of *N*-methylpropylamine attached to putrescine; however, variations between species mainly occur through the size of the polyamines formed. In a subsequent study, the Sumper *et al.* further characterized the silicification ability of the diatom components by employing polyamine repeats of *N*-methylpropylamine of between 15 and 21 repeat units and studying the resulting formation of silica nanospheres [86]. In this report, phosphate anions were identified as key contributors of both *in vivo* silica biomineralization as well as *in vitro* silicification as the size and amount of silica precipitated was dependent on both the concentration of polyamines as well as phosphate anions in solution. It was concluded through NMR and dynamic light scattering characterization that the self-assembly of polyamines mediated by phosphate anions is necessary for the formation of fused silica spheres between 50 and 700 nm in size. Since these findings have been reported, an increasing number of studies have used polyamines as silicification tools to control nanoparticle formation. Various groups have demonstrated successful

silicification using synthetically derived polyamines from short alkylamines to long chain polyamines of up to 15 propylamine subunits and cyclic polyamines [87-91].

1.4 Silaffins

1.4.1 Discovery of silaffins in sea diatoms

Kröger *et al*. first reported the identification and characterization of silaffins, peptides with *sil*ica *affin*ity, which are a group of polycationic peptides based on motifs isolated from the diatom *Cylindrotheca fusiformis* that enable the diatom to form its silica cell walls [71]. Upon further study of these cell walls and isolation of numerous polypeptides, three heavily modified peptides were show to have the ability to precipitate silica from silicic acid: silaffin-1A, -1B and 2. Using genomic analysis, silaffin-1A and -1B were determined to be processed forms of a larger precursor protein sil1p, containing seven homologous peptide sequences (R1 – R7; see Table 1 for sequence information) with repeat positively charged lysine and arginine residues. Lysine residues were further post-translationally modified with polyamines. A notable property of these isolated silaffin peptides is their ability to template the deposition of silica from precursors at a remarkable rate; clusters of fused spherical silica particles could be formed in sizes of up to 700 nm in diameter within only minutes. In addition, the amount of silica is proportional to the concentration of silaffin added, allowing for another degree of potential control. Lastly, a synthetic version of the R5 peptide also

precipitated silica in the presence of phosphate anions with activity at neutral pH; the lack of necessary post-translational modifications for silicification makes this peptide an attractive candidate for new strategies to template silica formation under mild reaction conditions.

Table 1: Amino acid sequences of all silaffin peptides. Adapted from [71].

Silaffin Peptide	Amino Acid Sequence
R1	SSKKSGSYYSYGTKKSGSYSGYSTKKSASRRIL
R2	SSKKSGSYSGYSTKKSGSRRIL
R3, R5, R7	SSKKSGSYSGSKGSKRRIL
R4, R6	SSKKSGSYSGSKGSKRRNL

1.4.2 Sequence analysis of silaffin R5

The discoveries of this work led researchers to believe that the long-chain polyamine modifications of silaffins play a key role in their silica-precipitating behavior and that synthetic and biomimetic fabrications could potentially be useful for silica materials applications. In later work, it was also determined that the serines of silaffins were also post-translationally modified with phosphate groups, imparting a zwitterionic nature to the peptides [92]. Specifically, silaffin-1A, a peptide without phosphorylation, does not have the silica-precipitating characteristics when in a buffer without phosphate,

while a fully modified silaffin maintains the property. Taken together, the evidence supported the conclusion that these peptides allowed for silica deposition through a self-assembly process in which electrostatic interactions allowed for a higher ordered structure of silaffins to form and upon which silica precursors condense [67,92].

In addition, properties of the formed silica were found to be controlled by another silaffin, silaffin-2 [93]. Unlike other silaffins, which had numerous positively charged long-chain polyamine modifications necessary for silica precipitation, silaffin-2 has numerous modifications that provide an anionic character, including residues with phosphate, sulfate and glucuronic acid modifications. Reactions containing both silaffin-1A (or LCPAs) and silaffin-2 in differing proportions can control silica pore sizes from tens up to hundreds of nanometers; this is thought to be due to the interactions of the highly-negative silaffin 2 occluding and interacting with the higher order assemblies from silaffin-1A [69,93]. The findings of silaffins within *C. fusiformis* and their silica-precipitating abilities were also corroborated by silaffins found *Thalassiosira pseudonana*, another diatom with ornate silica walls. In this work, researchers discovered that, although silaffins in *T. pseudonana* were not compositionally homologous to those in *C. fusiformis*, they maintain similar post-translational modifications of lysines as well as phosphorylation modifications, and provide the same structural template for the condensation of silica [94]. Indeed, regulatory silaffins in both species are modified by sulfate modification and glycosylation to maintain function.

Silaffin R5 is a 19 amino acid peptide sequence that contains a four lysines, which have previously been identified as a key contributor to its inherent silicification ability; however, the role and necessity of other residues within the sequence, as well as the distribution of lysines within the sequence required elucidation. Knecht and Wright were the first to functionally analyze the silica promoting ability of the silaffin R5 peptide by creating a series of 10 homologous peptide sequences that resembled the R5 peptide but contained key substitutions or deletions of certain motifs [95]. Specifically, they noted that deletion or substitution of the C-terminal RRIL motif with other sequences (*e.g.* AAIL) produced particles that either did not have or possessed reduced silicification ability. They hypothesized that the RRIL motif, possessing two charged amino acid resides next to two hydrophobic residues may allow for the transient assembly of silaffin peptides into micellar structures and are then crosslinked through the lysines and phosphate anions in solution to produce templates for the polycondensation of silica.

1.4.3 Applications of silaffins in biotechnology

The property of the silaffin peptides to cause the formation of silica from silicic acid precursors in a controlled and rapid manner has led to numerous applications, many employing the biomimetic R5 silaffin peptide. As discussed previously, encapsulation of enzymes and other biological entities within silica has been shown to confer numerous advantages, including stabilization and protection from adverse

conditions [68,69,96-98]. By employing silaffin-inspired techniques such as co-incubation of an enzyme with R5 silaffin or concatenation of silaffin with enzyme at the genetic level [22,98], the resultant immobilized enzymes retained enzymatic activity while exhibiting significantly improved thermal stability. In addition, silaffin R5 has also been used in facile holographic patterning of silica on surfaces [99]. Brott *et al.* demonstrated the effected incorporation of the R5 peptide within a composite material that was exposed upon laser excitation and was subsequently presented on the surface; co-incubation with silica precursors then resulted in the patterned silicification along a prescribed axis, demonstrating its potential for applications in nanopatterning. Silaffin R5 peptides have also been used as a tool to encapsulate and release cargo. Lechner and Becker have reported the use of silaffin R5 conjugated with a peptide ligand CG12AB (CGYHWYGYTPQNVI) through disulfide linkage, which is susceptible to reduction and thus release of the cargo. Subsequently, they demonstrated that this peptide conjugate was similarly able to produce silica in phosphate solution with average diameters of 600 - 900 nm; however, due to the inexact control of the silicification using R5, the silica particles fabricated in this study had a high polydispersity, which could not be controlled through both monomer and precursor concentration. A desirable combination of a controllable template with the silaffin R5 incorporated to imbue silicification ability would enhance the physical characteristics of such a release system.

One such potential conjugation partner would be the use of elastin-like polypeptides (ELPs).

1.5 Elastin-like polypeptides, self-assembly and applications

ELPs are a family of peptide polymers composed of the repeating pentapeptide sequence VPGXG, where X is the guest residue, which can be any amino acid except Pro (P). ELPs exhibit an aqueous lower-critical solution temperature (LCST) transition that is dependent on intrinsic material parameters, such as the ELP's guest residue (X) [100,101], molecular weight, and concentration [102], and extrinsic environmental factors, such as the type and concentration of salt [100,103,104]. ELPs can be encoded at the genetic level, expressed at high yield in *E. coli* and purified by exploiting their LCST behavior to produce monodisperse polypeptides that are entirely of the same composition, length, and physical properties; in addition, the ability to precisely encode complex block architectures at the gene level affords the possibility of creating polypeptides of enormous complexity with tight control. Chilkoti *et al.* have demonstrated in several previous papers that ELP block copolymers comprised of different ELP sequences with distinct LCSTs can form monodisperse micellar structures within specific temperature ranges (Figure 1) and can be used for applications such as drug delivery [105-107] and biosensing [103,108-110]. Diblock ELP sequences have been previously designed to incorporate moieties, such as peptides NGR and RGD, appended

to the hydrophilic ELP block, resulting in functionally decorated micelles, without disruption to the self-assembly process that can be used in the uptake of ELP nanoparticles by cells [105,109,111].

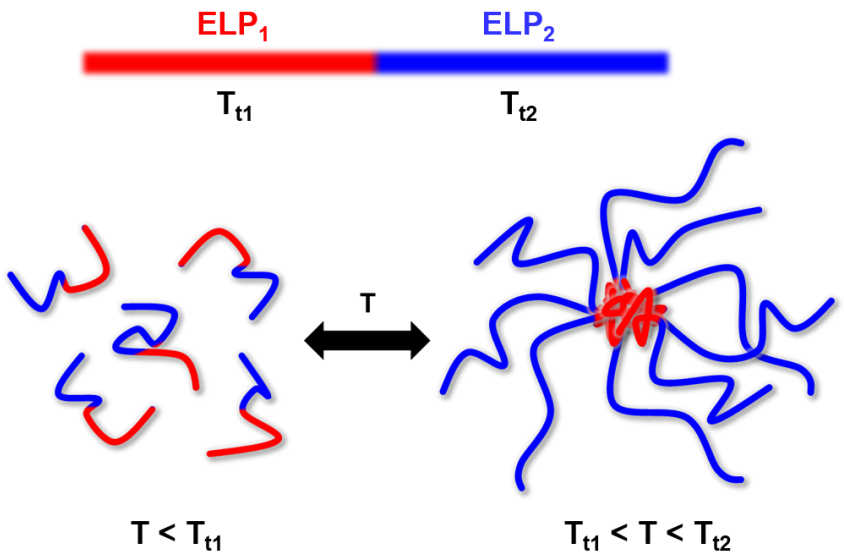

Figure 1: Construct design for micelle-forming diblock ELP consisting of ELP_1 ($Tt = Tt_1$) and ELP_2 ($Tt = Tt_2$). The diblock ELP is soluble when $T < Tt_1$ and forms micelles when $Tt_1 < T < Tt_2$. Figure adapted from [108].

The high degree of control of sequence from the genetic to peptide level allows for the construction of constructs that self-assemble, provide functionality and allow for facile chemistry on select portions of the sequence. The group has demonstrated numerous examples that conjugation of hydrophobic small molecules to hydrophilic ELP chains can result in the formation of nanoparticles. To highlight one example, MacKay *et al.* showed that conjugation of doxorubicin through a pH-labile linker inducing the self-assembly of ELP-doxorubicin nanoparticles for delivery showed

sustained release as well as significantly decreased tumor volume *in vivo* [112]. In another case, McDaniel *et al.* demonstrated that a variety of hydrophobic drugs can be conjugated to ELPs to form nanoparticles given the hydrophobicity of the drug to be able to drive the formation [113]. The genetic control and modular assembly of ELPs, allowing for the concatenation and insertion of other polypeptide sequences seamlessly, in addition to their ability to self-assemble through diblock assembly or conjugation of hydrophobes into highly uniform and monodisperse micelles, presents an appealing proposition for their application as templates for silaffin-mediated silicification to create hybrid polypeptide and silica nanoparticles.

1.6 Specific Aims

We proposed the use of elastin-like polypeptide self-assembled micelles that are monodisperse in size and construction to template the synthesis of hybrid silica nanoparticles to study its potential for the encapsulation and release for drugs as well as to characterize the degree of control of silicification in order to serve as a targeted delivery vehicle. By inserting a silaffin R5 peptide into a collection of different ELP constructs, we drove the presentation of silica-promoting motif at the corona of monodisperse micelle templates to promote the localized polycondensation of silica and fabricated hybrid silica-polypeptide materials. In addition, by conjugation of hydrophobic small molecule therapeutics such as doxorubicin to self-assembling ELP

constructs, we demonstrated sought to load and encapsulate drugs within the templated silica nanoparticles.

The approach as outlined in this work is to employ biologically-inspired silicification methodologies in the development of nanoscale assemblies of hybrid polypeptide and inorganic materials toward potential applications in drug delivery. This innovation uses the programmed assembly of genetically encoded polypeptides to template the formation of silicified nanoparticles in a simple and controlled manner, resulting in products of select size, composition and morphology; furthermore, the methodology highlighted in this work enables their formation under mild reaction conditions such as temperature, pH, and solvent.

1.6.1 Specific Aim 1

Aim 1 entails the proof-of-concept construction and study of an ELP and silaffin conjugate to probe the silicification potential of temperature-dependent polypeptide assembly templates. We employed the use of a diblock ELP construct, which self-assembles into spherical micelles upon the thermally-triggered phase transition of the more hydrophobic block, to characterize the dependence of silicification on the assembly and multivalent presentation of silaffin peptides. We further explored the degree of silica formation as a function of silica precursors as well as time and characterized the resulting nanoparticles using light scattering and electron microscopy.

Hypotheses addressed in Specific Aim 1:

1. Self-assembled ELP and silaffin R5 conjugates presenting multiple silica-promoting peptides at micelle coronae can serve as centers for silica polycondensation.
2. Silicification is subject to the temperature-dependent assembly of ELP and silaffin conjugate unimers (a single ELP chain) into micelles and that silica nanoparticles resulting from this reaction will result in particles with low size distributions.

1.6.2 Specific Aim 2

Aim 2 represents the study of silica particle formation and templating through the assembly of asymmetric amphiphiles toward its use as drug release vehicle. In this work, we inserted a silaffin R5 peptide within a single block ELP construct with a cysteine-rich trailer that self-assembles into spherical micelles upon conjugation with small hydrophobic molecules – the two used in this study were 1) *N*-benzylmaleimide and 2) BMPH-activated doxorubicin, a model cancer chemotherapeutic. We characterized the silicification of assemblies using both conjugates to study their size and resulting morphologies of the resulting hybrid silica particles. Finally, using the drug-conjugated micelle construct, we studied the pH-dependent release of drug from the encapsulated nanoparticle.

Hypotheses addressed in Specific Aim 2:

1. Asymmetric amphiphiles comprised of self-assembled ELP and silaffin conjugates of can serve as centers for silica polycondensation.
2. Silica nanoparticles formed through this process can encapsulate doxorubicin-conjugated ELPs and doxorubicin may be released from the silica nanoparticle matrix by cleavage of pH-labile linker.

1.6.3 Specific Aim 3

Aim 3 entails the study of the optimization of templates for silicification toward utilization of hybrid ELP and silica nanoparticles as a targeted carrier system. We constructed three ELP constructs, which self-assemble upon conjugation with *N*-(4-ethylphenyl)-maleimide, where the silica-promoting module was inserted at evenly-spaced regions along the ELP chain and would thus result, on average, in differential presentation of charge along the radial axis of the self-assembled templates. Using streptavidin-biotin as a proof-of-concept model for biospecific interaction, we characterized the degree of ligand availability beyond the silica shell.

Hypotheses addressed in Specific Aim 3:

1. Self-assembled micelles incorporating silica-promoting motifs at different locations along the ELP chain can promote the preferential polycondensation of silica in a similar manner to micelles presenting such motifs at the corona.

2. The location of inserted silaffin modules will influence both the morphology of resulting hybrid silica nanoparticles as well as the degree of availability of free ELP post-silicification.

1.7 Organization of the dissertation

This dissertation is organized such that each specific aim is addressed in its own chapter and is intended to encompass the research efforts toward one publication. Specific Aim 1 is investigated in Chapter 2, Specific Aim 2 in Chapter 3 and Specific Aim 3 in Chapter 4; finally, concluding remarks and future directions for this work are presented in Chapter 5.

2. Bio-Inspired Synthesis of Hybrid Silica Nanoparticles Templated from Elastin-like Polypeptide Micelles

The text and figures included in Chapter 2 were published in *Nanoscale*. The full citation for the article is: "Han, W., MacEwan, S. R., Chilkoti, A. & López, G. P. Bio-inspired synthesis of hybrid silica nanoparticles templated from elastin-like polypeptide micelles. Nanoscale 7, 12038-12044 (2015)." This work encompasses the aims set out in Specific Aim 1. Co-author Sarah MacEwan provided expertise in designing the oligonucleotides for the silaffin insert as well as general molecular biology techniques.

2.1 Chapter synopsis

The programmed self-assembly of block copolymers into higher order nanoscale structures offers many attractive attributes for the development of new nanomaterials for numerous applications including drug delivery and biosensing. The incorporation of biomimetic silaffin peptides in these block copolymers enables the formation of hybrid organic-inorganic materials, which can potentially enhance the utility and stability of self-assembled nanostructures. We demonstrate the design, synthesis and characterization of amphiphilic elastin-like polypeptide (ELP) diblock copolymers that undergo temperature-triggered self-assembly into well-defined spherical micelles. Genetically encoded incorporation of the silaffin R5 peptide at the hydrophilic terminus of the diblock ELP leads to presentation of the silaffin R5 peptide on the coronae of the micelles, which results in localized condensation of silica and the formation of near-

monodisperse, discrete, sub-100 nm diameter hybrid ELP-silica particles. This synthesis method, can be carried out under mild reaction conditions suitable for bioactive materials, and will enable the development of functional nanomaterials for applications in drug delivery, bioimaging and biosensing. Beyond silicification, the general strategies described herein may also be adapted for the synthesis of other biohybrid nanomaterials as well.

2.2 Introduction

Several biologically inspired methodologies for the facile synthesis of silica have been developed [21,75-77], and the discovery of peptides [71,73,78], proteins [79,80], and polymers [81] that facilitate the polymerization of silica under physiologically relevant conditions at controllable rates has expanded the utility of silica-stabilized organic materials. Two of the most prevalent biomimetic silica precipitants are polyamines and polypeptides that contain numerous lysine residues (e.g. poly-L-lysine), which have been used to template the formation of siliceous materials with various morphologies [89,114-117]. Kröger *et al*. first reported the identification and characterization of silaffins —peptides with *silica affinity*— which are a group of polycationic peptides based on motifs isolated from the diatom *Cylindrotheca fusiformis* that enable the diatom to form its silica cell walls [71]. Study of gene sequences revealed a sequence of 265 amino acids containing seven homologous peptides that catalyzed biosilicification. These peptides,

containing a high number of cationic residues (lysine and arginine), precipitate silica particles (of approximately 500 to 700 nm in diameter) under physiological conditions in a manner that depends on the concentration of the protein and solution pH. The same group also reported post-translational phosphorylation of the serine residues in the silaffin and modification of lysine residues with long-chain polyamines, and hypothesized that these post-translational modifications play an important role in silaffin-mediated silica condensation reactions [78]. However, the silaffin R5 peptide (see below for sequence) that is not post-translationally modified facilitates silicification in phosphate buffer [78,95]. Its lack of post-translational modification makes it an appealing candidate for applications in which it can be encoded in commonly used expression systems such as *E. coli*. The reported mechanism for silica mineralization of the silaffin R5 peptide depends on crosslinking of silaffin chains through solvent phosphate groups and presentation of a high density of cationic charges to favor silica condensation around the peptide [95]. The applications of this peptide have resulted in numerous demonstrations of silicification [22,97,98,118,119]. However, the uncontrolled self-assembly of these templates prior to silica deposition often results in a network of fused silica nanoparticles.

Herein, we demonstrate that silaffin R5 peptides fused to elastin-like polypeptides (ELPs) that self-assemble into monodisperse micelles can be used as templates for the controlled deposition of near monodisperse silica nanoparticles. Here

we show that, by appending the silaffin R5 peptide to the hydrophilic terminus of an ELP diblock copolymer, the resulting polypeptide maintains its ability to self-assemble into micelles and is able to serve as an effective template for silicification and the formation of near-monodisperse silica nanoparticles. These results set the stage for the synthesis of uniform hybrid ELP and silica nanoparticles for future applications in drug delivery, imaging and biosensing.

2.3 Materials and methods

2.3.1 Materials

Restriction enzymes BglI, NdeI, BseRI, AcuI, BamHI and XbaI, T4 DNA Ligase and calf intestinal phosphatase (CIP) were purchased from New England Biolabs (Ipswich, MA). pET-24a(+) vector was purchased from Novagen Inc. (Madison, WI). BL21 *E. coli* competent cells were purchased from EdgeBio (Gaithersburg, MD). Oligonucleotides were obtained from Integrated DNA Technologies, Inc. (Coralville, IA). Terrific Broth was purchased from MO BIO Labs, Inc. (Carlsbad, CA) and SDS-PAGE gels from BioRad, Inc. (Hercules, CA). Tetramethylorthosilicate (TMOS) was used as the silica precursor for condensation reactions and was obtained from Alfa Aesar (Ward Hill, MA). Quantifoil 300 mesh copper support grids (657-300-Cu) for cryogenic transmission electron microscopy were purchased from Electron Microscopy Sciences

(Hatfield, PA). Alexa Fluor 488 Fluorescent Dye was purchased from Life Technologies (Carlsbad, CA).

2.3.2 Construction of ELP-R5 silaffin gene

The ELP and silaffin R5-ELP (herein referred to as ELP-R5) genes were assembled by recursive directional ligation by plasmid reconstruction (PRe-RDL).[120] The diblock gene encodes for 60 pentapeptide repeats with the guest residue valine as the hydrophobic (core) block and 60 pentapeptide repeats with the guest residues alanine and glycine in a 1:1 ratio as the hydrophilic (corona) block. A leader DNA sequence that encodes for MGCGWP was incorporated, so as to include a unique cysteine (C) for thiol-mediated conjugation of Alexa Fluor 488 and a tryptophan (W) for quantification of the ELP by UV-vis spectrophotometry at 280 nm. A pET-24a(+) vector encoding the ELP sequence was isolated from *E. coli* cells and purified by miniprep. Another pET-24a(+) vector containing the silaffin R5 sequence was obtained by insertion of designed oligonucleotides, encoding R5 silaffin, into an empty vector, as previously described [100]. PRe-RDL was performed by digestion of the ELP-encoding vector with AcuI and BglI restriction enzymes, digestion of silaffin-R5-encoding vector with BseRI and BglI, and gel isolation of the desired DNA fragments from each restriction digestion (Figure 2). The expected number of base pairs for each cut for the ELP-containing band and Silaffin-containing band are 3206 and 3476 bp, respectively, which matches well with the gel image. T4 DNA ligase was used to ligate vector segments encoding the ELP

sequence and silaffin R5 and the ligated plasmid was transformed into BL21(DE3) *E. coli* for expression. The gene for a control ELP (ELP-GG), without the trailing silaffin sequence, was similarly constructed.

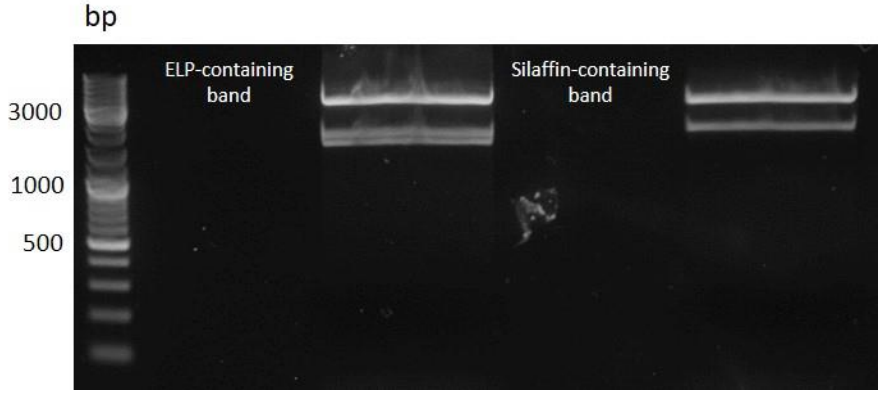

Figure 2: DNA agarose gel of PRe-RDL restriction and assembly of ELP-R5. The ELP-containing band ('A' cut) and Silaffin-containing band ('B' cut) are represented as the top bands in the left and right, respectively, lanes.

2.3.3 Expression and purification of ELP-R5 silaffin

Expression of ELP-R5 and ELP-GG was carried out in *E. coli* containing the assembled plasmids as described previously [120]. Fresh Terrific Broth (TB) culture media was prepared at 55 g/L, autoclaved and supplemented with 45 mg/mL kanamycin. A hyperexpression protocol was used for ELP expression that relies on the inherent leakiness of the T7 promoter [108]. A single colony of *E. coli* harboring an expression plasmid that encodes for an ELP of interest was used to inoculate a 50 mL starter culture in TB. After one day of culture at 37 ºC at 200 rpm, cells were centrifuged the following day and resuspended in 10 mL of fresh TB and transferred into 1 liter TB

and cultured at 37 ˚C and 200 RPM rotation for 24 h. Cells were then centrifuged, resuspended in phosphate buffered saline (PBS; pH 7.4) and lysed by sonication. Purification of ELP-R5 was carried out by inverse transition cycling (ITC), as previously described [121]. Briefly, one cycle of ITC consists of addition of NaCl and increase of temperature until solution becomes turbid, indicating that the ELP has transitioned, followed by centrifugation at 25 ˚C and 15,000 x g for 10 minutes to pellet the ELP, and resuspension of the pellet in fresh PBS or water. This step is followed by centrifugation at 4 ˚C and 15,000 x g for 10 minutes to remove irreversibly aggregated material, the supernatant is transferred to a new tube. Three cycles of ITC were sufficient to produce pure ELP-R5 polypeptides, as characterized by SDS-PAGE.

2.3.4 Silica deposition using the method of Kröger et al.

Silica deposition was carried out using methods similar to those previously described by Kröger *et al*. [78] For all reactions, 2.5 mg/mL final concentration of ELP-R5 (or ELP-GG control) in PBS or water was prepared and incubated at 37 ˚C for 15 min prior to reaction to ensure micelle formation. 1 M TMOS hydrolyzed in 1 mM HCl was prepared and mixed for 10 min by rotation at room temperature. The ELP-R5 solution was diluted to the final concentration and then hydrolyzed TMOS was added to the appropriate final TMOS concentration. The mixture was allowed to react for a set period of time, before centrifugation at 10,000 x g and resuspended in DI water.

2.3.5 Conjugation of fluorescent Alexa Fluor 488 to ELP-R5

Fluorescently conjugated ELP was prepared by reaction of the single cysteine residue in ELP-R5 (or ELP-GG), with Alexa Fluor 488-maleimide. 100 μM ELP-R5 (or ELP-GG) was prepared in PBS at room temperature and then a ten-fold excess of tris(2-carboxyethyl)phosphine (TCEP) was added to reduce disulfide bonds. A 10 mM stock solution of Alexa Fluor 488-maleimide was prepared and reacted with ELP-R5 (or ELP-GG control) at a molar ratio of fluor:ELP of 10:1. The reaction was allowed to continue for 12 h at 4 ˚C, the reaction mixture was then dialyzed using a 10K MWCO dialysis membrane (Thermo Scientific) to remove unreacted dye.

2.3.6 Characterization of silica encapsulation of ELP-R5

UV-vis spectrophotometry was performed on a Cary 300 UV-vis spectrophotometer (Agilent, Santa Clara, CA). 500 μL of a 20 μM ELP-R5 solution in water was aliquoted into a quartz crystal cuvette and placed into the sample well. The temperature dependent absorbance of the sample at 350 nm was measured from 20 ˚C to 60 ˚C at 0.1 ˚C increments and at a rate of 1 ˚C/min. Dynamic light scattering (DLS) was carried out on a DynaPro Plate Reader II (Wyatt Technology, Santa Barbara, CA). Measurements of hydrodynamic radii were made in triplicate, with each datum consisting of 10 acquisitions for 5 s each. The autocorrelation function was fitted by a regularization algorithm provided by the manufacturer to determine the hydrodynamic radius (R_h) of the ELPs. Zeta potential was measured on a Zetasizer Nano ZS (Malvern,

UK) with 90º scattering optics. 900 μL of an ELP was placed into a mini-quartz cuvet, and measured three times for each condition. Three measurements were then averaged to create a single datum. Cryo-transmission electron microscopy (cryo-TEM) was performed on a Tecnai G² Twin (FEI, Hillsboro, OR) at 200 keV. Samples were vitrified for cryo-TEM on a Vitrobot Mark III (FEI) using a 3 s blot time at -3 blot offset for all samples and imaged at a maximum of 15 electrons/Å² per image. Fluorescence microscopy was performed a Zeiss Axio Observer with temperature and humidity control with a 100x/1.45 oil Plan Apochromat DIC objective.

2.4 Results and discussion

2.4.1 ELP-R5 design and characterization

Figure 3A and B present a schematic and the amino acid sequence of the diblock ELP-R5 silaffin peptide. Raising the temperature above the critical micellization temperature (CMT) of ELP-R5 triggers its self-assembly into spherical micelles (Figure 3C), leading to the presentation of multiple copies of the R5 peptide on the corona of the micelle. We hypothesized that the presentation of a high local density of positively-charged residues in the silaffin R5 peptide at the corona of the micelle would selectively trigger the mineralization of silica.

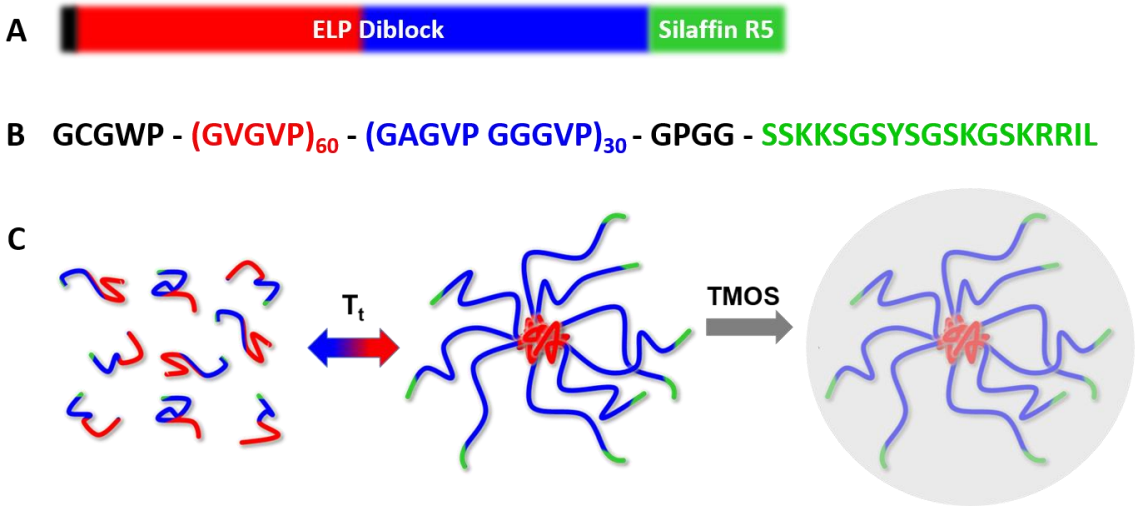

Figure 3: Schematic representation of materials and method. (A) Representation of ELP-R5 construct with C-terminal silaffin R5. (B) Amino acid sequence for ELP-R5 containing leading, micellar-core sequence for conjugation (black), inner block ELP with lower T_t (red), outer block ELP with higher T_t (blue), and silaffin R5 (green). (C) Representation of reaction process proceeding from assembly of ELP constructs into micelles, followed by addition of TMOS to produce silica nanoparticles.

We first characterized ELP-R5 to examine its self-assembly into spherical micelles and compared it to a diblock ELP-GG (negative control without silaffin) to determine whether appending the silaffin R5 peptide on the terminus of the ELP affects self-assembly. SDS-PAGE of purified ELP-R5 (Figure 4 Lane 2) was consistent with its theoretical molecular weight (49.8 kDa), as was the case for the ELP-GG construct (Figure 4 Lane 3; 47.8 kDa).

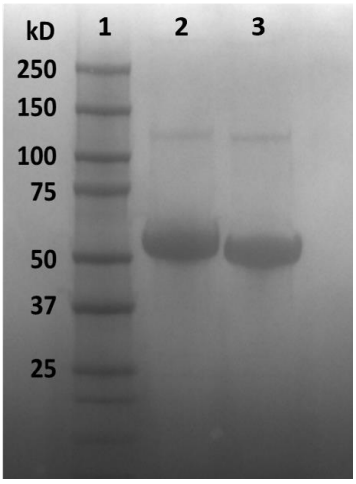

Figure 4: SDS-PAGE gel with polypeptide ladder (molecular weights shown), ELP-R5 (lane 1), and control ELP-GG (lane 2).

To determine the effect of the silaffin R5 peptide on micellization, we performed temperature-dependent turbidimetry and dynamic light scattering (DLS) measurements on a 25 μM solution of ELP-R5 in water (Figure 5, left side). The data show a slight increase in turbidity at approximately 33 ˚C, which is indicative of micelle formation[108], followed by a large increase in absorbance between 55 ˚C and 60 ˚C, resulting from the hydrophobic collapse of the coronal block and subsequent bulk aggregation of the ELP-R5 into micron size aggregates [108]. The temperature-dependent turbidity is in agreement with DLS measurements that show a similar increase in hydrodynamic radius (R_h) from ~9 nm (unimer) to 25 nm (micelle) at approximately 33 ˚C. In addition, the formation of micelles from ELP-R5 was reversible, such that micelles disassemble upon lowering the solution temperature below the T_t (data not shown), consistent with previous results obtained for similar systems [113].

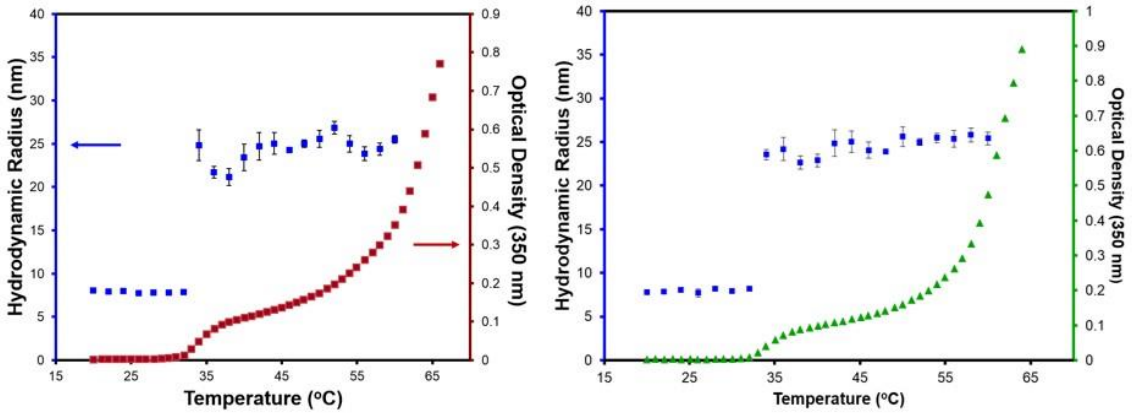

Figure 5: Dynamic light scattering (DLS) and turbidity measurement for 25 μM ELP-R5 (left) and ELP-GG (right) in water as a function of solution temperature. The R_h measured by DLS is plotted on the left vertical axis (blue) and the optical density at 350 nm (turbidity) is plotted on the right vertical axis (red & green, respectively).

These data are consistent with those measured for the control ELP-GG that does not contain the silaffin R5 peptide and indicate a small to negligible effect on micelle formation from attachment of the silaffin R5 peptide to the ELP (Figure 5; right side). These results suggest that micelle formation presents the silaffin R5 peptide on the corona of the micelle at a relatively high local concentration that we hypothesized should facilitate the condensation of silica.

2.4.2 Silicification using the modified Kröger method

To test this hypothesis, we next carried out silicification experiments to examine the formation of silica nanoparticles. Silicification reactions were first carried out in phosphate buffer using the method of Kröger *et al.* (see Materials and methods) at 37 ˚C for 30 s. These conditions resulted in the formation of clusters of relatively large fused spheres of silica with dimensions between 300 and 800 nm in diameter for ELP-R5

constructs (Figure 6). By contrast control experiments with the ELP-GG resulted in unappreciable formation of silica particles. This result is in agreement with previous studies that concluded that the assembly of silaffin mediated by the RRIL terminating sequence [95] in phosphate-containing solutions results in the formation and deposition of silica upon addition of silicic acid to form large, highly polydisperse and fused silica particles. Indeed, we suggest a similar mechanism in this circumstance, i.e., that silaffin R5-conjugated ELP is crosslinked through electrostatic interactions in the presence of phosphate anions and that the addition of silicic acid to this solution of assembled templates results in silica polycondensation [78,95].

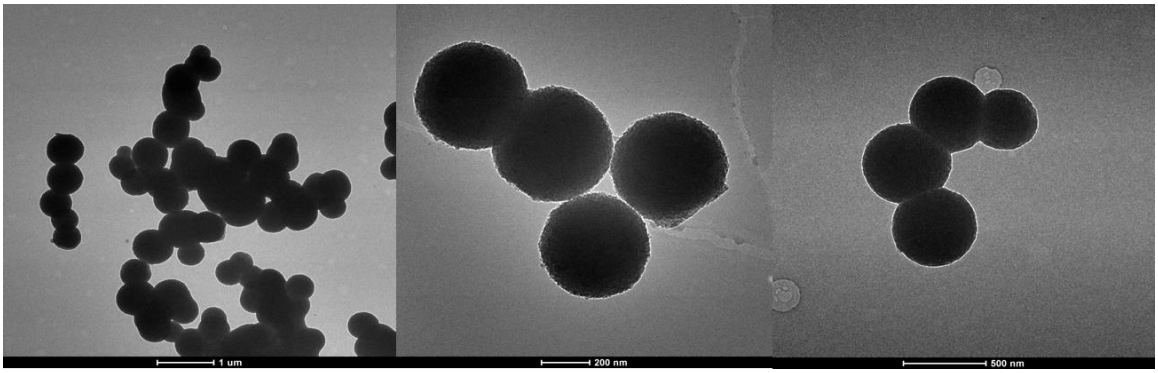

Figure 6: TEM images of particles resulting from the silicification of ELP-R5 micelles (2.5 mg/mL) carried out at 37 ˚C in the presence of phosphate (10 mM) with 100 mM TMOS for 30 seconds. Representative images shown from separate samples.

To demonstrate that ELP-R5 is encapsulated within the silica particles as a result of the silicification reaction, we conjugated fluorescent Alexa Fluor 488 to the single cysteine of ELP-R5, and carried out the same silicification reactions. We then analyzed the resulting samples by fluorescence microscopy (Figure 7). Comparison of the differential interference contrast (DIC) images with the fluorescence images shows that the resulting silica particles align with the fluorescent signal emitted by the Alexa Fluor 488, suggesting the presence of fluorescent ELP-R5 within the fused silica particles. This result provides evidence that it is possible to employ ELP fusions with silaffin R5 to template the formation and arrangement of silica deposition and that their formation in phosphate buffer was driven by the mechanism described above.

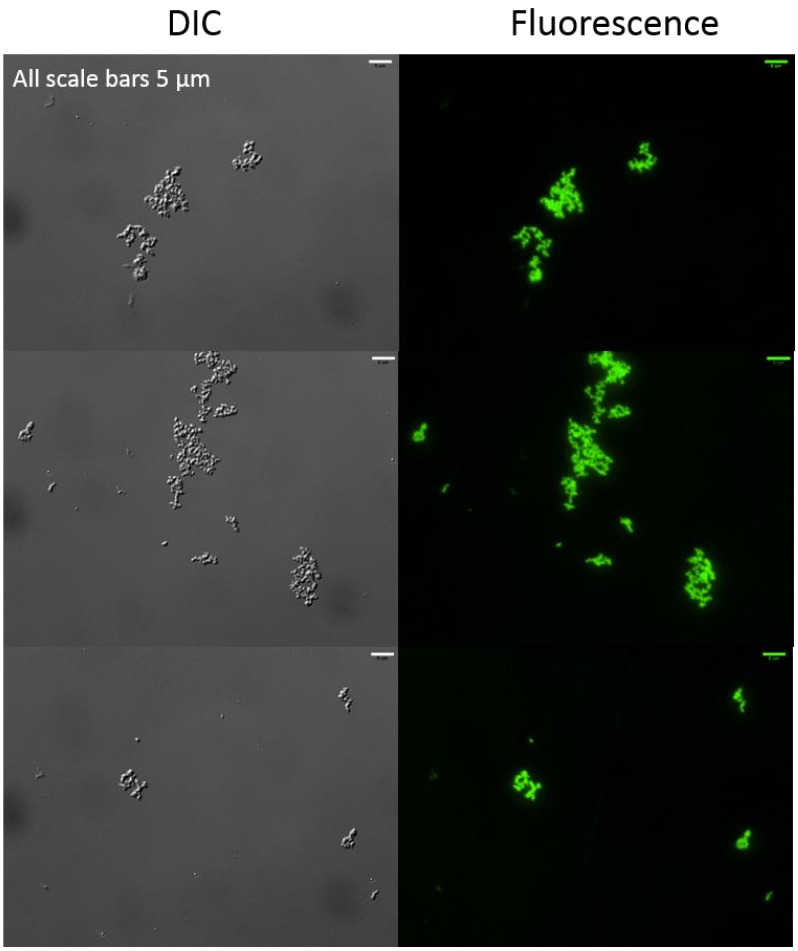

Figure 7: Differential interference contrast (DIC; left) and fluorescence (right) images of silicified core-conjugated Alexa Fluor 488 ELP-R5 micelles formed through phosphate-mediated crosslinking of silaffin R5 peptides. Images are of particles in PBS.

2.4.3 ELP-R5 micelle templated silicification of monodisperse hybrid nanoparticles

We next hypothesized that a predetermined, controlled assembly of highly-monodisperse, micellar templates for silica deposition using ELP constructs, presenting silaffin peptides at the coronae accomplished without the addition of phosphate in

solution, would lead to silica nanoparticles that are similarly individualized and monodisperse. We incubated solutions of ELP-R5 micelles in water with TMOS for varying periods of time at 37 ºC (a temperature that is greater than the CMT of ELP-R5 in water) and characterized the reaction products by cryo-TEM and light scattering. Cryo-TEM showed that the silica particles obtained by reaction 100 mM TMOS in the presence of ELP-R5 (2.5 mg/mL) at 37 ºC for 8 h are of uniform size and discrete (i.e., not fused together as observed for reactions in the presence of phosphate ion, Figure 8). Interestingly the uniform particles are packed in a roughly hexagonal lattice within the vitreous ice; the lack of particles near the center of the grid hole is likely due to a decrease in the thickness of vitreous ice within the grid hole. Image analysis of >200 particles throughout the grid showed that the silica nanoparticles are near monodisperse in size with a mean diameter of 51 ± 4.8 nm.

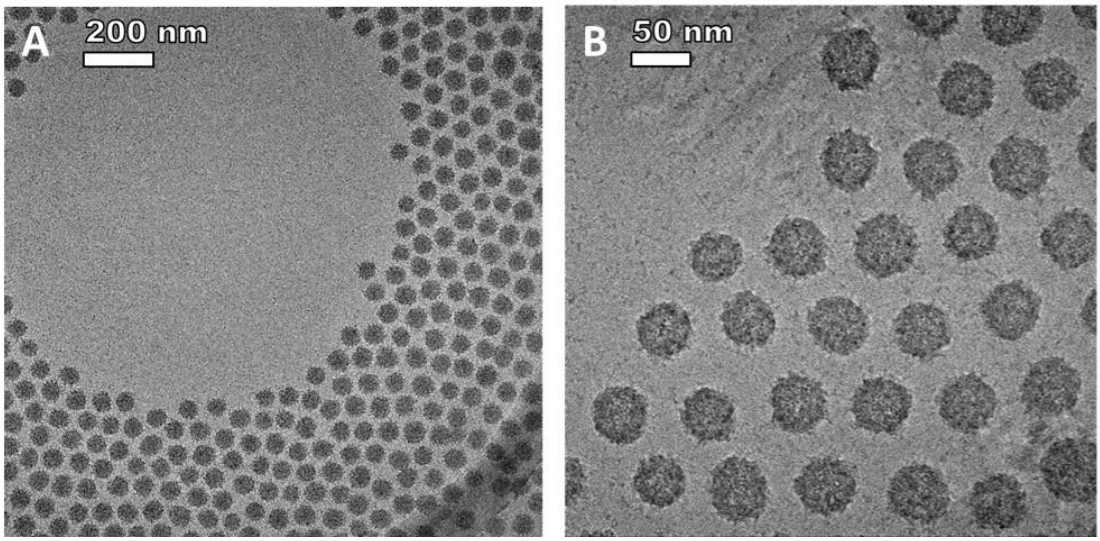

Figure 8: Characterization of biosilicification of ELP constructs (A) and (B) Cryogenic transmission electron microscopy images of ELP-R5 silica nanoparticles after 8 hour reaction with hydrolyzed TMOS at 100 mM. Scale bars are 200 nm (A) and 50 nm (B).

Furthermore, zeta potential measurements for ELP-GG control micelles and ELP-R5 micelles prior to, and post silicification were obtained (Figure 9). In contrast to ELP-R5 micelles alone (middle), which exhibit a positive zeta potential of 8.1 ± 0.7 mV, hybrid ELP-R5 silica particles formed through exposure to 100 mM TMOS for 8 hours resulted in a zeta potential of -27.1 ± 3.0 mV, due to the deposition of silica around the micelles and associated negative surface charge of deprotonated silanol groups. DLS measurements were also taken in a time-course study of the formation of silica on ELP-R5 (Figure 10) using three different final TMOS concentrations – 10 mM, 50 mM and 100 mM. The R_h increased from ~25 nm before the reaction to ~35 nm for each of the three concentrations. Interestingly, at all TMOS concentrations studied, there is a general trend in the data that suggests that the growth in the size of the nanoparticles upon

silicification occurs during the first hour of measurement, after which no further significant growth is observed.

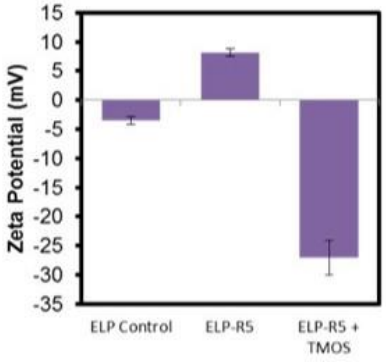

Figure 9: Zeta potential measurement of nanoparticles of control ELP-GG (left), ELP-R5 without TMOS (center) and ELP-R5 with TMOS (right).

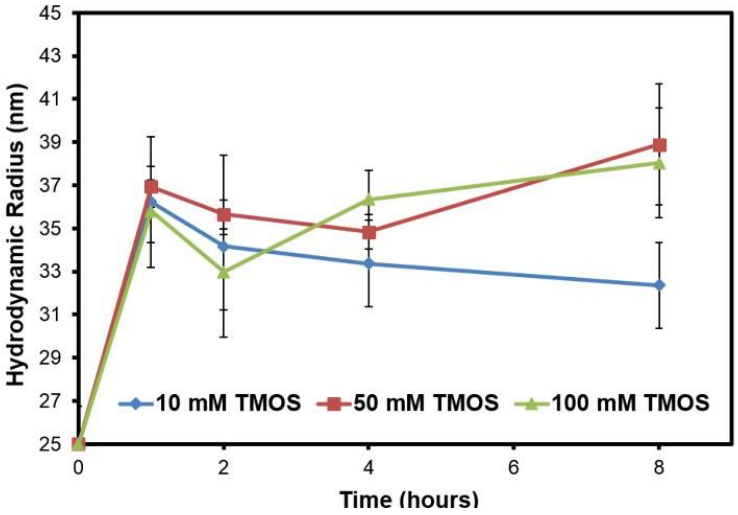

Figure 10: Time course measurements of hydrodynamic radii of ELP-R5 with 10 mM (circles, blue), 50 mM (squares, red) and 100 mM (triangles, green) TMOS.

Importantly, we found the uniform silicification and formation of hybrid nanoparticles to be dependent on both the presence of the silaffin R5 peptide and the micelles (Figure 11). While the ELP-R5 micelles resulted in a formation of hybrid particles of uniform size, both the ELP-GG control micelle without silaffin R5 peptide and the unassembled ELP-R5 unimer (i.e. silicified at 25 ºC, a temperature that is below the CMT of 33 ºC of ELP-R5 in water) resulted in a lack of silica particles under nearly identical experimental conditions. This is strong evidence that the presentation of a high local density of positive charges from the lysine and arginine residues of the silaffin R5 through micellization of the ELP-R5 construct is necessary to serve as growth centers for silica deposition on the nanoparticles.

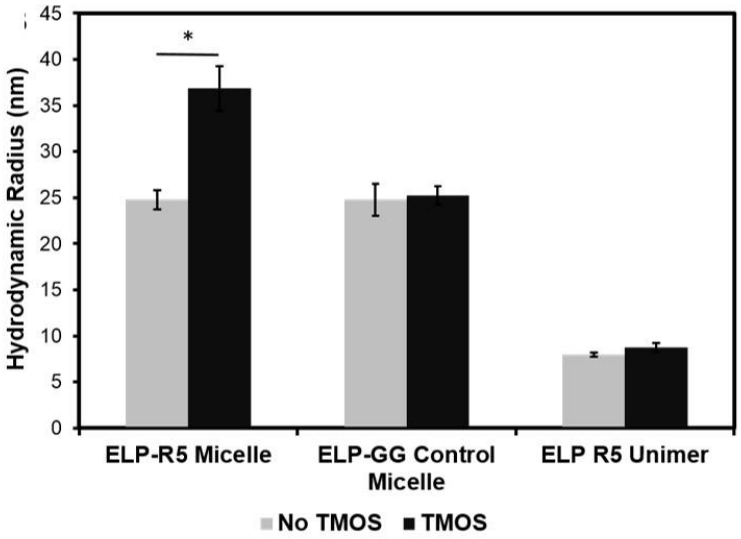

Figure 11: Hydrodynamic radii of ELPs prior to (left, grey bars) and after (right, black bars) incubation with 100 mM hydrolyzed TMOS for 8 h. *ELP-R5 micelle construct showed a significant ($p < 0.05$) increase in size.

2.5 Conclusion

We report the synthesis of discrete and monodisperse nanoparticles containing silica and an engineered polypeptide in a temperature- and assembly- dependent manner. By combining the temperature-triggered self-assembly of ELPs into monodisperse micelles with the silicification properties of the silaffin R5 peptide in water, we demonstrate the formation of very uniform, hybrid silica-polypeptide nanoparticles using a simple, isothermal reaction that may be suitable for biomedical or biotechnological applications. For example, this method is promising for encapsulation of therapeutic or imaging moieties within silica stabilized ELP nanoparticles. Furthermore, conjugation of the silaffin R5 to other self-assembling peptides that provide access to diverse nanoparticle morphologies may enable the facile synthesis of silica stabilized hybrid particles of various sizes and morphologies. Finally, the design of more complex, functional, self-assembling ELPs that incorporate multiple biomineralization-promoting tags may enable the fabrication of more complex hybrid nanomaterials.

2.6 Chapter acknowledgements

This work is supported by NSF's Research Triangle MRSEC (DMR-1121107). W.H. acknowledges support through a NIH Biotechnology Predoctoral Training Fellowship and the Center for Biological and Tissue Engineering (NIH Grant No. 5T32GM008555-18). The authors thank the staff of the Duke University Shared Materials

Instrumentation Facility and Light Microscopy Core Facility for their expert technical assistance.

3. Self-Assembled Hybrid Elastin-like Polypeptide / Silica Nanoparticles Enable Triggered Drug Release

The text and figures included in Chapter 3 represent yet unpublished work and encompasses the aims set out in Specific Aim 2.

3.1 Chapter synopsis

The discovery of biomimetic polypeptides that enable the biomineralization of synthetic and biosynthetic materials has resulted in the development of hybrid materials that incorporate inorganic components for potential application in drug delivery, enzyme immobilization, and surface modification. Here, we describe an approach that uses micellar assemblies of an elastin-like polypeptide (ELP) modified with silica-promoting sequences and drug conjugates, which are subsequently encapsulated within the silica matrix. Incorporation of a lysine-rich tag derived from the silaffin R5 peptide to the N-terminus of a hydrophilic ELP that self-assembles upon conjugation of hydrophobic molecules at the C-terminus results in the formation of spherical micelles with conjugated drug embedded in the core and a corona that is decorated with the silaffin peptide. These micelles serve as the building blocks for the polycondensation of silica into uniform, hybrid polypeptide-silica nanoparticles. We demonstrate proof-of-concept examples using a model hydrophobic small molecule and doxorobucin, small molecule chemotherapeutic, and further show pH-dependent doxorubicin release from the hybrid nanoparticles.

3.2 Introduction

Material systems comprising silica components are widely used in biotechnology and medicine due to their numerous attractive features – silica affords a range of comparatively simple, yet flexible chemistries using commercially available reagents, and silica based materials exhibit robust structural and mechanical stability, and importantly are non-toxic and biocompatible [5,75,122,123]. Consequently, the use of silica-based materials have grown significantly in the past few decades for biosensing [12,124,125], drug delivery [5,58,60] and biomaterials [21,75,76,126]. Notably, templated formation of mesoporous silica nanoparticles has drawn substantial attention for effective, triggered delivery of various therapeutics [61,64,127,128] with the advantages of high and multi-drug loading capacity as well as release rate tunability; however, these materials often require harsh reaction conditions and multi-step processing to fabricate [129,130], that limit the types of molecules that can be encapsulated. These limitations can be alleviated by taking cues from nature, and provide the motivation for this paper.

Biomimetic and biologically-inspired strategies for the formation of silica stem from the observation that natural organisms are able to direct biosilica deposition within mild reaction environments rapidly and with intricate precision over micro- and nano-length scales [71,77,131]. To date, numerous proteins [71,73,78-81] have been isolated and characterized as important players in nature's exquisite silicification capabilities, *i.e.* the ability to drive the deposition of silica onto an organic template. In addition,

synthetic polymers [114-117,132], possessing similar chemical and structural features as their biological counterparts, have also contributed to our silicification toolbox. One of the most widely studied natural siliceous components is the silaffin family of polypeptides, which were first discovered by Kröger *et al.* [71] within the 813 bp *sil1* gene sequence of the sea diatom species, *Cylindrotheca fusiformis* . Upon further analysis [78,81] specific post-translational modifications were identified — phosphorylation of serine residues and long-chain polyamine modification of the various lysine residues— that play a vital role in the ability of silaffins to direct the deposition of silica. Interestingly, however, the silaffin R5 peptide without any post-translational modifications also facilitates silicification in the presence of phosphate anions. It is hypothesized that silicification occurs by transient self-assembly of individual silaffin peptides through the charge neutralization of lysines by phosphate groups, which provides the high local cationic environment necessarily for facile silicification [78,129,133]. Silaffin R5 has since been explored for biotechnological applications such as enzyme immobilization [22,98,119], cell encapsulation [134], and nanomaterial patterning [118,135]. Although silaffin R5 has previously been used in the encapsulation of drugs in particles [136], a limitation to its further application in this application space is the uncontrolled template crosslinking, which may result in networks of silica particles as well as the imprecise control of nanoparticle size leading to polydisperse nanoparticles.

In a previous study [137], our group demonstrated that the incorporation of a silaffin R5 sequence into a diblock elastin-like-polypeptide (ELP), which self-assembles into spherical micelles displaying the R5 peptides on the micellar surface, provides the necessary reaction environment to template the formation of monodisperse silica nanoparticles. We also showed that silicification is dependent on both the presence of silaffin R5 as well as the assembly of individual ELP molecules (i.e., unimers) into micelles, and envisioned potential applications such as drug release for the system, enabled by the facile design and expression of desired ELP constructs. ELPs are polypeptides with the repeat pentapeptide motif VPGXG, where X may be any amino acid except proline, and exhibit a lower critical transition temperature (LCST) in water that dependent on a variety of factors, including intrinsic parameters like polypeptide composition of guest residue X, molecular weight, concentration, as well as extrinsic parameters like the type and concentration of salts [100-102,104]. ELPs are an attractive material system because they can be encoded at the genetic level to provide complete control of the amino acid sequence and chain length and can be expressed at a high level in *Escherichia coli*. Exploitation of the thermally responsive phase behavior of ELPs also allows facile and rapid purification of both the polypeptide as well as its peptide or protein fusions following expression from E. coli lysate [103,121]. Furthermore, ELP offer an immense range of possible designs at the gene level; they can be genetically fused to peptide and proteins [138,139], intricate block architectures can be designed at

the gene level [103,111,137] and ELPs can be designed with precisely located conjugation sites for the post-expression conjugation of non-genetically encodable moieties that can drive their self-assembly [103,112,140,141]. Within the research space of drug delivery, ELPs have been used as a carrier for small molecule drugs and peptides to improve their pharmacokinetics and tissue [112,140-142].

Herein, we report the design and characterization of silica-promoting ELPs that self-assemble into micelles through the conjugation with one of two hydrophobic molecules: *N*-benzylmaleimide or the chemotherapeutic doxorubicin. We demonstrate that both designs are able to similarly template the formation of silica encapsulated nanoparticles and that it is possible to program the release of drug from the particles. Further, we hypothesize that these findings, in conjunction with the precise design potential of genetically encoded ELPs, may allow for the fabrication of a hybrid ELP / silica nanoparticle platform for targeted delivery of drugs.

3.3 Materials and methods

3.3.1 Materials

Restriction enzymes BglI, NdeI, BseRI, AcuI, BamHI and XbaI, T4 DNA Ligase and calf intestinal phosphatase (CIP) were purchased from New England Biolabs (Ipswich, MA). BL21 *E. coli* competent cells were purchased from EdgeBio (Gaithersburg, MD). Oligonucleotides were obtained from Integrated DNA

Technologies, Inc. (Coralville, IA). Terrific Broth was purchased from MO BIO Labs, Inc. (Carlsbad, CA) and SDS-PAGE gels from BioRad, Inc. (Hercules, CA). Miniprep and Gel Extraction Kits were purchased from Qiagen (Venlo, Netherlands). Tetramethylorthosilicate (TMOS) was obtained from Alfa Aesar (Ward Hill, MA). Formvar-copper 200 mesh (FF200-Cu) grids for transmission electron microscopy were purchased from Electron Microscopy Sciences (Hatfield, PA). Oregon Green Carboxylic Acid, Succinimidyl Ester, wheat germ agglutinin Alexa Fluor 594 conjugate, and Image-iT Fixation/Permeabilization Kit were purchased from Thermo Fisher Scientific (Waltham, MA). HT-29 cells, McCoy's 5a Growth Medium, Dulbecco's phosphate buffered saline (DBPS), Hank's balanced salt solution (HBSS) and fetal bovine serum (FBS) were purchased from ATCC (Manassas, VA).

3.3.2 Construction of sp-ELP and con-ELP genes

Genes encoding silica-promoting ELP (sp-ELP) and control ELP (con-ELP) sequences were constructed by recursive directional ligation by plasmid reconstruction (PRe-RDL) [120] of an ELP gene that has a C-terminal cysteine-rich trailer sequence followed by of either a silica-promoting sequence (sp-ELP) or control sequence (con-ELP) at the N-terminus. The ELP gene, which encodes a 40 pentapeptide VPGAG repeat in a pET-24a(+) vector (plasmid A), and another pET-24a(+) vector that contains a DNA sequence that encodes a $(CGG)_8$ sequence (plasmid B) were obtained from a previous study [143]. The plasmid containing the ELP sequence (plasmid A) was digested with

AcuI and BglI restriction nucleases, the plasmid containing the trailer sequence (plasmid B) was digested with BseRI and BglI), and both were segments were gel isolated and purified using a Qiagen Gel Extraction kit. Subsequently both DNA fragments were ligated together using T4 DNA ligase and transformed into BL21(DE3) cells for *E. coli* expression. To insert the silica-promoting or control nucleotide sequences (Figure 12) at the 5′-end of the ELP gene, the A+B plasmid product of PRe-RDL was digested with NdeI and BseRI, dephosphorylated using calf intestinal phosphatase (CIP), and purified using a Qiagen Purification Kit. Reconstituted and annealed oligos containing either the silica-promoting tag or a control tag were incubated with the digested vector and ligated using T4 DNA ligase, transformed into chemically competent *E. coli* and expressed as previously described [138].

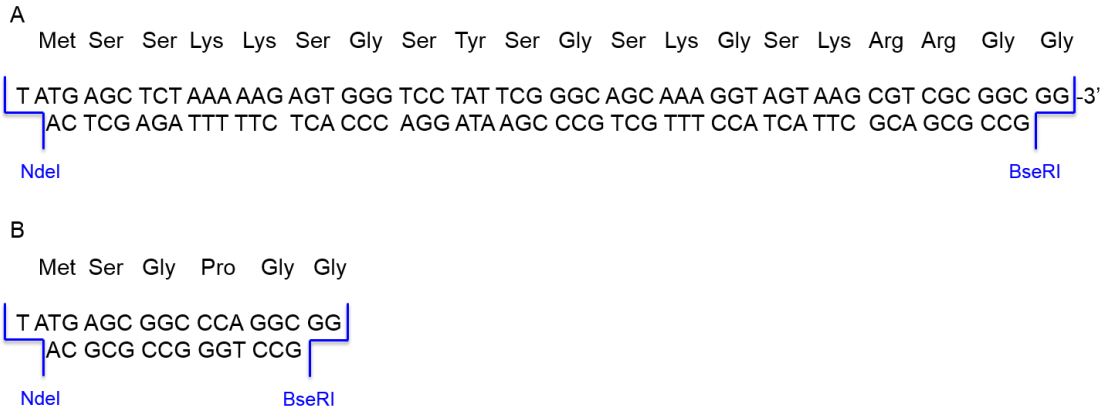

Figure 12: Oligonucleotide inserts for creation of sp-ELP (A) and control ELP constructs (B). For each A and B, top : amino acid sequence; bottom: sense (5′ -> 3′) and antisense (3′ -> 5′) oligonucleotide sequence. Restriction enzyme recognition sites and base pair overhangs indicated with blue lines.

3.3.3 Expression and purification of sp-ELP and con-ELP

Expression of sp-ELP and con-ELP was carried out in *E. coli* containing the assembled plasmids as described previously [137]. Fresh terrific broth (TB) culture media was prepared at 55 g/L, autoclaved and supplemented with 45 mg/mL kanamycin. A hyperexpression protocol was used for ELP expression that relies on the inherent leakiness of the T7 promoter [108]. A single colony of *E. coli* harboring an expression plasmid that encodes for an ELP of interest was used to inoculate a 50 mL starter culture in TB. After one day of culture at 37 ºC at 200 rpm, cells were centrifuged the following day and resuspended in 10 mL of fresh TB and transferred into 1 liter TB and cultured at 37 ˚C and 200 rpm rotation for 24 h. Cells were then centrifuged, resuspended in phosphate buffered saline (PBS; pH 7.4) and lysed by sonication. Purification of polypeptide was carried out by inverse transition cycling (ITC), as previously described [121]. Briefly, one cycle of ITC consists of addition of NaCl and increase of temperature until solution becomes turbid, indicating that the ELP has transitioned, followed by centrifugation at 25 ˚C and 15,000 x g for 10 minutes to pellet the ELP, and resuspension of the pellet in fresh PBS or water supplemented by 20 mM TCEP, pH 7. This step is followed by centrifugation at 4 ˚C and 15,000 x g for 10 minutes to remove irreversibly aggregated material, the supernatant is transferred to a new tube. Three cycles of ITC were sufficient to produce pure polypeptides, as characterized by SDS-PAGE.

3.3.4 Conjugation of N-benzylmaleimide and BMPH-activated doxorubicin

Conjugation of *N*-benzylmaleimide (BM) and *N*-β-maleimidopropionic acid hydrazide- (BMPH) activated doxorubicin (Dox) was carried out as previously described [112,113]. Briefly, 10 mg of lyophilized sp-ELP was resuspended in 900 μL of 10 mM phosphate buffer supplemented with 20 mM tris(2-carboxyethyl)phosphine hydrochloride (TCEP), pH 7. 50 mM *N*-benzylmaleimide in DMSO was added to reach 1 mL total reaction volume and allowed to react for 3 h. The product was then purified by usage of a PD10 column as well as dialyzed two times for 4 h each using dialysis cassettes. The purified samples were then lyophilized for storage and buffer exchange.

For conjugation with BMPH-activated doxorubicin, BMPH is first reacted with doxorubicin in which the hydrazide moiety of BMPH reacts with the carbonyl moiety of the doxorubicin to form a hydrazone bond and subsequent linkage of maleimide to doxorobucin. 50 mg of BMPH was dissolved in 10 mL anhydrous methanol in a glass tube and 110 mg doxorubicin was dissolved in anhydrous methanol in a round bottom flask, supplemented with 100 μL trifluoroacetic acid. The BMPH solution was subsequently added to the doxorobucin solution while stirring and allowed to react overnight in the dark and at room temperature. The methanol was then removed by rotary evaporation and replaced with 10 mL fresh anhydrous methanol. 250 mg lyophilized sp-ELP was resuspended in 2 mL water and supplemented with TCEP to a final concentration of 30 mM, pH 7, and incubated for 15 min to break disulfide bonds. 5

M NaCl was then added to phase separate the ELP, which was further separated via ultracentrifugation at 14,000 x g for 10 min, and resuspended in 5 mL 0.1 M/1 mM phosphate/EDTA buffer, pH 7. The BMPH-activated doxorubicin solution was then added dropwise to the ELP solution while stirring and reacted overnight in the dark and at room temperature. sp-ELP-Dox was purified using Amicon Ultra centrifugal filters (EMD Millipore; Billerica, MA) with a 10 kDa molecular weight cutoff.

3.3.5 Characterization of silica encapsulation of sp-ELP-BM and sp-ELP-Dox

Dynamic light scattering (DLS) was carried out on a DynaPro Plate Reader II (Wyatt Technology; Santa Barbara, CA). Measurements of hydrodynamic radii (R_h) were made in triplicate, with each measurement consisting of 10 acquisitions for 5 s each. The autocorrelation function was fitted by a regularization fit provided by the manufacturer to determine the R_h. Zeta potential was measured on a Zetasizer Nano ZS (Malvern Instruments; Malvern, UK) with 90º scattering optics. 900 μL of an ELP sample was placed into a mini-quartz cuvet, and measured three times for each condition. Three measurements were then averaged to create a single data point. Transmission electron microscopy (TEM) was performed on a Tecnai G^2 Twin (FEI Company; Hillsboro, OR) at 200 keV.

3.3.6 Cell culture method

Subculturing of HT-29 cells followed the instructions provided by the ATCC website and in T-75 flasks. Briefly, used culture medium was removed and cells were rinsed using DPBS. 3 mL of 0.25% (w/v) Trypsin/EDTA solution was added to the flask and allowed to incubate for 15 min at 37^0 C. Subsequently, 6 mL 10% FBS supplemented McCoy's 5A medium was added to the flask and the entire solution was transferred to a 50 mL conical tube, centrifuged at 120 x g for 10 min to pellet the cells, and the supernatant was removed. Finally, 5 mL fresh 10% FBS supplemented McCoy's 5A medium was added to the tube, pipetted up and down to resuspend cells, and 1 mL of cells were transferred to a new T-75 flask containing 11 mL of the aforementioned growth medium (*i.e.*, subcultivation ratio of 1:5).

3.3.7 Fluorescence microscopy of cellular uptake of free doxorubicin, ELP micelles and ELP / silica nanoparticles

HT-29 colorectal adenocarcinoma cells (ATCC; see Supplementary Materials for subculture methodology) were seeded at 1 x 10^5 cells/cm^2 on 35 mm culture dishes with a No. 0 coverslip window attachment (MatTek Corporation; Ashland, MA). Cells were incubated with control Doxorobucin, sp-ELP-Dox micelle and sp-ELP-Dox silica nanoparticle treatments, washed with Hank's balanced salt solution (HBSS) twice, fixed using the fixative solution of an Image-iT® Fixation/Permeabilization Kit, stained with wheat germ agglutinin Alexa Fluor 594 conjugate, and finally washed four times further.

Imaging was conducted using a Leica SP5 inverted confocal microscope using a 63x/1.20 water objective and the data was analyzed using Leica LAS AF software.

3.4 Results and discussion

3.4.1 Silica-promoting ELP design and characterization

Our modular design of amphiphilic, silica-promoting ELPs begins at the amino acid sequence level with three distinct polypeptide subunits: an N-terminal silaffin R5 peptide motif, a hydrophilic ELP sequence, and a C-terminal trailer containing eight cysteine residues for conjugation (Figure 13A). We utilized the thiol-rich trailer region of the polypeptides for covalent conjugation of hydrophobic molecules that have been previously demonstrated to result in sufficient hydrophobicity to drive self-assembly of the conjugation product [112,113]. For this study, we utilized two hydrophobic molecules: (1) *N*-benzylmaleimide, for proof-of-concept using a model small hydrophobic molecule, and (2) doxorubicin, a chemotherapeutic drug (Figure 13B). Upon micellization of ELP unimers post-conjugation, we hypothesized that the abundance of positively-charged residues in the corona of the micelles due to the silica-promoting R5 sequence would lead to the preferential polycondensation of silica in the presence of silica-forming monomers (e.g., hydrolyzed tetramethyl orthosilicate, TMOS) to form uniform nanoparticles encapsulating the polypeptide template and drug (Figure 13C).

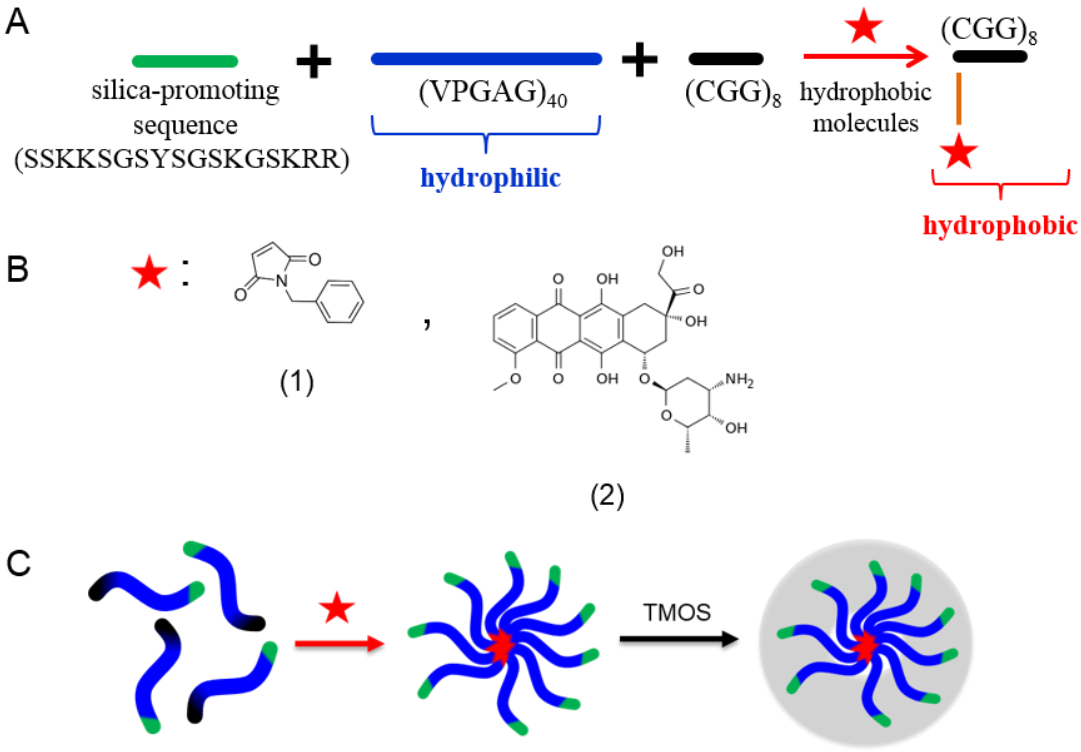

Figure 13: Schematic representation of ELP sequence, conjugation and self-assembly of hybrid silica-ELP nanoparticles. (A) Representation of silica-promoting ELP sequence (sp-ELP) with an N-terminal silaffin R5 peptide leader (green) appended to a hydrophilic ELP block (blue) and a cysteine-rich C-terminal trailer for conjugation (black). The Control ELP (con-ELP) contains the ELP and cysteine-rich trailer and lacks the the silica-promoting R5 leader. (B) Conjugation of hydrophobic molecules (red stars) leads to the self-assembly of ELP micelles. Hydrophobes: N-Benzylmaleimide (1) and Doxorubicin (2). (C) Upon hydrophobe conjugation, ELP unimers self-assemble into spherical micelles and serve as templates for the polycondensation of silica from hydrolyzed TMOS.

First, we recombinantly expressed, purified, and characterized the silica-promoting ELP (sp-ELP) construct, as well as a control ELP (con-ELP) construct that is identical to sp-ELP, but which lacks the silica-condensation-promoting motif. We performed SDS-PAGE on purified samples of sp-ELP and con-ELP and determined that

the observed bands matched the theoretical molecular weights of 18.7 kDa and 16.8 kDa for sp-ELP and con-ELP, respectively. Further, the purification by inverse transition cycling (ITC) of both constructs resulted in highly pure samples for subsequent analysis.

3.4.2 Silicification using sp-ELP-BM micelle construct

To study the silicification ability of sp-ELP, we first covalently conjugated the polypeptide to *N*-benzylmaleimide (sp-ELP-BM) and characterized the resulting materials using light scattering and TEM. DLS measurements of sp-ELP-BM at 100 μM in water show a mean R_h of 19.2 ± 0.3 nm, indicative of the formation of self-assembled micelles. Next, we carried out time-course silicification experiments with hydrolyzed TMOS at 10 mM (triangles) and 100 mM of TMOS (circles) over the course of 4 h (Figure 14A). For both precursor concentrations, the observed size of the sp-ELP-BM particles increased, and in particular for the 100 mM TMOS samples, the R_h increased from ~19 nm to ~24 nm over the length of study, while the R_h of micelles with no TMOS (squares) showed no significant change in size. In contrast, the control ELP (con-ELP-BM; Figure 15; left side) exhibited no significant difference in measured particle size over the same period of time. Subsequently, we imaged both the R5-modified and control samples after reaction with 100 mM TMOS for 4 h using TEM. TEM confirmed that the sp-ELP-BM construct (Figure 14B) forms near-monodisperse silica nanoparticles with a mean diameter of 42.1 ± 5.5 nm as calculated by image processing of the TEM images, which is in agreement with DLS. In contrast, no silica particles were visible over the TEM grid

(image not shown) for the negative control, con-ELP-BM. Interestingly, the electron density contrast visible in the TEM images of the spherical sp-ELP-BM silica particles clearly suggest a core-shell structure comprising a shell of silica with high electron density that encapsulates lower electron density core, that presumably contains the ELP and encapsulated small molecule. This observation is in contrast to our previous study [137] in which we utilized a self-assembled diblock ELP system and observed silica growth along the entire radial axis of the nanoparticles. This suggests that the core of sp-ELP-BM micelles may be more hydrophobic and tightly packed than those studied previously, that precludes the penetration of silica condensation into the ELP core, thereby leading to a core-shell morphology.

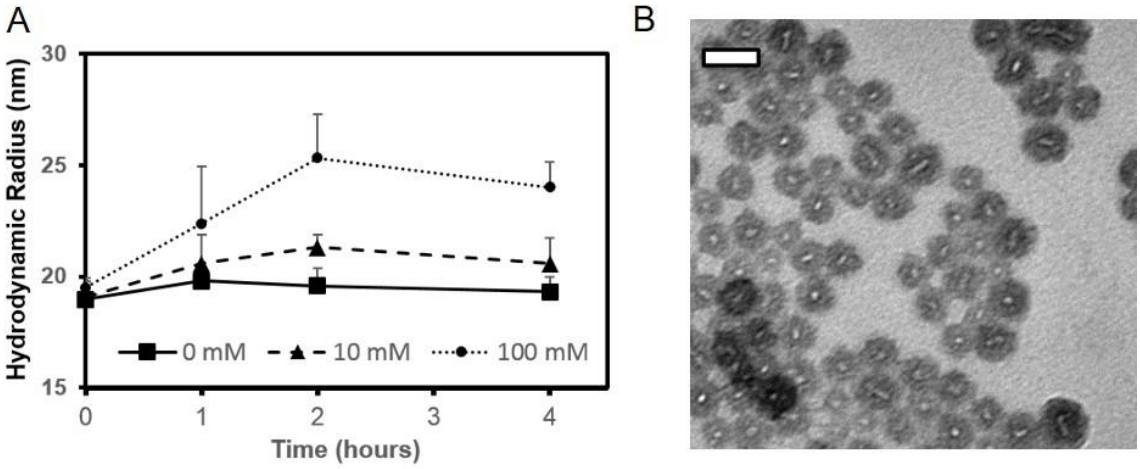

Figure 14: Characterization of the silicification of sp-ELP *N*-benzylmaleimide (sp-ELP-BM). (A) Time course measurements of hydrodynamic radii of sp-ELP-BM with different concentrations of TMOS (0, 10, 100 mM). (B) Representative transmission electron microscopy image of silica nanoparticles templated from sp-ELP-BM with 100 mM hydrolyzed TMOS for 4 hours; scale bar: 50 nm.

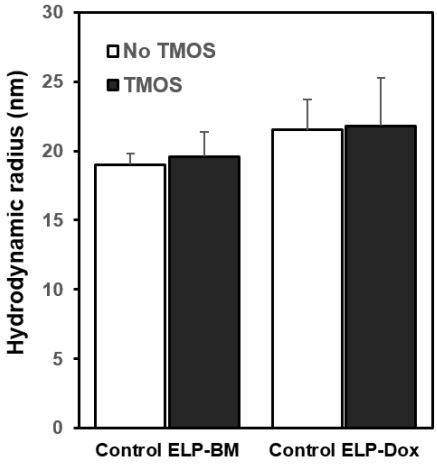

Figure 15: Hydrodynamic radii of control silicification experiments. Control ELP-BM and Control ELP-Dox without TMOS (white) and post silicification (black) with 100 mM TMOS for 4 hours.

We next measured the zeta potential of the sp-ELP-BM micelles prior to and post silicification (as well as con-ELP-BM micelles) (Figure 16). While sp-ELP-BM micelles (dotted bar) exhibited a zeta potential of 8.7 ± 1.2 mV –likely resulting from the positively-charged lysine and arginine residues at the surface of the micelle– post-silicification particles (filled bar) exhibited a zeta potential of -31.2 ± 4.6 mV, suggesting the coverage of polypeptide residues with silica and the presence of negatively charged surface silanol groups, which is in agreement with previous studies with templated nanoparticles by silica deposition [116,137].

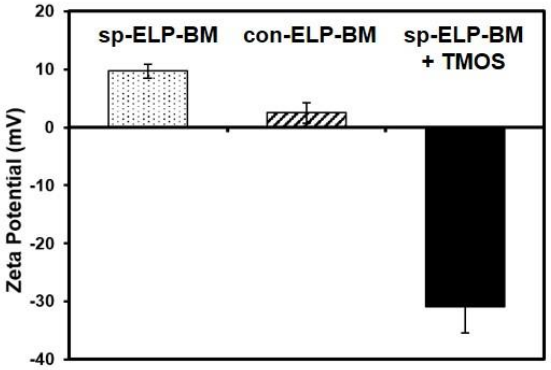

Figure 16: Zeta potential measurements of sp-ELP-BM micelles (dots), ELP-BM micelles (diagonal stripes) and sp-ELP-BM silicified nanoparticles (solid).

3.4.3 Silicification using sp-ELP-Dox micelle construct

Satisfied with the proof-of-concept demonstration using N-benzylmaleimide, we segued to doxorubicin, a small molecule cancer drug that is hence of greater utility.

Because the drug must be released from the nanoparticle to be therapeutically effective, we relied upon a strategy that we have previously implemented to release doxorubicin from ELP nanoparticles [112,144]. In this approach, the drug is linked to the ELP through an acid-labile hydrazone bond, which is cleaved at pH < 6 in solution and hence releases drug within the acidic environment of late endosomes and lysosomes of cells [145-147]. To insert the internal hydrazone bond between the drug and ELP, a heterobifunctional linker, N-β-maleimidopropionic acid hydrazide (BMPH) was first conjugated to the 13'-keto position of doxorubicin, and the product of this reaction was then conjugated to the ELP via reaction of the maleimide group in the product with the cysteine residues in the ELP; conjugation of multiple copies of the drug triggers self-assembly of the ELP into spherical micelles that are termed sp-ELP-Dox. We performed a time-course silicification study for sp-ELP-Dox (Figure 17A) in which we incubated solutions of the conjugate micelles at 100 μM in water in the presence of 10 mM (triangles) and 100 mM (circles) hydrolyzed TMOS over the span of 4 hs. DLS measurements showed that the R_h of the 10 mM experimental group increased from 21.2 ± 1.1 nm to 23.2 ± 1.1 nm and that of the 100 mM TMOS group increased from 21.5 ± 0.8 nm to 25.3 ± 1.9 nm after 4 h while the size of the control, sp-ELP-Dox incubated with no silica precursor, did not change significantly with time. We next imaged sp-ELP-Dox silica nanoparticles obtained after 4 h incubation with 100 mM TMOS by TEM (Figure 17B) and again observed spherical, core-shell nanoparticles measuring 47.8 ± 7.5 nm in

diameter. Both of these findings are in agreement with the previous sp-ELP-BM construct data and further demonstrate the silicification of the sp-ELP-Dox conjugate. Lastly, con-ELP-Dox micelles did not exhibit silicification (Figure 15; right side), providing further evidence that the formation of silica nanoparticles is dependent on the presence of the silica-promoting R5 peptide motif.

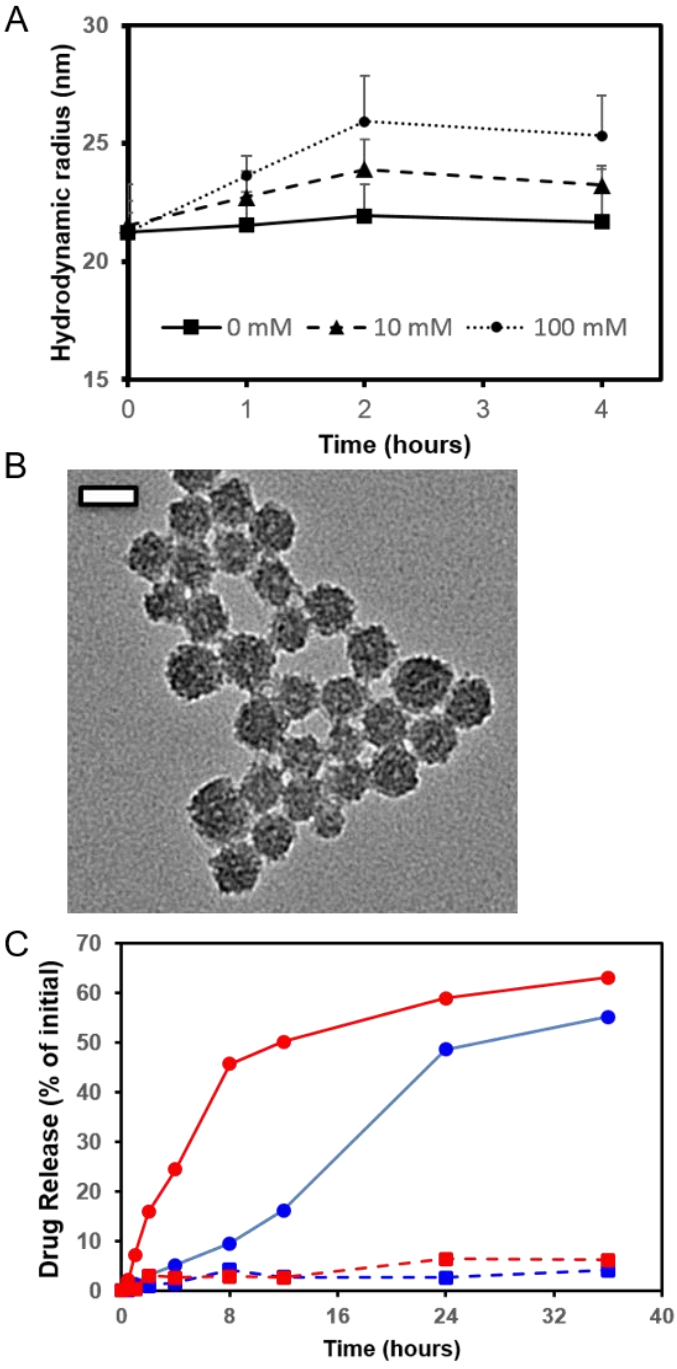

Figure 17: Characterization of silicification and release of sp-ELP doxorubicin (sp-ELP-Dox). (A) Time course measurements of R_h of sp-ELP-Dox with different concentrations of TMOS (0, 10, 100 mM). (B) Representative TEM image of silica nanoparticles templated from sp-ELP-Dox with 100 mM hydrolyzed TMOS for 4 h;

scale bar: 50 nm. (C) Doxorubicin release as a function of time as measured by absorbance spectrophotometry for sp-ELP-Dox micelles without silica (red) and sp-ELP-Dox silica nanoparticles (blue) at pH 7.4 (squares) and pH 5.0 (circles).

3.4.4 pH-triggered release from silicified sp-ELP-Dox micelles

We next studied the pH-triggered release of doxorubicin from sp-ELP-Dox silica nanoparticles by measurement of the characteristic spectrophotometric absorbance of doxorubicin at 480 nm and characterizing the amount of drug released as a fraction of initial drug loading (Figure 17C) by incubation at either pH 7.4 or 5.0 for a set amount of time, adjustment of pH to 7.4 to stop further release, separation using a microcentrifuge ultrafiltration unit, and measurement of absorbance of doxorubicin (at 480 nm) in the filtrate. Percent release from sp-ELP-Dox silica (blue), calculated as a fraction of the initial fluorescence level, for samples at pH 7.4 (square markers) indicated that only ~4% of doxorubicin is released after 36 h, while samples at pH 5.0 (circle markers) showed significantly greater, 55% drug released after 36 h incubation. The release data suggest that silica encapsulation of doxorubicin loaded ELP micelles does not prevent the pH-dependent release of drug. In comparison, we also conducted the same release experiment using only sp-ELP-Dox micelles (red) without silicification in order to characterize the release of Dox from only a micellar nanoparticle carrier. The sp-ELP-Dox micelles demonstrated greater initial release rate, liberating ~45% of Dox after 8 h and 63% after 36 h, greater than that of the silicified nanoparticles; this is in general

agreement with the previous study for the micelle release for a ELP and doxorubicin conjugate, which exhibited a similar release profile [112]. Interestingly, the silicified particles show a delay in the pH-mediated release of Dox, potentially due to the silica shell preventing the cleavage of the hydrazine bond or degradation of the polypeptide and silica particle. However, the total accumulated release after 36 hours suggests that both types of particles maintain their pH responsiveness.

3.4.5 Cellular uptake of doxorubicin-encapsulated ELP-silica nanoparticles

To further explore the potential of sp-ELP-Dox silica nanoparticles as a tool in the delivery of therapeutics, we investigated their uptake in cancer cells by confocal fluorescence microscopy (Figure 18). We incubated HT-29 colorectal adenocarcinoma cells with free doxorubicin (Figure 18A-C), sp-ELP-Dox micelles (Figure 18D-F), and sp-ELP-Dox silica nanoparticles (Figure 18G-I) for 10 min, 2 h and 24 h. The cells primarily appear in the form of cellular aggregates, each containing a number of individual cells that may be observed using the cell stain as a guide. Free doxorubicin is observed in cell nuclei as early as 10 minutes, while a minute fluorescent is observed with the sp-ELP-Dox micelle sample, suggesting an initial release of Dox, and no fluorescence is detected in the silica encapsulated sp-ELP-Dox sample, which is in agreement with a previous study [112]. At 2 h, the fluorescence signal from sp-ELP-Dox micelle samples is greater than that of the sp-ELP-Dox silica nanoparticles, and lastly at 24 h incubation, the

doxorubicin fluorescence within cells incubated with sp-ELP-Dox silica nanoparticles intensifies moderately, indicating further release and accumulation (Figure 18I). The cell uptake data is in general agreement with the *in vitro* release characterization, which suggests that doxorubicin remains conjugated to ELP and encapsulated in silica until the low pH environment of cellular endosomes after uptake triggers the cleavage and subsequent release of drug [148].

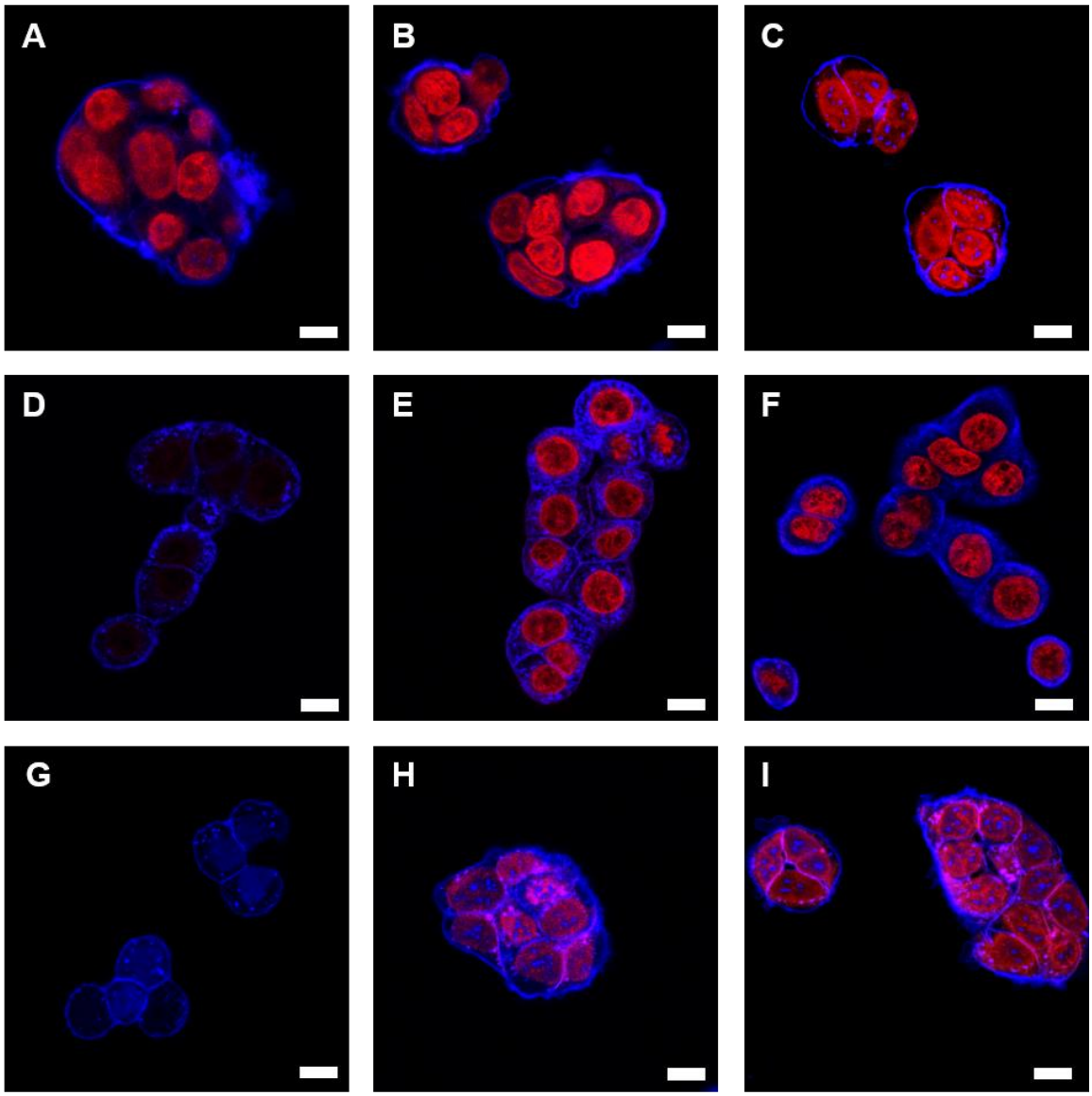

Figure 18: Cellular uptake of Doxorubicin-encapsulated ELP-silica nanoparticles by HT-29 cells. Confocal fluorescence microscopy of free doxorubicin (A-C), sp-ELP-Dox micelles without silica (D-F), and sp-ELP-Dox silica particles (G-I) at 10 min (A, D, G), 2 hours (B, E, H) and 24 hours (C, F, I). Colors: Doxorubicin (red) and cell stain (blue); scale bar: 10 μm)

3.5 Conclusion

We report the design, fabrication and application of ELP templated silica nanoparticles towards the programmable release of the chemotherapeutic, doxorubicin. By incorporating a silica-promoting motif derived from the synthetic silaffin R5 peptide into a modular ELP construct, we demonstrate that the self-assembly of hydrophobe-conjugated sp-ELP micelles can drive the polycondensation of silica-precursors to form uniform, hybrid core-shell nanoparticles. Further, we show that the addition of a stabilizing layer of silica does not prevent the pH-dependent release of encapsulated drug and that this material system may be utilized in future *in vivo* drug delivery studies. In addition, the precise control of polypeptide sequence and the broad availability of additional conjugation partners may enable the incorporation of moieties for targeted delivery applications. Furthermore, the discovery and integration of additional biomineralization tags into the design of self-assembled polypeptide micelles may result in more complex hybrid biomaterials with valuable biomedical applications such as imaging and theragnostics.

3.6 Chapter acknowledgements

This work is supported by NSF's Research Triangle MRSEC (DMR-1121107). W.H. acknowledges support from the NIH Biotechnology Predoctoral Training Fellowship (NIH Grant No. 5T32GM008555-18). The authors would like to especially

thank Parisa Yousefpour of the Chilkoti Lab for providing advice and technical assistance in the conjugation of Dox and thank the staff of the Duke University Light Microscopy Core Facility (LMCF) for training and support with confocal fluorescence microscopy.

4. Optimization of Elastin-like Polypeptide / Silica Nanoparticles formed by Bioinspired Silicification for Biospecific Targeting

The text and figures included in Chapter 4 represents yet unpublished work and encompasses the aims set out in Specific Aim 3. Co-author Lei Tang provided expertise in quartz crystal microbalance theory and operation.

4.1 Chapter synopsis

Regio-specific control of the composition and properties of nanomaterials is highly important in developing new material systems towards biotechnological applications such as drug delivery and biosensing. While biologically-inspired mineralization strategies have opened up numerous avenues to incorporate mechanically robust and chemically stable elements and imbue these assemblies with desired characteristics, their fabrication and control can still be improved. We report a relatively simple approach that uses self-assembled elastin-like-polypeptide (ELP) spherical micelles to template silica nanoparticles that retain and display a genetically-encoded peptide motif beyond the periphery of the as-formed silica shell. We incorporate a silica-promoting, modified silaffin motif at specific sites along the polypeptide chain of ELPs that comprise template micelles and show that constructs containing these programmed modifications yield different and well-defined nanoparticle properties as characterized through dynamic and static light scattering, transmission electron microscopy, fluorescence spectrophotometry, and quartz crystal

microbalance measurements. Together, these data demonstrate the potential to create hybrid polypeptide / silica nanomaterials that enhance the control of silica deposition and enable the retention of biospecific targeting attributes of the underlying components of the micellar template.

4.2 Introduction

Methodologies for silica biomineralization, specifically biomimetic and biologically-inspired strategies to generate silica, have garnered a significant attention in the past few decades [6,75,131], owing largely to the successful and increasing technological application of silica-based materials [5,122,149,150] and a growing understanding of how nature generates biosilica in rapid and intricate manner under physiological conditions [71,73,75,79-81,135]. From this greater insight, an assortment of synthetic and biological materials have been co-opted to drive silica formation and create silica with ordered, hierarchical structure [151-154] and towards biotechnological applications such as enzyme [21,22,98,119] and cell encapsulation [134,155] as well as drug delivery [136,156], Silica materials have attracted such attention because they have been found to possess a robust and versatile structural scaffold and support properties as well as suitable biocompatibility for biological applications.

One family of polypeptides that has been especially well-studied with regards to biomineralization and applications has been the silaffins, which are derived from the

marine diatom, *Cylindrotheca fusiformis* [71,78,93]. These peptides (dubbed R1 – R7) are post-translationally modified *in vivo* and have been implicated as a key player in the formation of the silica cell walls that diatoms use as frameworks and for protection. Further analysis demonstrated that these modifications were vital in the self-assembly and templating of silica deposition from precursors [78,95]. In addition, the R5 peptide was also found to have siliceous activity without modifications due to its inherent ability to form template centers in the presence of phosphate ions in solution [95,157]. Since their discovery, biomimetic silaffin peptides have be used in a variety of biological applications[97,98,118,136]; however, their use as a means for forming biofunctional hybrid nanoparticles has been limited by reduced regio-specific control of biomineralization (i.e., silicification) at high resolution. Our group has previously shown that genetically encoded elastin-like polypeptides (ELPs) that self-assemble into micelles and that contain copies of the silaffin R5 sequence displayed at the corona can drive the deposition of silica to form near monodisperse hybrid particles that encapsulate an underlying micellar core [137]. In addition, we have demonstrated the conjugation, encapsulation, and subsequent release of small hydrophobic drugs from a polypeptide / silica nanoparticle system. However, one of the most attractive features of ELPs is that they can be programmed to express peptide motifs for biospecific recognition applications, which may be lost upon silica encapsulation; we sought a desirable union

of both materials properties –silica nanoencapsulation while maintaining capacity for biospecific recognition– in a single synthetic step.

ELPs, comprised of the pentapeptide repeat GXGVP (where X is any amino acid except proline), are derived from the natural tropoelastin and notably demonstrate characteristic lower critical solution temperature (LCST) phase behavior in aqueous solution dependent on their composition and concentration, among other factors.[100-104,138] Importantly, due to their LCST behavior and the fact that they can be genetically designed, expressed and purified at high efficiencies [121,138], ELPs have been widely studied as drug carriers for applications in cancer and diabetes therapy [139-142,158]. In addition, the exquisite control over the peptide sequence has enabled various ELP-based approaches to the self-assembly of protein micelles that present multiple copies of a peptide motif at the corona, potentiating enhanced cellular recognition and uptake [56,105,108,109,111].

Herein, we detail the design of ELP constructs that contain silica-promoting modified silaffin sequences at various locations along the polypeptide chain to explore the potential for exposure of ELP termini beyond a silicified nanoparticle as a proof-of-concept for applications of hybrid ELP / silica nanomaterials in targeting and biosensing.

4.3 Materials and methods

4.3.1 Materials

Restriction enzymes BglI, NdeI, BseRI, AcuI, BamHI and XbaI, T4 DNA Ligase and calf intestinal phosphatase (CIP) were purchased from New England Biolabs (Ipswich, MA). EB5α and BL21 (DE3) *E. coli* competent cells were purchased from EdgeBio (Gaithersburg, MD). Oligonucleotides were obtained from Integrated DNA Technologies, Inc. (Coralville, IA). Terrific broth (TB) was purchased from MO BIO Labs, Inc. (Carlsbad, CA) and SDS-PAGE gels from BioRad, Inc. (Hercules, CA). Miniprep and Gel Extraction Kits were purchased from Qiagen (Venlo, Netherlands). N-(4-Ethylphenyl)-maleimide and Streptavidin-Cy3 were purchased from Sigma Aldrich (St. Louis, MO). EZ-Link™ Sulfo-NHS-Biotin, Slide-A-Lyzer™ Dialysis Cassettes, EMD Millipore Amicon Ultra-0.5, 100 kDa Centrifugal Filter Units and Streptavidin were purchased from Thermo Fisher Scientific (Waltham, MA). PD10 disposable desalting columns were purchased from GE Healthcare Life Sciences (Pittsburgh, PA). Tetramethylorthosilicate (TMOS) was obtained from Alfa Aesar (Ward Hill, MA). Formvar-copper 200 mesh (FF200-Cu) grids for transmission electron microscopy were purchased from Electron Microscopy Sciences (Hatfield, PA). Gold (5 MHz) QCM sensors were purchased from Biolin Scientific (Stockholm, Sweden); Biotin PEG Thiol and PEG Thiol were purchased from Polypure AS (Oslo, Norway).

4.3.2 PRe-RDL construction of sp-ELP and c-ELP gene sequences in plasmid DNA

The silica-promoting ELP (sp-ELP) and control ELP (c-ELP) genes were assembled by a multi-step concatenation process. Specifically, each construct began with plasmids containing four fundamental sequences: 1) a 40 pentapeptide VPGAG block, 2) an 80 pentapeptide VPGAG block, 3) a modified silaffin sequence, and 4) a cysteine-rich trailer sequence (Figure 19). Through two sequential steps and using recursive directional ligation by plasmid reconstruction (PRe-RDL) [120], the pieces were concatenated. Both ELP genes and the conjugation trailer, $(CGG)_8$, were obtained from previous studies and were harbored in pET-24a(+) vectors with the appropriate restriction recognition sites necessary for PRe-RDL. For PRe-RDL, the plasmid containing the N-terminal sequence (plasmid A) was digested with AcuI and BglI restriction nucleases, the plasmid containing the C-terminal sequence (plasmid B) was digested with BseRI and BglI), and both were segments were gel isolated and purified using a Qiagen Gel Extraction kit. Subsequently both DNA fragments were ligated together using T4 DNA ligase and transformed into EB5α *E. coli* competent cells for subsequent cloning and expression. For the control ELP (c-ELP), the modified silaffin sequence was not incorporated. Upon completion and confirmation of the gene sequences, each construct plasmid was then transformed into BL21 (DE3) *E. coli* competent cells for expression and purification.

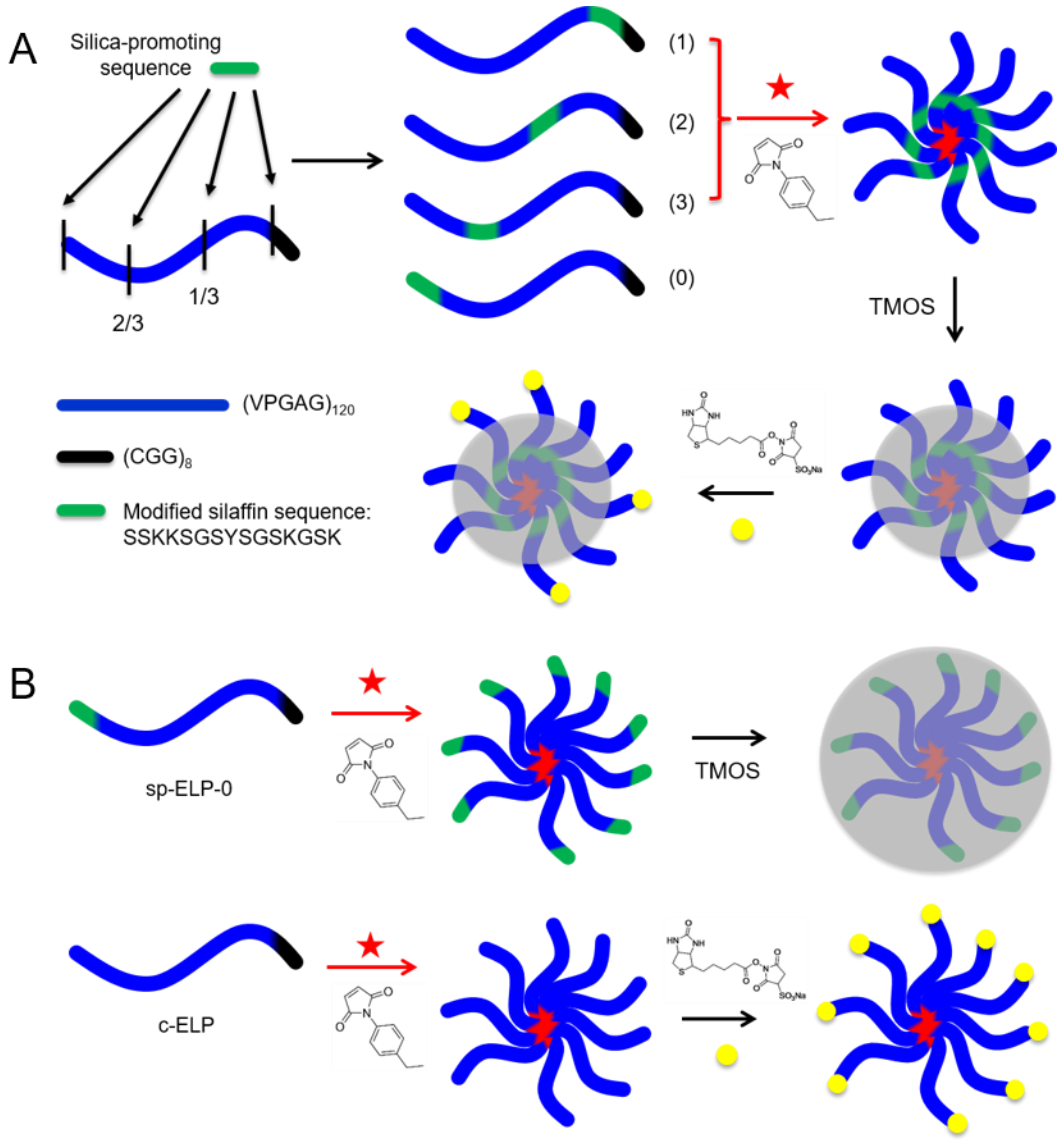

Figure 19: Schematic representation of study of selective silica formation on silica-promoting protein micelle constructs. (A) Three experimental constructs –sp-ELP-1, -2, -3– are synthesized with a modified silaffin sequence either (1) adjacent to the cysteine-rich conjugation motif, (2) 1/3 or (3) 2/3 of the way into the segment lengths within the ELP constructs. *N*-(4-Ethylphenyl)-maleimide (red stars) is used to drive assembly of ELP unimers into micelles. Post-silicification, ELP surface exposure is assayed by biotinylation of the N-terminal amine of the peptides. (B) Schematic representations of control ELPs. sp-ELP-0 contains the silica-promoting motif at the N-terminus of the peptide sequence. c-ELP lacks a silica-promoting motif and is used as a positive control for N-terminal biotinylation of the ELP-based micelles.

4.3.3 Expression and purification of ELP constructs in E. coli bacteria

Expression of sp-ELP and c-ELP was carried out in *E. coli* containing the assembled plasmids as described previously.[137] Fresh Terrific Broth (TB) culture media was prepared at 55 g/L, autoclaved and supplemented with 45 mg/mL kanamycin. A hyperexpression protocol was used for ELP expression that relies on the inherent leakiness of the T7 promoter [108]. A single colony of *E. coli* harboring an expression plasmid that encodes for an ELP of interest was used to inoculate a 50 mL starter culture in TB. After one day of culture at 37 ºC at 200 rpm, cells were centrifuged the following day and resuspended in 10 mL of fresh TB and transferred into 1 liter TB and cultured at 37 ˚C and 200 rpm rotation for 24 h. Cells were then centrifuged, resuspended in phosphate buffered saline (PBS; pH 7.4) and lysed by sonication. Purification of polypeptide was carried out by inverse transition cycling (ITC), as previously described [121]. Briefly, one cycle of ITC consists of addition of NaCl and increase of temperature to 40 ˚C until solution becomes turbid, indicating that the ELP has transitioned, followed by centrifugation at 40 ˚C and 15,000 x g for 10 minutes to pellet the ELP, and resuspension of the pellet in fresh PBS or water supplemented by 20 mM TCEP, pH 7 to prevent formation of disulfide bonds. This step is followed by centrifugation at 4 ˚C and 15,000 x g for 10 minutes to remove irreversibly aggregated material, the supernatant is transferred to a new tube. Three cycles of ITC were sufficient to produce pure polypeptides, as characterized by SDS-PAGE.

4.3.4 Conjugation of N-(4-ethylphenyl)-maleimide to sp-ELP-n and c-ELP constructs

Conjugation of *N*-(4-ethylphenyl)-maleimide was carried out as previously described [112,113]. Briefly, 10 mg of lyophilized silica-promoting ELP construct (sp-ELP-n) or control ELP lacking a silica-promoting tag (c-ELP) was resuspended in 850 μL of 10 mM phosphate buffer supplemented with 20 mM tris(2-carboxyethyl)phosphine hydrochloride (TCEP), pH 7. 50 mM N-(4-ethylphenyl)-maleimide in DMSO was added to reach 1 mL total reaction volume (additional DMSO was added to solubilize the hydrophobe upon mixing with ELP) and allowed to react for 3 hours. The product was then purified by usage of a PD10 column (as well as dialyzed two times for 4 hours each using Slide-A-Lyzer™ dialysis cassettes. The purified samples were then lyophilized for storage and buffer exchange.

4.3.5 Characterization of silica encapsulation of sp-ELP-n and c-ELP assemblies

Dynamic light scattering (DLS) was carried out on a DynaPro Plate Reader II (Wyatt Technology; Santa Barbara, CA). Measurements of hydrodynamic radii were made in triplicate, with each measurement consisting of 10 acquisitions for 5 s each. The autocorrelation function was fitted by a regularization fit provided by the manufacturer to determine the hydrodynamic radius (R_h). Transmission electron microscopy (TEM) was performed on a Tecnai G^2 Twin (FEI Company; Hillsboro, OR) at 200 keV. Static light scattering measurements were performed on an ALV/CGS-3 system at 1 mg/mL

ELP concentration per sample; each sample was processed by passage through a .44 μm PTFE filter prior to analysis. Experimental runs were performed at scattering angles of 20º to 150º in 5º increments with three runs per sample performed and limited to a 5% variance between runs.

4.3.6 Biotinylation of ELP constructs at the N-terminus

Biotinylation of ELP constructs was carried out using the EZ-Link sulfo-NHS-biotin system. ELP micelles or hybrid ELP and silica nanoparticles were prepared in solution and reacted with 10-fold excess of sulfo-NHS-biotin in ultrapure water. For c-ELP, to reduce the amount of biotinylation of amines on lysine residues, the pH was adjusted to 7.0 and the ratio of biotin to ELP was lowered to 1:1. The reaction was allowed to proceed for 1 hour at room temperature (4 hours for c-ELP micelles) and subsequently dialyzed twice to remove unconjugated biotin and change buffer if necessary. Samples were used immediately in subsequent studies.

4.3.7 Fluorescence study of biotinylated sp-ELP-n and c-ELP

50 μM final concentration biotinylated ELP micelles or ELP / silica nanoparticles in 450 μL solution were allowed to react with fluorescently (Cy3) labeled streptavidin in 50 μL while gently shaking for 1 hour. Subsequently, unbound streptavidin-Cy3 was removed by ultracentrifugation with Amicon ultrafiltration tubes with a 50 kDa molecular weight cutoff – since the cutoff is close to the size of the streptavidin molecule, 5 rounds of purification were necessary to ensure sufficient removal as

previously described [159]. The samples were then equilibrated back to the initial volume, and 50 μL of sample was aliquoted into a 384 well plate for analysis. Sample plates were then excited at 500 nm for 1.0 s to quantify fluorescence.

4.3.8 QCM sensor preparation and cleaning

5 MHz gold-coated quartz sensors were first plasma cleaned for 2 minutes and subsequently cleaned with piranha solution (100 μL/sample) to ensure a suitable initial surface or to remove adsorbates from a previous run. The sensors were then rinsed with ethanol five times. To create a mixed monolayer of PEG-thiol and biotin-PEG-thiol on the surface of the QCM sensor, the sensor was incubated in 100 μL of 50 mM PEG-thiol and 0.5 mM biotin-PEG-thiol (1% biotinylated PEG ratio) in a 1:1 water-ethanol solution for 16 hours, and subsequently rinsed with ethanol five times, sonicated for 3 minutes, rinsed with ethanol five times, and dried for storage or immediate use.

4.3.9 QCM study of biotinylated sp-ELP-n and c-ELP

50 μM biotinylated ELP micelles or ELP / silica nanoparticles were used throughout this study. QCM sensors coated by exposure to 1% biotin-PEG-thiol (see above) were used in conjunction with a Biolin Scientific Q-Sense 4-channel Analyzer system. The data for the 5^{th} and 7^{th} overtone data points were collected for each sample at a constant flow rate of 100 μL/min throughout the course of each set of measurements. Each channel was first equilibrated with PBS until the signal was constant for 15 minutes; afterward, 25 μg/mL streptavidin was flowed over the biotinylated sensors for

8 minutes to create an adlayer of bound protein, which was then washed with PBS for another 10 minutes. A buffer exchange to pure water was performed for 10 minutes or until the signal reestablished as constant. Samples containing experimental nanoparticles in water were then flowed for 8 minutes and lastly washed with water for 10 minutes.

4.4 Results and discussion

4.4.1 Silica-promoting ELP construct design and fabrication

In order to ascertain whether it is possible to selectively promote the formation of silica shells around self-assembled micellar templates and maintain free polypeptide chain at the coronal termini, we designed a family of ELPs that contain silaffin tags at specific locations along the micelle forming ELPs (i.e, unimers). While the characteristically random coil chains do not align along the radial axis, we hypothesized that the selective placement of the tags along a relatively long ELP sequence, combined with stochastic average radial distance of each tag from the assembled polypeptide micellar core, would result in significant difference in the resulting silica shells. The basis of each ELP construct in this study is a 120 pentapeptide repeat of the sequence VPGAG, appended to a trailer sequence containing eight cysteine residues, which are employed as conjugation sites to drive self-assembly (Figure 19A). To this foundation we inserted, at the genetic level, a silica-promoting, modified silaffin sequence (N-

SSKKSGSYSGSKGSK -C) at four locations along the base ELP construct: at the interface between the ELP and cysteine-rich trailer (sp-ELP-1), forty and eighty pentapeptides upstream from the trailer (sp-ELP-2 and -3, respectively), and finally at the N-terminus of the construct as a control (sp-ELP-0). To drive the self-assembly of ELP unimers into micelles, we conjugated a small hydrophobic, thiol-reactive maleimide, *N*-(4-ethylphenyl)-maleimide (Figure 19A red star; EPM) to the cysteine rich sequence at the C-terminus of the modified ELPs; we chose a slightly more hydrophobic [113] molecule than in our previous study [137] to ensure that all constructs would form micelles for subsequent experiments. Specifically, we hypothesized that the formation of micelles containing silica-promoting motifs would result in the polycondensation of silica preferentially when incubated with precursors, and importantly, that the design differences between unimer constructs would lead to differential exposure of ELP chains at the periphery of the silica nanoparticle. We probed for such contrasts by using the highly specific and robust streptavidin-biotin interaction and biotinylation (yellow circle in Figure 19) of free N-terminal amines on exposed ELPs post-silicification.

In addition, we constructed two control ELPs – an aforementioned negative control ELP (sp-ELP-0) that presents the modified silaffins at the corona of the micelle - as well as a positive control ELP (c-ELP) that contains no silica-promoting motif (Figure 19B). In a previous study, we demonstrated that the presence of the silaffin sequence is essential to the silicification of micellar templates [137], and thus reasoned that micellar

assembly and biotinylation of the c-ELP construct would result in nanoparticles presenting the highest degree of biotin for study. All constructs, including their full sequence and theoretical molecular weight, are detailed in Table 2.

Table 2: sp-ELP construct sequences and theoretical molecular weights

Construct	Sequence	Theoretical Molecular Weight ($g \cdot mol^{-1}$)
sp-ELP-1	N- (M)SGP $(GAGVP)_{120}$ GGSSKKSGSYSGSKGSKGG $(CGG)_8$ -C	49.2×10^3
sp-ELP-2	N- (M)SGP $(GAGVP)_{80}$ GGSSKKSGSYSGSKGSKGG $(GAGVP)_{40}$ $(CGG)_8$ -C	49.2×10^3
sp-ELP-3	N- (M)SGP $(GAGVP)_{40}$ GGSSKKSGSYSGSKGSKGG $(GAGVP)_{80}$ $(CGG)_8$ -C	49.2×10^3
sp-ELP-0	N- (M)SSKKSGSYSGSKGSKGG $(GAGVP)_{120}$ $(CGG)_8$ -C	48.9×10^3
c-ELP	N- (M)SGP $(GAGVP)_{120}$ $(CGG)_8$ -C	47.5×10^3

4.4.2 Sp-ELP-n* and c-ELP characterization by DLS and TEM

We next characterized the silicification and resulting hybrid silica / ELP nanoparticles from the different constructs using dynamic light scattering and electron microscopy. We first determined the hydrodynamic radii of EPM-conjugated ELPs (indicated by * following the construct; *e.g. sp-ELP-1**) pre- and post-silicification for 4 hours with TMOS (Figure 20A). Although there were no statistically significant differences between the R_h of the ELP micelles and the silicified nanoparticles between constructs, it is interesting to note that the change in R_h for sp-ELP-1* from 35.5 nm to 47.8 nm was less than that of sp-ELP-2*, -3* and control sp-ELP-0* - 32.7 nm to 53.1 nm, 29.3 nm to 45.5 nm, and 29.7 nm to 53.0 nm, respectively. In addition, the TEM images of the resulting hybrid nanoparticles (Figure 20B) show more clearly defined core-shell

morphologies for sp-ELP-2* and -3*, in agreement with control sp-ELP-0*, as compared to sp-ELP-1*. These data together may suggest that a construct with the silica-promoting tag near the micellar core will result in silica formation within the interior of the micelle and may not envelop the entirety the micellar template.

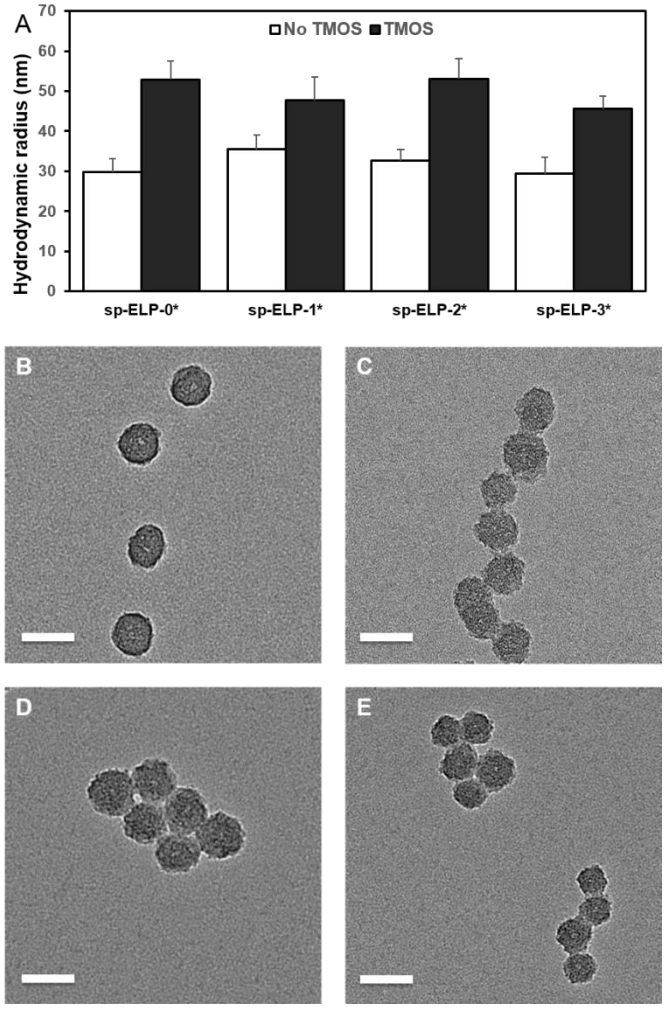

Figure 20: Characterization of silicification of sp-ELP micelle constructs using dynamic light scattering and transmission electron microscopy. (A) Measurements of hydrodynamic radii of sp-ELP micelle constructs (white) and with incubation with

100 mM TMOS, 4 hours (black). (C-E) Transmission electron microscopy images of resulting silica nanoparticles; scale bar: 100 nm.

4.4.3 Static light scattering characterization of sp-ELP micelles and sp-ELP / silica nanoparticles

To further characterize the impact on silicification on the micellar templates as well as highlight the differences between constructs, we performed static light scattering to determine the radius of gyration (R_g) and the measured molecular weight (M_w) of the micelles and resulting hybrid nanoparticles. For each construct and experimental condition, we measured the angle-dependent scattering intensity using 25 μM ELP equivalent micelles or hybrid nanoparticles from θ of 25º to 150º and subsequently generated Guinier plots of Kc/R_θ as a function of θ (Figure 21). From this information, and using the Raleigh equation,

$$\frac{Kc}{R_\theta} = \left(\frac{1}{M_w} + 2A_2C\right)\frac{1}{P_\theta}$$

we determined the M_w and R_g for each condition using the scattering intensity at θ = 0º and the slope of the Guinier plot, respectively, and compiled the results in Table 3.

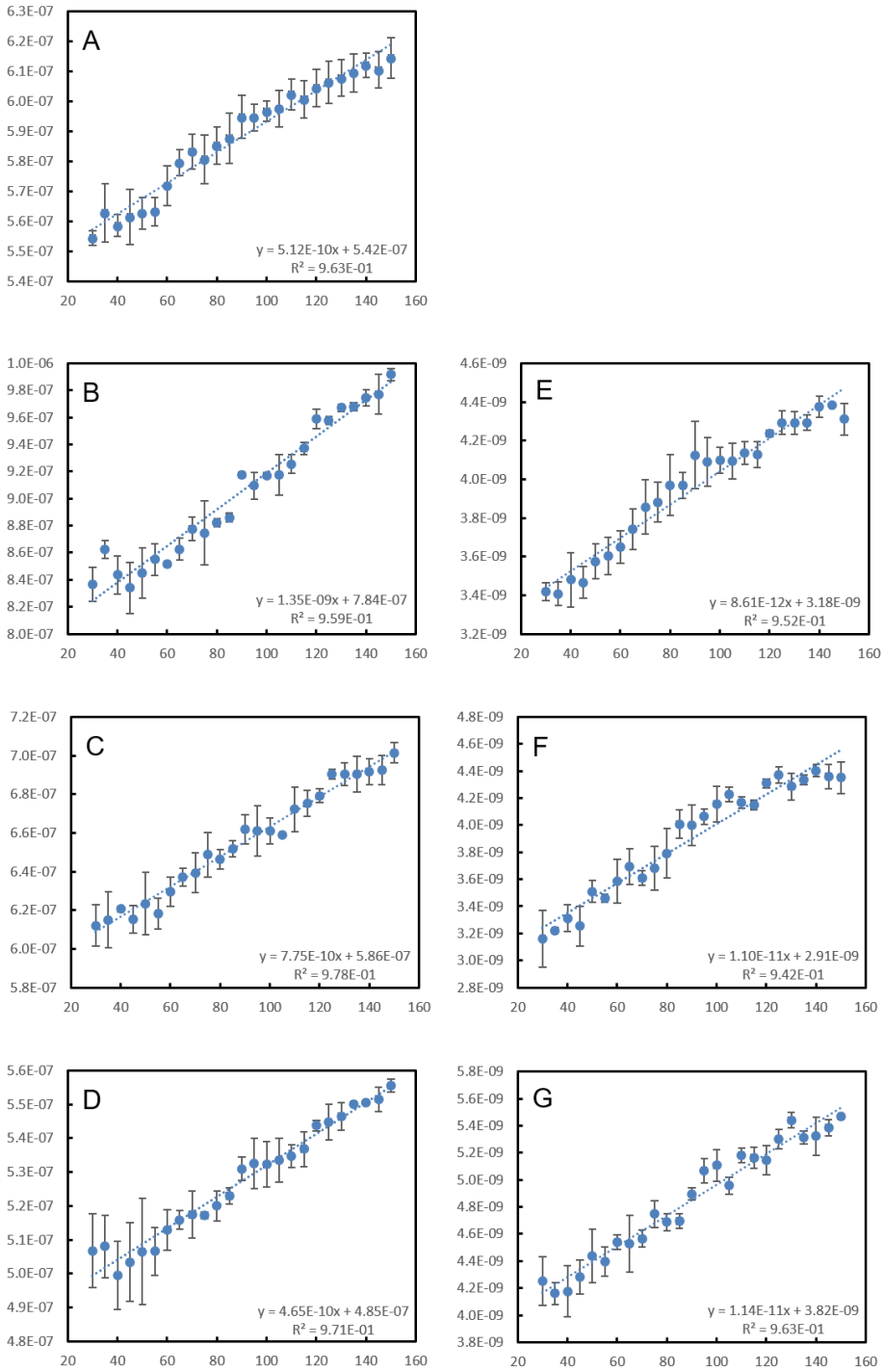

Figure 21: Guinier plots showing Kc/R_θ vs. θ (degrees) obtained from static light scattering of ELP micelles and ELP-silica hybrid nanoparticles at 25 μM. Control

c-ELP micelle (A) and sp-ELP-1*, -2*, -3* without silica (B-D) and with silica (E-G) shown with regression.

Table 3: ELP micelle and ELP-silica nanoparticle characterization by static and dynamic light scattering

Construct	ELP Unimer MW ($g \cdot mol^{-1}$)	R_g (nm) [a]	R_h (nm) [b]	ρ [c]	Measured MW ($g \cdot mol^{-1}$) [a]	N_{agg} [d]
c-ELP	47.5×10^3	21.1	28.2	0.748	1.76×10^6	37
sp-ELP-1*, w/o silica	49.2×10^3	28.4	35.5	0.800	1.28×10^6	26
sp-ELP-2*, w/o silica	49.2×10^3	24.8	32.7	0.758	1.63×10^6	33
sp-ELP-3*, w/o silica	49.2×10^3	22.7	29.3	0.775	2.01×10^6	41
sp-ELP-1*, w/ silica	49.2×10^3	37.1	47.8	0.776	2.94×10^8	n.d.
sp-ELP-2*, w/ silica	49.2×10^3	43.0	53.1	0.810	3.12×10^8	n.d.
sp-ELP-3*, w/ silica	49.2×10^3	39.5	45.5	0.868	2.43×10^8	n.d.

[a] R_g, the radius of gyration, and Measured MW (molecular weight) were obtained by static light scattering (see Figure S2); [b] R_h, the hydrodynamic radius was obtained by dynamic light scattering; [c] ρ, shape factor, was obtained by dividing the radius of gyration by hydrodynamic radius; [d] N_{agg}, the number of ELP unimers per micelle, was obtained by through the molecular weight of an individual ELP unimers.

First, using the theoretical molecular weight of the unimers, combined with the measured and calculated micellar molecular weights, we obtained the aggregation number (N_{agg}) for each sp-ELP construct, *i.e.* the average number of ELP unimers per assembled micelle. The resulting N_{agg} values were ~26, 33, and 41 for sp-ELP-1*, -2, and 3*, respectively; the differences between experimental constructs may reflect the axial placement of the modified silaffin sequence. For instance, the proximity of the cationic motif to the C-terminal conjugation trailer and therefore the hydrophobic core may hinder denser packing of ELP chains per micelle. As the silica-promoting tag is moved towards the N-terminus and away from the hydrophobic core, we observe that the aggregation number is more in line with that of the c-ELP construct and previous

studies [113]. In addition, by combining the dynamic and static light scattering data, we calculated the shape factor, $\rho = R_g/R_h$, for each experimental construct prior to and post silicification, which provides information about the distribution of mass for each construct. Interestingly, the ρ for sp-ELP-1* decreased from 0.800 to 0.776, while that of sp-ELP-2* and -3* increased from 0.758 and 0.775 to 0.810 and 0.868, respectively. To more accurately study the exposure of ELP, and specifically its N-terminus, beyond the periphery of the silica nanoparticles, we performed two biophysical studies utilizing the biotin-streptavidin binding interaction: 1) a fluorescently-labeled streptavidin binding study in solution and 2) a QCM study of binding of hybrid nanoparticles to streptavidin adsorbed on "planar" surfaces.

4.4.4 Fluorescence assay of biotinylated sp-ELP and c-ELP silicified nanoparticles using fluorescent streptavidin

To explore whether the ELPs are present on the surface of the hybrid nanoparticles, we exploited the amine at the N-terminus of each polypeptide sequence which can be covalently biotinylated using *N*-hydroxysuccinimide activation and reaction. By attempting to biotinylate the free N-termini of the ELP micelles after silicification, we intended to mimic the presentation of peptide targeting and recognition ligands that may be incorporated into this system for future applications. In the first study, we investigated the reactivity of biotinylated ELP / silica nanoparticles with free, fluorescent streptavidin in solution by co-incubation, followed by purification from free, unbound streptavidin and excitation/detection of the Cy3 fluorophore-labeled streptavidin

(Figure 22). As expected, the positive control, biotinylated c-ELP construct, exhibited the highest degree of fluorescent signal at $11.05 \pm 1.14 \times 10^3$ a.u., which was statistically significant ($p < 0.05$) compared to all other experimental samples. For the silicified constructs, sp-ELP-1* nanoparticles displayed a signal of $6.18 \pm 0.91 \times 10^3$ a.u., which was also significantly higher than that of sp-ELP-2* and 3* at $2.63 \pm 0.69 \times 10^3$ a.u. and $2.10 \pm 0.47 \times 10^3$ a.u., respectively. We additionally utilized two types of negative controls: samples that were not biotinylated as well as samples exposed to fluorescent streptavidin that was preblocked with free biotin (*i.e.* streptavidin-Cy3 pre-incubated and saturated with free biotin). Interestingly, only the sp-ELP-1* silica nanoparticles showed a significantly higher fluorescence signal, suggesting a specific interaction between biotin ligands conjugated to the ELP micelles and streptavidin in solution, lending further support to the conclusion that ELP was retained on the surface of the hybrid nanoparticles for this construct. Conversely, the difference in fluorescence for sp-ELP-1* compared to the positive control c-ELP sample shows that a large fraction of ELP N-terminal ends are likely encapsulated within the silica matrix and is in agreement with the random coil nature of the free polypeptide chains [160].

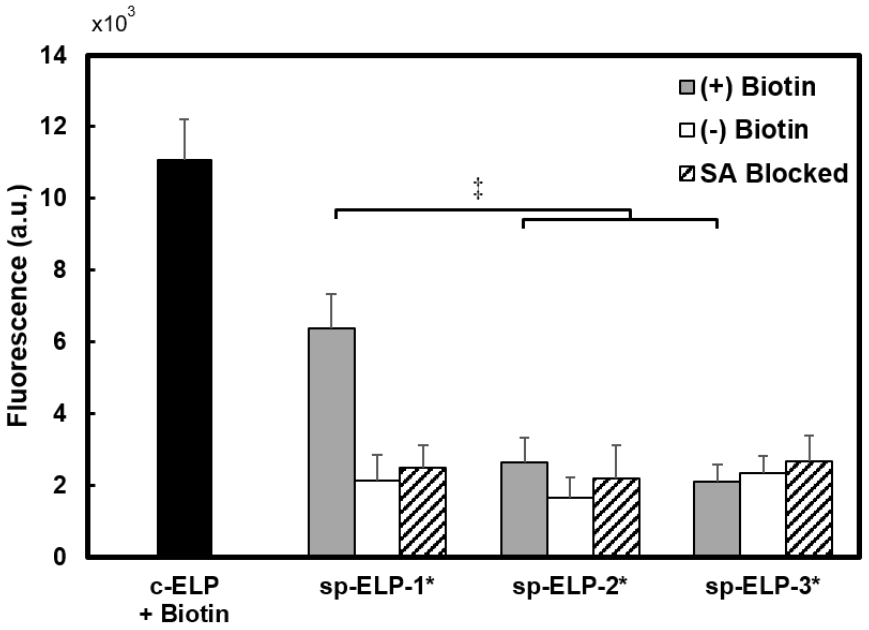

Figure 22: Cy3 fluorescence study of biotinylated sp-ELP silica nanoparticle constructs - 50 μM ELP incubated with Streptavidin-Cy3 conjugate and purified. c-ELP + Biotin (no silica) positive control (black bar) is plotted against biotinylated (striped bars) and negative control non-biotinylated (white bars) silicified sp-ELP-1*, -2*, -3* micelles. Excitation: 1 sec; ‡: $p < 0.05$.

To approximate the concentration of fluorescently labeled streptavidin adsorbed to each sample, we constructed a standard curve based on fluorescence of free streptavidin-Cy3 (Figure 23). The regression fit is highly linear, $R^2 = 0.9989$, and allows for a simple conversion of fluorescence to concentration. For the c-ELP sample, we obtain a streptavidin concentration of 34.68 ± 3.58 μM, or approximately 69.3% binding (given ~50 μM ELP) and for the sp-ELP-1* sample, we obtain a concentration of 19.39 ± 2.86 μM, or approximately 38.8% binding. However, these data are likely affected by imperfections in the purification of free streptavidin-Cy3 post-reaction or the non-specific adsorption of streptavidin to the hybrid particles themselves.

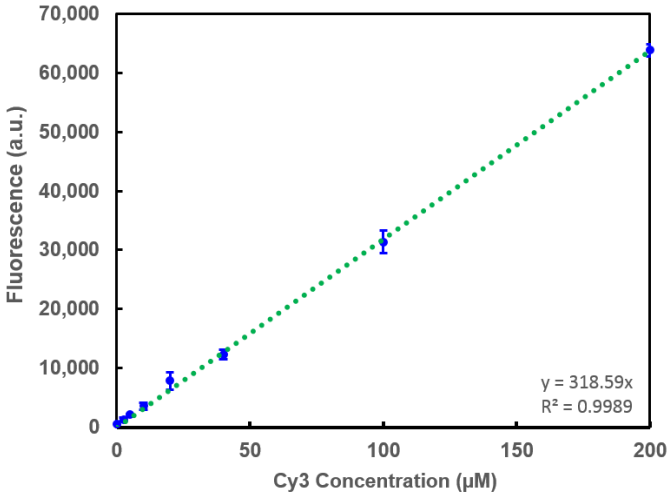

Figure 23: Steptavidin-Cy3 fluorescence standard for given concentrations; excitation: 1 sec.

4.4.5 Quartz crystal microbalance study of biotinylated sp-ELP and c-ELP silicified nanoparticles

To further study the selective application of silica upon silica-promoting ELP templates, we employed quartz crystal microbalance measurements in which we first flowed free streptavidin over a biotinylated PEG-thiol monolayer on a gold QCM sensor, and then flowed biotinylated or un-biotinylated sample over the sensor to study the accumulation of mass on the sensor surface (Figure 24A). Representative QCM frequency (ΔF; 5^{th} overtone) data for the biotinylated experimental groups are shown in (Figure 25) and their corresponding dissipation results are shown in (Figure 26); we observe an average frequency change as a result of streptavidin binding to be -8.76 ± 0.72 Hz in addition to a dissipation change of $0.09 \pm 0.04 \times 10^{-6}$, and is characteristic of streptavidin immobilization on the surface of the sensors.

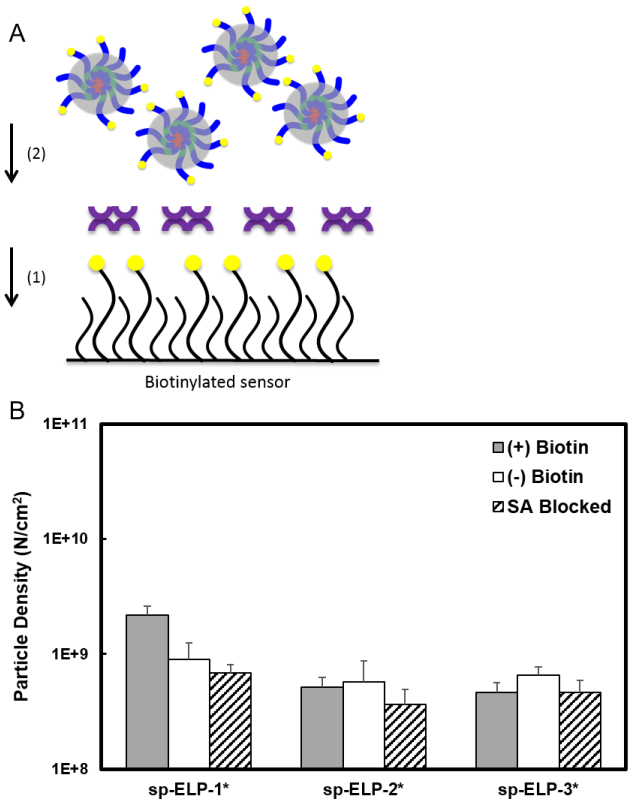

Figure 24: (A) Schematic representation of quartz crystal microbalance assay for biotinylation of ELP post-silicification. A biotinylated gold QCM sensor is (1) incubated with free streptavidin, washed and (2) incubated with sp-ELP silica nanoparticle constructs. (B) Approximate number of particles bound using each construct – sp-ELP-1*, 2*, 3* silica nanoparticles (grey bars) and controls using non-biotinylated nanoparticles (white bars) and incubation with sensors with incorporated blocked streptavidin (diagonal pattern bars). Values obtained by dividing mass from QCM data by individual nanoparticle mass.

By incorporating the previously discussed molecular weight from SLS for each construct into the measured ΔF (Hz) – the change in frequency – for nanoparticle loading, we can arrive at an approximation of the particle density that has attached to the surface, specifically and non-specifically (Figure 24B). We utilized two negative controls to

investigate specificity. a control in which the ELP/silica particles are not biotinylated (white bars) as well as a control in which we flowed excess free biotin over the sensor after the initial streptavidin coverage to pre-block the available binding sites of the streptavidin (diagonal bars). Both controls are used to gauge the amount of non-specific adsorption of nanoparticles onto the protein-covered surface. In considering both the un-biotinylated and pre-blocked streptavidin controls, there is evidence of significant non-specific interaction between the nanoparticles and the surface, likely due to the nonspecific adsorption of streptavidin onto the hybrid particles.

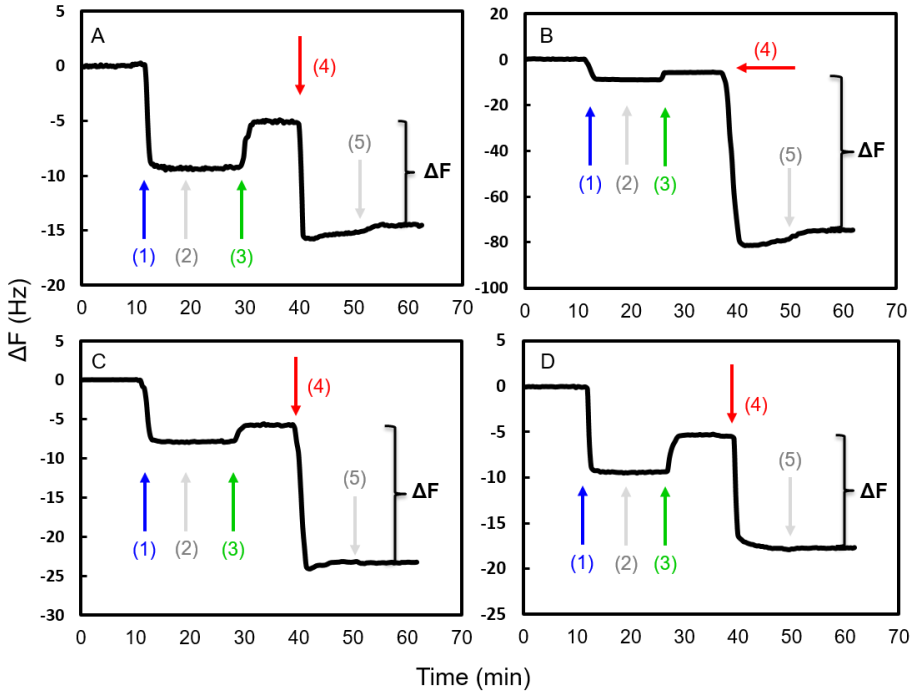

Figure 25: Representative quartz crystal microbalance frequency measurements of sp-ELP silica nanoparticles binding to a streptavidin-covered biotinylated gold sensor. Sequence of events include flow of free streptavidin (1; blue) to cover biotinylated surface, wash with PBS (2; grey), buffer exchange to milli-Q H_2O (3; green), sample flow (4; red), and a final wash (5; grey). Samples are labeled as positive control c-ELP (A) and sp-ELP-1*, -2*, 3* silica (B-D) with biotinylation.

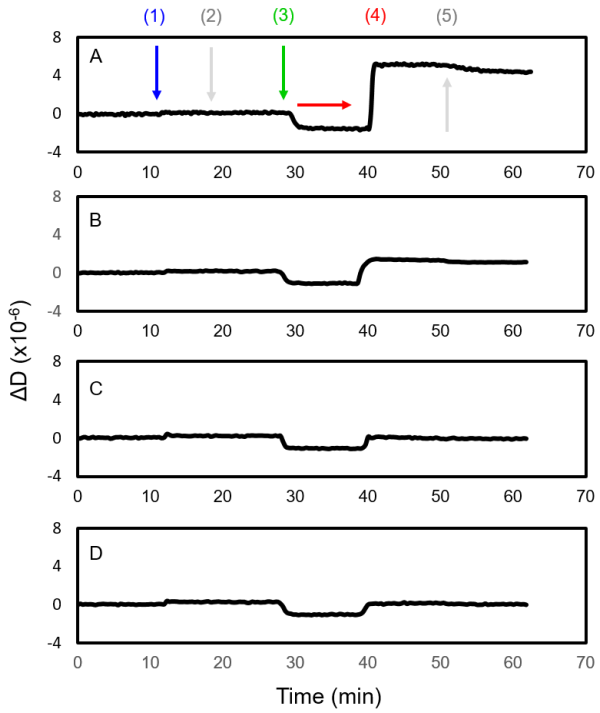

Figure 26: Representative quartz crystal microbalance dissipation measurements of sp-ELP silica nanoparticles binding to a streptavidin-covered biotinylated gold sensor. Sequence of events include flow of free streptavidin (1; blue) to cover biotinylated surface, wash with PBS (2; grey), buffer exchange to milli-Q H_2O (3; green), sample flow (4; red), and a final wash (5; grey). Samples are labeled as positive control c-ELP (A) and sp-ELP-1*, -2*, 3* silica (B-D) with biotinylation.

Unfortunately, as both interaction types are competing for the streptavidin bound to the sensor surface, it may be difficult to de-convolute the data to obtain a better understanding of the differences in specificity between the experimental constructs beyond subtraction of the control data. However, we do observe an increased number of particles bound for silicified sp-ELP-1* at 2.49 x 10^9 particles/cm^2 compared to that of silicified sp-ELP-2* and 3*, 5.97 x 10^8 particles/cm^2 and 5.36 x 10^8 particles/cm^2, respectively. This approximately four-fold increase in particle surface adherence may

suggest an increased availability of biotinylated ELP unimers, resulting in the increased specific interaction of the biotin and streptavidin and beyond physical adsorption.

4.5 Conclusions

The programmed placement of a modified silaffin tag within an ELP construct that self assembles into spherical micelles upon conjugation of hydrophobes results in significant differences in nanoparticle morphology and reactivity. We report the silicification of a family of silica-promoting ELP constructs that demonstrate the selective application of a silica shell and differential exposure of free ELP termini when the silicification module is encoded near the core of the assembled micelle. While a free N-terminus itself does not represent a specific ligand or recognition motif in this study, we hypothesize that the availability of free ELP beyond silica encapsulation grants additional control and supports the potential for additional functionality of the hybrid ELP and silica platform. When combined with our previous studies demonstrating the potential for ELP / silica nanoparticles to be used to encapsulate and release drugs, these findings may enable the fabrication of more complex ELP and silica biosensing and drug delivery assemblies through constructs that are driven to self-assemble with drug conjugation, encapsulated and stabilized by silica shell formation and targeted via exposed, genetically encoded peptide sequences.

4.6 Chapter acknowledgements

This work is funded by NSF's Research Triangle MRSEC (DMR-1121107). W.H. acknowledges support from the NIH Biotechnology Predoctoral Training Fellowship (NIH Grant No. 5T32GM008555-18). The authors thank the staff of the Duke University Shared Materials Instrumentation Facility for their expertise in electron microscopy.

5. Conclusion and Future Directions

5.1 Summary

The work presented in this dissertation represents a systematic study of templating the formation of silica from self-assembled elastin-like polypeptides to create a hybrid nanomaterial that has potential for application as a carrier for the delivery of therapeutics. By taking advantage of the biologically-inspired material toolbox in both silaffin-mediated silicification as well as the precise compositional control of peptide sequence and thermally-dependent phase behavior of elastin-like polypeptides, we demonstrated that monodisperse silica nanoparticles could be fabricated rapidly and under physiologically relevant conditions in temperature, pH and in aqueous solution. We synthesized a variety of silica nanoparticles based mainly on the construction of the underlying ELP template and showed that silicification using this methodology could be used to encapsulate hydrophobic small molecules for release as well as to potentially retain the peptide-targeting functionality of the template. Overall, the work was organized into three studies that revolved around this central theme.

In Chapter 2, we described the fundamental proof-of-concept demonstration that silaffin-presenting diblock ELP micelles could be used to drive the formation of monodisperse, spherical silica. By selectively appending the silaffin motif to an ELP construct that assembles with increased temperature, we demonstrated that both the presence of the silica promoter and self-assembly was required to organize sufficient

local charge density to promote silicification and proved the polypeptide template was encapsulated with the silica matrix using fluorescence microscopy. In Chapter 3, we expanded upon this basis to study the encapsulation and release of the small hydrophobic molecule doxorubicin from the silica matrix. In this case, we used a conjugation-driven ELP assembly system where conjugation with such hydrophobes would result in the formation of spherical micelles with the drug at the core. Similarly to the first study, we found that self-assembly of the template was required for silicification of sub-100 nm silica particles (~42 nm for *N*-benzylmaleimide and ~47 nm for BMPH-activated doxorubicin), but unlike the first study, we found that silicification in this case resulted in core-shell silica morphologies. Finally, we were able to show release of doxorubicin from the derived silica shells through cleavage of the drug from the core of the micelle template. In Chapter 4, we studied the potential for silica and elastin-like polypeptide nanoparticles towards application as a targeted delivery vehicle. Using a conjugation-driven ELP assembly system again, we inserted the silaffin peptide at different locations along the ELP to create three experimental constructs, which subsequently self-assemble to present the silica-promoting motif at different radial spaces on average. We found that the construct containing the silaffin insertion closest to the assembled micellar core was significantly different than the other constructs and remained susceptible to N-terminal ELP biotinylation through streptavidin binding studies. This finding may open the possibility of future application of this material to

include targeting ligands and further characterization as a desired drug carrier. Overall, we believe this hybrid material platform has potential to be useful in biomedical and materials science applications; while a significant portion of this work represents proof-of-concept studies of silicification using ELP templates, the findings within this thesis has potentiated a number of future directions that may enhance the attractiveness of the hybrid material system.

5.2 Future Directions

5.2.1 Utilization of diverse silica precursor combinations

Throughout the work described in this thesis, we generated all of the silica through hydrolysis and polycondensation of tetramethoxysilane (TMOS), a tetra-functional silica precusor that reacts to form four siloxane bonds and results in a highly crosslinked matrix. However, there is great potential to expand upon this singular precursor to more fully explore the rich world of alkoxysilane monomers that have been previously characterized. Shields *et al.* have recently reported the study of siloxane gels generated from a variety of such monomers, including di-functional dimethoxymethylsilane (DMODMS) , tri-functional trimethoxymethylsilane (TMOMS), TMOS, chemically-reactive vinyltrimethoxysilane (VTMOS), and most importantly mixtures of these hetero-functional monomers [161]. Through the incorporation of different ratios of monomers, they were able to generate particles of variable density and

porosity as well as enable surface functionality through presentation of vinyl groups. The use of such monomers within the silica-promoting ELP system would be interesting for two reasons: 1) the ability to template similarly sized particles with variable porosity may affect drug release and 2) the ability to include functional groups on the surface may enhance the potential for appending targeting ligands to the nanoparticle surface. For the first consideration, it would be interesting to template particles using TMOS (as we have already demonstrated) as well as using differing ratios of DMODMS:TMOS and TMOMS:TMOS by drug-conjugated ELP micelles and subsequently trigger release. Particles with different porosities may respond to the triggering signal more rapidly as well as release drugs at varying rates. In the second consideration, the use of a mixture of VTMOS and TMOS to silicify hybrid nanoparticles would result in the exposure of vinyl groups on the surface through polycondensation. We have initially explored the use of different precursors by characterizing the silicification of the diblock ELP used in Chapter 2 with 10:1 TMOS:VTMOS and 10:1 TMOS:ATMOS (Figure 27). By covering the surface of the resulting particles with vinyl and amine groups, it may be possible to incorporate surface targeting ligands through click or *N*-hydroxysulfosuccinimide chemistries. This may be used in conjunction with the biorecognition ability afforded by ELP as studied in Chapter 4 and may further be used to study uptake of encapsulated nanoparticles within cells.

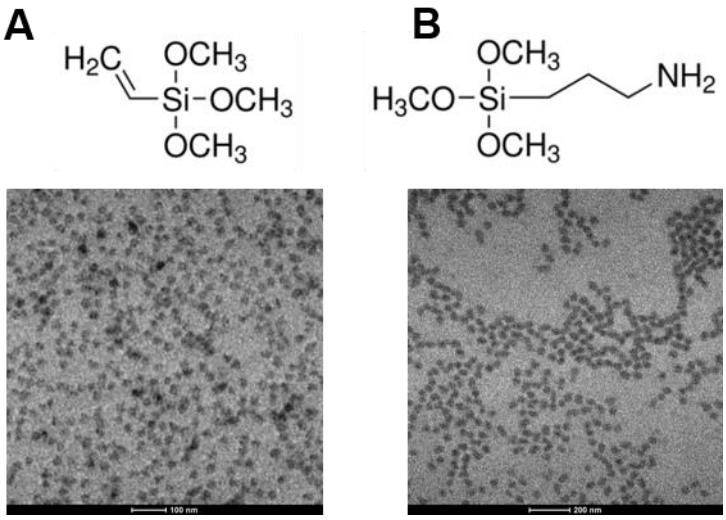

Figure 27: Silicification of diblock ELP micelles with mixtures of alkoxysilane monomers 10:1 TMOS:VTMOS (A) and 10:1 TMOS:ATMOS (B). ELP micelles at 1 mg/mL incubated at 37º C were reacted at 100 mM total precursor concentration for 4 hours and characterized by transmission electron microscopy.

5.2.2 In Vivo Targeting and Cell Uptake of ELP and Silica Nanoparticles

In Chapter 4, we studied the selective application of silica in order to assess the potential for targeting using this system by encoding peptide targeting motifs within the ELP construct and the exposure of ELP through the silicified silica shell. Indeed, the retention of ELP biorecognition ability would significantly enhance the value of hybrid ELP and silica nanoparticles and we have thus far demonstrated a proof-of-concept using biotinylation of the N-terminal amine on exposed ELP chains. The next logical step in further characterizing the selective silicification of ELP templates would be to genetically encode a peptide targeting ligand to the N-terminus of the ELP constructs

and to explore whether they retain function post-silicification. The use of peptides to target preferentially expressed markers on tumor cells has been well studied and numerous short peptides have been identified using biomimicry and phage display.[41,162,163] One such peptide, Asn-Gly-Arg (NGR), has been identified to selectively bind to an isoform of aminopeptidase-N (CD13), which is overexpressed on tumor vasculature and employed in as a targeting ligand previously [164-166]. Simnick *et al.* has also demonstrated that the incorporation and decoration of NGR peptides (as well as other targeting peptides such as RGD) on self-assembled ELP micelles can be used to enhance delivery to tumors [56,167]. We have similarly designed a family of ELPs that incorporate NGR at the N-terminus and are presented at the coronae of self-assembled ELP micelles upon conjugation (Figure 28).

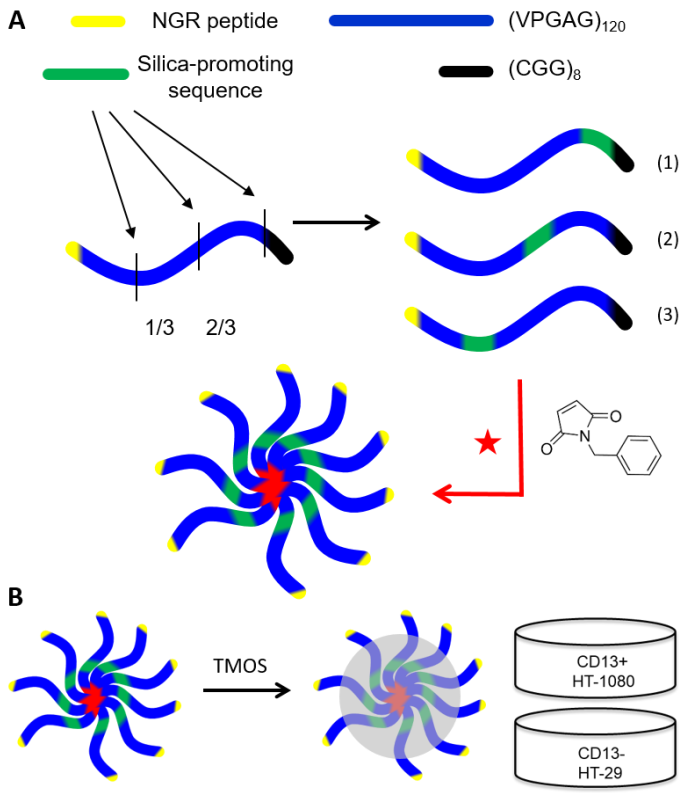

Figure 28: Schematic representation of the study of cell uptake of silicified assembled NGR-sp-ELPs. (A) Insertion of a modified silaffin sequence creates three experimental constructs (NGR-sp-ELP-1, -2, -3) that self-assemble into micelles upon conjugation with *N*-benzylmaleimide (red star). (B) NGR-presenting hybrid ELP and silica nanoparticles are incubated with CD13+ HT-1080 fibrosarcoma and CD13- HT-29 adenocarcinoma cells.

To reproduce the experimental setup of the study in Chapter 4, it would be necessary to generate three ELP constructs that have a silica-promoting motif inserted along the ELP axis at varying locations (Figure 28A). If the results in the study were to be reproduced, we may expect that only NGR-sp-ELP-1 silicified micelles may be preferentially uptaken by CD13+ cells such as HT-1080 fibrosarcoma compared to both

the other experimental constructs (NGR-sp-ELP-2, -3) as well as controls without the NGR decoration (Figure 28B). Specifically, we would first culture both HT-1080 and HT-29 cells in open-window chambers and subsequently incubate them with each population of fluorescently labeled polypeptide / silica nanoparticles post-silicification. Using a combination of fluorescence microscopy and flow cytometry, we would characterize the ligand/receptor mediated preferential uptake, if any, of the various nanoparticle populations. This experimental design, from a materials perspective, would enable us to far better understand the regio-specificity of silicification by modulation of the placement of the silica-promoting tag. With regards to the biomedical application, the ability to combine both silicification and active targeting within a single ELP micelle construct would allow us to fabricate a targeted nanoparticle delivery system that both encapsulates the cargo in silica as well as retains the polypeptide biorecognition functionality.

We have previously begun to characterize this system and found that, indeed, the constructs do in fact produce silica particles similar to those previously studied (Figure 29). A concern with this direction is the potential for the positively charged arginine residue to promote silicification in addition to the silica-promoting module. If this is the case, then it will be necessary to explore the literature to find peptide targeting sequences that do not require the usage of a positively charged amino acid. However, the availability of the sp-ELP-1 N-terminal amine suggests that a singular charge may be

insufficient to accumulate silica from polycondensation and block the utilization of the peptide.

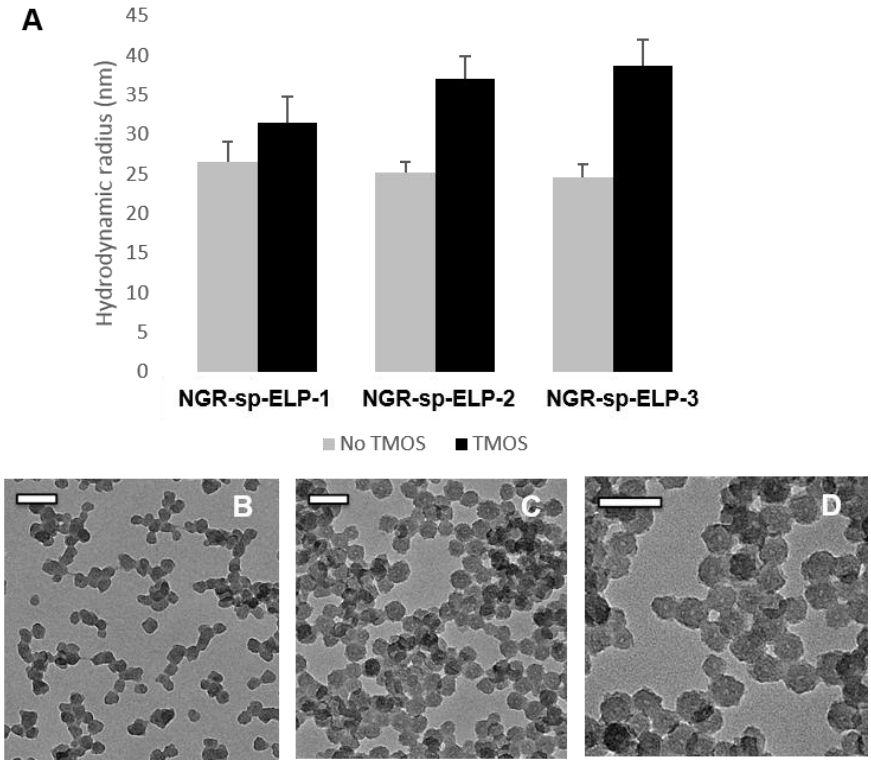

Figure 29: Light scattering and electron microscopy characterization of silicified ELP and silica nanoparticles using NGR-sp-ELP constructs. (A) Hydrodynamic radii of NGR-sp-ELP-1, -2, -3 micelles without (grey bars) and with (black bars) incubation with 100 mM TMOS for 4 hours. The particles were subsequently characterized using TEM with NGR-sp-ELP-1 (B), -2 (C), -3 (D) particles as templates. Scale bar: 100 nm.

In summary, this thesis describes the use of self-assembling elastin-like polypeptide constructs to template the formation and encapsulation by silica using a biologically-inspired silaffin peptide motif, which may have potential as nanoscale carriers for the delivery of therapeutics. With additional study, this system may allow

for the facile fabrication of silica-stabilized, tunable, and targeted nanoparticles that may fulfill a need in cancer therapy.

References

1 Iler, R. K. *The Chemistry of Silica: Solubility, Polymerization, Colloid and Surface Properties and Biochemistry of Silica*. (Wiley, 1979).

2 Stöber, W., Fink, A. & Bohn, E. Controlled growth of monodisperse silica spheres in the micron size range. *Journal of colloid and interface science* **26**, 62-69 (1968).

3 Rosenholm, J. M., Mamaeva, V., Sahlgren, C. & Lindén, M. Nanoparticles in targeted cancer therapy: mesoporous silica nanoparticles entering preclinical development stage. *Nanomedicine* **7**, 111-120 (2012).

4 Tang, L. & Cheng, J. Nonporous silica nanoparticles for nanomedicine application. *Nano today* **8**, 290-312 (2013).

5 Barbe, C. *et al.* Silica particles: a novel drug-delivery system. *Advanced materials* **16**, 1959-1966 (2004).

6 Steven, C. R. *et al.* Bioinspired silica as drug delivery systems and their biocompatibility. *Journal of Materials Chemistry B* **2**, 5028-5042 (2014).

7 Kim, J., Kim, L. & Kim, C. Size control of silica nanoparticles and their surface treatment for fabrication of dental nanocomposites. *Biomacromolecules* **8**, 215-222 (2007).

8 Hartlen, K. D., Athanasopoulos, A. P. & Kitaev, V. Facile preparation of highly monodisperse small silica spheres (15 to> 200 nm) suitable for colloidal templating and formation of ordered arrays. *Langmuir* **24**, 1714-1720 (2008).

9 Arriagada, F. & Osseo-Asare, K. Synthesis of nanosize silica in a nonionic water-in-oil microemulsion: effects of the water/surfactant molar ratio and ammonia concentration. *Journal of colloid and interface science* **211**, 210-220 (1999).

10 Osseo-Asare, K. & Arriagada, F. Preparation of SiO2 nanoparticles in a non-ionic reverse micellar system. *Colloids and surfaces* **50**, 321-339 (1990).

11 Osseo-Asare, K. & Arriagada, F. Growth kinetics of nanosize silica in a nonionic water-in-oil microemulsion: a reverse micellar pseudophase reaction model. *Journal of colloid and interface science* **218**, 68-76 (1999).

12 Wang, C., Ma, Z., Wang, T. & Su, Z. Synthesis, Assembly, and Biofunctionalization of Silica-Coated Gold Nanorods for Colorimetric Biosensing. *Advanced Functional Materials* **16**, 1673-1678 (2006).

13 Wang, Z. L., Gao, R. P., Gole, J. L. & Stout, J. D. Silica nanotubes and nanofiber arrays. *Advanced materials* **12**, 1938-1940 (2000).

14 Harada, M. & Adachi, M. Surfactant-Mediated Fabrication of Silica Nanotubes. *Advanced materials* **12**, 839-841 (2000).

15 Adachi, M., Harada, T. & Harada, M. Formation processes of silica nanotubes through a surfactant-assisted templating mechanism in laurylamine hydrochloride/tetraethoxysilane system. *Langmuir* **16**, 2376-2384 (2000).

16 Yang, H., Ozin, G. A. & Kresge, C. T. The role of defects in the formation of mesoporous silica fibers, films, and curved shapes. *Advanced materials* **10**, 883-887 (1998).

17 Brinker, C. J. & Scherer, G. W. *Sol-gel science: the physics and chemistry of sol-gel processing*. (Academic press, 2013).

18 Barbé, C. *et al.* Silica Particles: A Novel Drug-Delivery System. *Advanced materials* **16**, 1959-1966 (2004).

19 Wang, Y. & Caruso, F. Enzyme encapsulation in nanoporous silica spheres. *Chemical Communications*, 1528-1529 (2004).

20 Wang, Y. & Caruso, F. Mesoporous silica spheres as supports for enzyme immobilization and encapsulation. *Chemistry of Materials* **17**, 953-961 (2005).

21 Betancor, L. & Luckarift, H. R. Bioinspired enzyme encapsulation for biocatalysis. *Trends in Biotechnology* **26**, 566-572 (2008).

22 Luckarift, H. R., Spain, J. C., Naik, R. R. & Stone, M. O. Enzyme immobilization in a biomimetic silica support. *Nat Biotech* **22**, 211-213 (2004).

23 Livage, J., Roux, C., Da Costa, J., Quinson, J. & Desportes, I. Immunoassays in sol-gel matrices. *Journal of Sol-Gel Science and Technology* **7**, 45-51 (1996).

24 Gill, I. & Ballesteros, A. Encapsulation of biologicals within silicate, siloxane, and hybrid sol-gel polymers: an efficient and generic approach. *Journal of the American Chemical Society* **120**, 8587-8598 (1998).

25 Larson, D. R. *et al.* Silica nanoparticle architecture determines radiative properties of encapsulated fluorophores. *Chemistry of materials* **20**, 2677-2684 (2008).

26 Ow, H. *et al.* Bright and Stable Core−Shell Fluorescent Silica Nanoparticles. *Nano Letters* **5**, 113-117 (2005).

27 Choi, J. *et al.* Core-shell silica nanoparticles as fluorescent labels for nanomedicine. *Journal of biomedical optics* **12**, 064007-064007-064011 (2007).

28 Benezra, M. *et al.* Multimodal silica nanoparticles are effective cancer-targeted probes in a model of human melanoma. *The Journal of clinical investigation* **121**, 2768-2780 (2011).

29 Gerion, D. *et al.* Paramagnetic silica-coated nanocrystals as an advanced MRI contrast agent. *The Journal of Physical Chemistry C* **111**, 12542-12551 (2007).

30 Taylor, K. M. *et al.* Mesoporous silica nanospheres as highly efficient MRI contrast agents. *Journal of the American Chemical Society* **130**, 2154-2155 (2008).

31 Tang, L. *et al.* Aptamer-Functionalized, Ultra-Small, Monodisperse Silica Nanoconjugates for Targeted Dual-Modal Imaging of Lymph Nodes with Metastatic Tumors. *Angewandte Chemie International Edition* **51**, 12721-12726 (2012).

32 Chen, J.-F., Ding, H.-M., Wang, J.-X. & Shao, L. Preparation and characterization of porous hollow silica nanoparticles for drug delivery application. *Biomaterials* **25**, 723-727 (2004).

33 Huo, Q. *et al.* A New Class of Silica Cross-Linked Micellar Core−Shell Nanoparticles. *Journal of the American Chemical Society* **128**, 6447-6453 (2006).

34 Tan, A., Simovic, S., Davey, A. K., Rades, T. & Prestidge, C. A. Silica-lipid hybrid (SLH) microcapsules: a novel oral delivery system for poorly soluble drugs. *Journal of controlled release* **134**, 62-70 (2009).

35 Cancer Facts & Figures 2016. (American Cancer Society, Atlanta, 2016).

36 Hanahan, D. & Weinberg, Robert A. Hallmarks of Cancer: The Next Generation. *Cell* **144**, 646-674.

37 Sun, T. *et al.* Engineered nanoparticles for drug delivery in cancer therapy. *Angewandte Chemie International Edition* **53**, 12320-12364 (2014).

38 Brown, M. L., Lipscomb, J. & Synder, C. The Burden of Illness of Cancer: Economic Cost and Quality of Life. *Annual Review of Public Health* **22**, 91-113 (2001).

39 Mariotto, A. B., Robin Yabroff, K., Shao, Y., Feuer, E. J. & Brown, M. L. Projections of the Cost of Cancer Care in the United States: 2010–2020. *Journal of the National Cancer Institute* (2011).

40 Seiwert, T. Y., Salama, J. K. & Vokes, E. E. The concurrent chemoradiation paradigm—general principles. *Nature clinical practice Oncology* **4**, 86-100 (2007).

41 Peer, D. *et al.* Nanocarriers as an emerging platform for cancer therapy. *Nature Nanotechnology* **2**, 751-760 (2007).

42 Bae, Y. H. & Park, K. Targeted drug delivery to tumors: Myths, reality and possibility. *Journal of Controlled Release* **153**, 198-205 (2011).

43 Wang, A. Z., Langer, R. & Farokhzad, O. C. Nanoparticle Delivery of Cancer Drugs. *Annual Review of Medicine* **63**, 185-198 (2012).

44 Brannon-Peppas, L. & Blanchette, J. O. Nanoparticle and targeted systems for cancer therapy. *Advanced Drug Delivery Reviews* **64, Supplement**, 206-212 (2012).

45 Yuan, F. *et al.* Vascular permeability in a human tumor xenograft: molecular size dependence and cutoff size. *Cancer research* **55**, 3752-3756 (1995).

46 Hobbs, S. K. *et al.* Regulation of transport pathways in tumor vessels: Role of tumor type and microenvironment. *Proceedings of the National Academy of Sciences* **95**, 4607-4612 (1998).

47 Matsumura, Y. & Maeda, H. A new concept for macromolecular therapeutics in cancer chemotherapy: mechanism of tumoritropic accumulation of proteins and the antitumor agent smancs. *Cancer research* **46**, 6387-6392 (1986).

48 Maeda, H., Nakamura, H. & Fang, J. The EPR effect for macromolecular drug delivery to solid tumors: Improvement of tumor uptake, lowering of systemic toxicity, and distinct tumor imaging in vivo. *Advanced Drug Delivery Reviews* **65**, 71-79 (2013).

49 Xiong, H. Q. *et al.* Cetuximab, a monoclonal antibody targeting the epidermal growth factor receptor, in combination with gemcitabine for advanced pancreatic cancer: a multicenter phase II Trial. *Journal of Clinical Oncology* **22**, 2610-2616 (2004).

50 Weiner, L. M. & Adams, G. P. New approaches to antibody therapy. *Oncogene* **19**, 6144-6151 (2000).

51 Dhar, S., Gu, F. X., Langer, R., Farokhzad, O. C. & Lippard, S. J. Targeted delivery of cisplatin to prostate cancer cells by aptamer functionalized Pt (IV) prodrug-PLGA–PEG nanoparticles. *Proceedings of the National Academy of Sciences* **105**, 17356-17361 (2008).

52 Farokhzad, O. C. *et al.* Nanoparticle-aptamer bioconjugates a new approach for targeting prostate cancer cells. *Cancer research* **64**, 7668-7672 (2004).

53 Schiffelers, R. M. *et al.* Cancer siRNA therapy by tumor selective delivery with ligand-targeted sterically stabilized nanoparticle. *Nucleic Acids Research* **32**, e149 (2004).

54 Li, J. *et al.* Fusion protein from RGD peptide and Fc fragment of mouse immunoglobulin G inhibits angiogenesis in tumor. *Cancer gene therapy* **11**, 363-370 (2004).

55 Curnis, F. *et al.* Differential binding of drugs containing the NGR motif to CD13 isoforms in tumor vessels, epithelia, and myeloid cells. *Cancer Research* **62**, 867-874 (2002).

56 Simnick, A. J. *et al.* In vivo tumor targeting by a NGR-decorated micelle of a recombinant diblock copolypeptide. *Journal of Controlled Release* **155**, 144-151 (2011).

57 Yonenaga, N. *et al.* RGD-based active targeting of novel polycation liposomes bearing siRNA for cancer treatment. *Journal of Controlled Release* **160**, 177-181 (2012).

58 He, Q. & Shi, J. MSN Anti-Cancer Nanomedicines: Chemotherapy Enhancement, Overcoming of Drug Resistance, and Metastasis Inhibition. *Advanced materials* **26**, 391-411 (2014).

59 Tarn, D. *et al.* Mesoporous Silica Nanoparticle Nanocarriers: Biofunctionality and Biocompatibility. *Accounts of Chemical Research* **46**, 792-801 (2013).

60 Li, Z., Barnes, J. C., Bosoy, A., Stoddart, J. F. & Zink, J. I. Mesoporous silica nanoparticles in biomedical applications. *Chemical Society reviews* **41**, 2590-2605 (2012).

61 Slowing, I. I., Vivero-Escoto, J. L., Wu, C.-W. & Lin, V. S. Y. Mesoporous silica nanoparticles as controlled release drug delivery and gene transfection carriers. *Advanced Drug Delivery Reviews* **60**, 1278-1288 (2008).

62 Grün, M., Lauer, I. & Unger, K. K. The synthesis of micrometer-and submicrometer-size spheres of ordered mesoporous oxide MCM-41. *Advanced materials* **9**, 254-257 (1997).

63 Rosenholm, J. M. *et al.* Targeting of porous hybrid silica nanoparticles to cancer cells. *ACS nano* **3**, 197-206 (2008).

64 Meng, H. *et al.* Codelivery of an Optimal Drug/siRNA Combination Using Mesoporous Silica Nanoparticles To Overcome Drug Resistance in Breast Cancer in Vitro and in Vivo. *ACS Nano* **7**, 994-1005 (2013).

65 Xue, M. *et al.* pH-operated mechanized porous silicon nanoparticles. *Journal of the American Chemical Society* **133**, 8798-8801 (2011).

66 Schroder, H., Wang, X., Tremel, W., Ushijima, H. & Muller, W. Biofabrication of biosilica-glass by living organisms. *Natural Product Reports* **25**, 455-474 (2008).

67 Hildebrand, M. Diatoms, Biomineralization Processes, and Genomics. *Chemical Reviews* **108**, 4855-4874 (2008).

68 Dickerson, M., Sandhage, K. & Naik, R. Protein- and Peptide-Directed Syntheses of Inorganic Materials. *Chemical Reviews* **108**, 4935-4978 (2008).

69 Patwardhan, S. Biomimetic and bioinspired silica: recent developments and applications. *Chem Commun* **47**, 7567-7582 (2011).

70 Patwardhan, S. & Clarson, S. Silicification and biosilicification. *Silicon Chemistry* **1**, 207-214 (2002).

71 Kröger, N., Deutzmann, R. & Sumper, M. Polycationic Peptides from Diatom Biosilica That Direct Silica Nanosphere Formation. *Science* **286**, 1129-1132 (1999).

72 Shimizu, K., Cha, J., Stucky, G. & Morse, D. Silicatein α: Cathepsin L-like protein in sponge biosilica. *Proceedings of the National Academy of Sciences* **95**, 6234-6238 (1998).

73 Wenzl, S., Hett, R., Richthammer, P. & Sumper, M. Silacidins: Highly Acidic Phosphopeptides from Diatom Shells Assist in Silica Precipitation In Vitro. *Angewandte Chemie* **120**, 1753-1756 (2008).

74 Kröger, N. Prescribing diatom morphology: toward genetic engineering of biological nanomaterials. *Current opinion in chemical biology* **11**, 662-669 (2007).

75 Patwardhan, S. V. Biomimetic and bioinspired silica: recent developments and applications. *Chemical Communications* **47**, 7567-7582 (2011).

76 Patwardhan, S. V., Clarson, S. J. & Perry, C. C. On the role(s) of additives in bioinspired silicification. *Chemical Communications*, 1113-1121 (2005).

77 Dickerson, M. B., Sandhage, K. H. & Naik, R. R. Protein- and Peptide-Directed Syntheses of Inorganic Materials. *Chemical Reviews* **108**, 4935-4978 (2008).

78 Kroger, N., Lorenz, S., Brunner, E. & Sumper, M. Self-assembly of highly phosphorylated silaffins and their function in biosilica morphogenesis. *Science* **298**, 584-586 (2002).

79 Shimizu, K., Cha, J., Stucky, G. D. & Morse, D. E. Silicatein α: Cathepsin L-like protein in sponge biosilica. *Proceedings of the National Academy of Sciences* **95**, 6234-6238 (1998).

80 Cha, J. N. *et al.* Silicatein filaments and subunits from a marine sponge direct the polymerization of silica and silicones in vitro. *Proceedings of the National Academy of Sciences* **96**, 361-365 (1999).

81 Kröger, N., Deutzmann, R., Bergsdorf, C. & Sumper, M. Species-specific polyamines from diatoms control silica morphology. *Proceedings of the National Academy of Sciences* **97**, 14133-14138 (2000).

82 Cha, J. *et al.* Silicatein filaments and subunits from a marine sponge direct the polymerization of silica and silicones in vitro. *Proceedings of the National Academy of Sciences* **96**, 361-365 (1999).

83 Müller, W. *et al.* Silicateins, the major biosilica forming enzymes present in demosponges: Protein analysis and phylogenetic relationship. *Gene* **395**, 62-71 (2007).

84 Rai, A. & Perry, C. C. Facile fabrication of uniform silica films with tunable physical properties using silicatein protein from sponges. *Langmuir* **26**, 4152-4159 (2009).

85 Müller, W., Wang, X., Jochum, K. & Schröder, H. Self-healing, an intrinsic property of biomineralization processes. *IUBMB life* **65**, 382-396 (2013).

86 Sumper, M., Lorenz, S. & Brunner, E. Biomimetic Control of Size in the Polyamine-Directed Formation of Silica Nanospheres. *Angewandte Chemie* **115**, 5350-5353 (2003).

87 Belton, D. J., Patwardhan, S. V., Annenkov, V. V., Danilovtseva, E. N. & Perry, C. C. From biosilicification to tailored materials: Optimizing hydrophobic domains and resistance to protonation of polyamines. *Proceedings of the National Academy of Sciences* **105**, 5963-5968 (2008).

88 Belton, D. J., Patwardhan, S. V. & Perry, C. C. Spermine, spermidine and their analogues generate tailored silicas. *Journal of Materials Chemistry* **15**, 4629-4638 (2005).

89 Bernecker, A. *et al.* Tailored Synthetic Polyamines for Controlled Biomimetic Silica Formation. *Journal of the American Chemical Society* **132**, 1023-1031 (2009).

90 Masse, S., Laurent, G. & Coradin, T. Influence of cyclic polyamines on silica formation during the Stober process. *Physical chemistry chemical physics : PCCP* **11**, 10204-10210 (2009).

91 Masse, S. *et al.* Modification of the Stöber process by a polyazamacrocycle leading to unusual core-shell silica nanoparticles. *Langmuir* **24**, 4026-4031 (2008).

92 Kröger, N., Lorenz, S., Brunner, E. & Sumper, M. Self-Assembly of Highly Phosphorylated Silaffins and Their Function in Biosilica Morphogenesis. *Science* **298**, 584-586 (2002).

93 Poulsen, N., Sumper, M. & Kröger, N. Biosilica formation in diatoms: Characterization of native silaffin-2 and its role in silica morphogenesis. *Proceedings of the National Academy of Sciences* **100**, 12075-12080 (2003).

94 Poulsen, N. & Kröger, N. Silica Morphogenesis by Alternative Processing of Silaffins in the Diatom Thalassiosira pseudonana. *Journal of Biological Chemistry* **279**, 42993-42999 (2004).

95 Knecht, M. R. & Wright, D. W. Functional analysis of the biomimetic silica precipitating activity of the R5 peptide from Cylindrotheca fusiformis. *Chemical Communications*, 3038 (2003).

96 Luckarift, H., Spain, J., Naik, R. & Stone, M. Enzyme immobilization in a biomimetic silica support. *Nat Biotech* **22**, 211-213 (2004).

97 Sano, K.-I., Minamisawa, T. & Shiba, K. Autonomous Silica Encapsulation and Sustained Release of Anticancer Protein. *Langmuir* **26**, 2231-2234 (2010).

98 Marner, W. D., Shaikh, A. S., Muller, S. J. & Keasling, J. D. Enzyme immobilization via silaffin-mediated autoencapsulation in a biosilica support. *Biotechnology Progress* **25**, 417-423 (2009).

99 Brott, L. *et al.* Ultrafast holographic nanopatterning of biocatalytically formed silica. *Nature* **413**, 291-293 (2001).

100 McDaniel, J. R., Radford, D. C. & Chilkoti, A. A unified model for de novo design of elastin-like polypeptides with tunable inverse transition temperatures. *Biomacromolecules* **14**, 2866-2872 (2013).

101 Urry, D. W. *et al.* Temperature of polypeptide inverse temperature transition depends on mean residue hydrophobicity. *Journal of the American Chemical Society* **113**, 4346-4348 (1991).

102 Meyer, D. E. & Chilkoti, A. Quantification of the Effects of Chain Length and Concentration on the Thermal Behavior of Elastin-like Polypeptides. *Biomacromolecules* **5**, 846-851 (2004).

103 MacEwan, S. R. & Chilkoti, A. Elastin-like polypeptides: biomedical applications of tunable biopolymers. *Biopolymers* **94**, 60-77 (2010).

104 Cho, Y. *et al.* Effects of Hofmeister Anions on the Phase Transition Temperature of Elastin-like Polypeptides. *The Journal of Physical Chemistry B* **112**, 13765-13771 (2008).

105 MacEwan, S. R. & Chilkoti, A. Controlled Apoptosis by a Thermally Toggled Nanoscale Amplifier of Cellular Uptake. *Nano Letters* **14**, 2058-2064 (2014).

106 Shi, P. *et al.* Elastin-based protein polymer nanoparticles carrying drug at both corona and core suppress tumor growth in vivo. *Journal of Controlled Release* **171**, 330-338 (2013).

107 Shah, M. *et al.* A rapamycin-binding protein polymer nanoparticle shows potent therapeutic activity in suppressing autoimmune dacryoadenitis in a mouse model of Sjögren's syndrome. *Journal of Controlled Release* **171**, 269-279 (2013).

108 Dreher, M. R. *et al.* Temperature Triggered Self-Assembly of Polypeptides into Multivalent Spherical Micelles. *Journal of the American Chemical Society* **130**, 687-694 (2007).

109 MacEwan, S. R. & Chilkoti, A. Digital Switching of Local Arginine Density in a Genetically Encoded Self-Assembled Polypeptide Nanoparticle Controls Cellular Uptake. *Nano Letters* **12**, 3322-3328 (2012).

110 Ghoorchian, A., Chilkoti, A. & López, G. P. Simple Assay for Proteases Based on Aggregation of Stimulus-Responsive Polypeptides. *Analytical Chemistry* **86**, 6103-6110 (2014).

111 Hassouneh, W. *et al.* Unexpected Multivalent Display of Proteins by Temperature Triggered Self-Assembly of Elastin-like Polypeptide Block Copolymers. *Biomacromolecules* **13**, 1598-1605 (2012).

112 MacKay, J. A. *et al.* Self-assembling chimeric polypeptide-doxorubicin conjugate nanoparticles that abolish tumours after a single injection. *Nature materials* **8**, 993-999 (2009).

113 McDaniel, J. R. *et al.* Self-assembly of thermally responsive nanoparticles of a genetically encoded peptide polymer by drug conjugation. *Angewandte Chemie* **52**, 1683-1687 (2013).

114 Jan, J.-S., Lee, S., Carr, C. S. & Shantz, D. F. Biomimetic Synthesis of Inorganic Nanospheres. *Chemistry of Materials* **17**, 4310-4317 (2005).

115 Jan, J.-S. & Shantz, D. F. Biomimetic Silica Formation: Effect of Block Copolypeptide Chemistry and Solution Conditions on Silica Nanostructure. *Advanced materials* **19**, 2951-2956 (2007).

116 Yuan, J.-J., Mykhaylyk, O. O., Ryan, A. J. & Armes, S. P. Cross-Linking of Cationic Block Copolymer Micelles by Silica Deposition. *Journal of the American Chemical Society* **129**, 1717-1723 (2007).

117 Li, Y., Du, J. & Armes, S. P. Shell cross-linked micelles as cationic templates for the preparation of silica-coated nanoparticles: strategies for controlling the mean particle diameter. *Macromolecular rapid communications* **30**, 464-468 (2009).

118 Brott, L. L. *et al.* Ultrafast holographic nanopatterning of biocatalytically formed silica. *Nature* **413**, 291-293 (2001).

119 Naik, R. R., Tomczak, M. M., Luckarift, H. R., Spain, J. C. & Stone, M. O. Entrapment of enzymes and nanoparticles using biomimetically synthesized silica. *Chemical Communications*, 1684-1685 (2004).

120 McDaniel, J. R., MacKay, J. A., Quiroz, F. G. a. & Chilkoti, A. Recursive Directional Ligation by Plasmid Reconstruction Allows Rapid and Seamless Cloning of Oligomeric Genes. *Biomacromolecules* **11**, 944-952 (2010).

121 Hassouneh, W., Christensen, T. & Chilkoti, A. Elastin-Like Polypeptides as a Purification Tag for Recombinant Proteins. *Current Protocols in Protein Science* **61**, 6.11.11-16.11.16 (2001).

122 Avnir, D., Coradin, T., Lev, O. & Livage, J. Recent bio-applications of sol–gel materials. *Journal of Materials Chemistry* **16**, 1013-1030 (2006).

123 Yang, P., Gai, S. & Lin, J. Functionalized mesoporous silica materials for controlled drug delivery. *Chemical Society reviews* **41**, 3679-3698 (2012).

124 Slowing, I. I., Trewyn, B. G., Giri, S. & Lin, V. Y. Mesoporous silica nanoparticles for drug delivery and biosensing applications. *Advanced Functional Materials* **17**, 1225-1236 (2007).

125 Wu, Y., Chen, C. & Liu, S. Enzyme-functionalized silica nanoparticles as sensitive labels in biosensing. *Analytical Chemistry* **81**, 1600-1607 (2009).

126 Yi, D. K. *et al.* Silica-coated nanocomposites of magnetic nanoparticles and quantum dots. *Journal of the American Chemical Society* **127**, 4990-4991 (2005).

127 Zhao, Y., Trewyn, B. G., Slowing, I. I. & Lin, V. S.-Y. Mesoporous silica nanoparticle-based double drug delivery system for glucose-responsive controlled release of insulin and cyclic AMP. *Journal of the American Chemical Society* **131**, 8398-8400 (2009).

128 Vivero-Escoto, J. L., Slowing, I. I., Wu, C.-W. & Lin, V. S.-Y. Photoinduced intracellular controlled release drug delivery in human cells by gold-capped

mesoporous silica nanosphere. *Journal of the American Chemical Society* **131**, 3462-3463 (2009).

129 Lechner, C. C. & Becker, C. F. Silaffins in silica biomineralization and biomimetic silica precipitation. *Marine drugs* **13**, 5297-5333 (2015).

130 Lechner, C. C. & Becker, C. F. Modified silaffin R5 peptides enable encapsulation and release of cargo molecules from biomimetic silica particles. *Bioorganic & medicinal chemistry* **21**, 3533-3541 (2013).

131 Belton, D., Paine, G., Patwardhan, S. V. & Perry, C. C. Towards an understanding of (bio) silicification: the role of amino acids and lysine oligomers in silicification. *Journal of Materials Chemistry* **14**, 2231-2241 (2004).

132 Yuan, J. J. & Jin, R. H. Multiply Shaped Silica Mediated by Aggregates of Linear Poly(ethyleneimine). *Advanced materials* **17**, 885-888 (2005).

133 Lechner, C. C. & Becker, C. F. W. A sequence-function analysis of the silica precipitating silaffin R5 peptide. *Journal of Peptide Science* **20**, 152-158 (2014).

134 Yang, S. H. *et al.* Biomimetic Encapsulation of Individual Cells with Silica. *Angewandte Chemie International Edition* **48**, 9160-9163 (2009).

135 Wong Po Foo, C. *et al.* Novel nanocomposites from spider silk–silica fusion (chimeric) proteins. *Proceedings of the National Academy of Sciences of the United States of America* **103**, 9428-9433 (2006).

136 Lechner, C. C. & Becker, C. F. W. Modified silaffin R5 peptides enable encapsulation and release of cargo molecules from biomimetic silica particles. *Bioorganic & Medicinal Chemistry* **21**, 3533-3541 (2013).

137 Han, W., MacEwan, S. R., Chilkoti, A. & López, G. P. Bio-inspired synthesis of hybrid silica nanoparticles templated from elastin-like polypeptide micelles. *Nanoscale* **7**, 12038-12044 (2015).

138 Trabbic-Carlson, K., Liu, L., Kim, B. & Chilkoti, A. Expression and purification of recombinant proteins from Escherichia coli: Comparison of an elastin-like polypeptide fusion with an oligohistidine fusion. *Protein Science* **13**, 3274-3284 (2004).

139 Amiram, M., Luginbuhl, K., Li, X., Feinglos, M. N. & Chilkoti, A. A depot-forming glucagon-like peptide-1 fusion protein reduces blood glucose for five days with a single injection. *Journal of Controlled Release* **172**, 144-151 (2013).

140 McDaniel, J. R., Callahan, D. J. & Chilkoti, A. Drug delivery to solid tumors by elastin-like polypeptides. *Advanced Drug Delivery Reviews* **62**, 1456-1467 (2010).

141 McDaniel, J. R., MacEwan, S. R., Dewhirst, M. & Chilkoti, A. Doxorubicin-conjugated chimeric polypeptide nanoparticles that respond to mild hyperthermia. *Journal of Controlled Release* **159**, 362-367 (2012).

142 MacEwan, S. R. & Chilkoti, A. Applications of elastin-like polypeptides in drug delivery. *Journal of Controlled Release* **190**, 314-330 (2014).

143 McDaniel, J. R. *et al.* Noncanonical Self-Assembly of Highly Asymmetric Genetically Encoded Polypeptide Amphiphiles into Cylindrical Micelles. *Nano Letters* **14**, 6590-6598 (2014).

144 Mastria, E. M. *et al.* Doxorubicin-conjugated polypeptide nanoparticles inhibit metastasis in two murine models of carcinoma. *Journal of Controlled Release* **208**, 52-58 (2015).

145 Haag, R. Supramolecular drug-delivery systems based on polymeric core–shell architectures. *Angewandte Chemie International Edition* **43**, 278-282 (2004).

146 Hrubý, M., Koňák, Č. & Ulbrich, K. Polymeric micellar pH-sensitive drug delivery system for doxorubicin. *Journal of Controlled Release* **103**, 137-148 (2005).

147 Bae, Y., Fukushima, S., Harada, A. & Kataoka, K. Design of environment-sensitive supramolecular assemblies for intracellular drug delivery: Polymeric micelles that are responsive to intracellular pH change. *Angewandte Chemie International Edition* **42**, 4640-4643 (2003).

148 Bae, Y. *et al.* Preparation and biological characterization of polymeric micelle drug carriers with intracellular pH-triggered drug release property: tumor permeability, controlled subcellular drug distribution, and enhanced in vivo antitumor efficacy. *Bioconjugate chemistry* **16**, 122-130 (2005).

149 Guerrero-Martinez, A., Perez-Juste, J. & Liz-Marzan, L. M. Recent progress on silica coating of nanoparticles and related nanomaterials. *Advanced materials* **22**, 1182-1195 (2010).

150 Jain, T. K., Roy, I., De, T. K. & Maitra, A. Nanometer Silica Particles Encapsulating Active Compounds: A Novel Ceramic Drug Carrier. *Journal of the American Chemical Society* **120**, 11092-11095 (1998).

151 Cha, J. N., Stucky, G. D., Morse, D. E. & Deming, T. J. Biomimetic synthesis of ordered silica structures mediated by block copolypeptides. *Nature* **403**, 289-292 (2000).

152 Yuan, J. J. & Jin, R. H. Multiply shaped silica mediated by aggregates of linear poly (ethyleneimine). *Advanced materials* **17**, 885-888 (2005).

153 Patwardhan, S. V., Maheshwari, R., Mukherjee, N., Kiick, K. L. & Clarson, S. J. Conformation and Assembly of Polypeptide Scaffolds in Templating the Synthesis of Silica: An Example of a Polylysine Macromolecular "Switch". *Biomacromolecules* **7**, 491-497 (2006).

154 Khripin, C. Y., Pristinski, D., Dunphy, D. R., Brinker, C. J. & Kaehr, B. Protein-Directed Assembly of Arbitrary Three-Dimensional Nanoporous Silica Architectures. *ACS Nano* **5**, 1401-1409 (2011).

155 Meunier, C. F., Dandoy, P. & Su, B.-L. Encapsulation of cells within silica matrixes: Towards a new advance in the conception of living hybrid materials. *Journal of Colloid and Interface Science* **342**, 211-224 (2010).

156 Allouche, J., Boissiere, M., Hélary, C., Livage, J. & Coradin, T. Biomimetic core–shell gelatine/silica nanoparticles: A new example of biopolymer-based nanocomposites. *Journal of Materials Chemistry* **16**, 3120-3125 (2006).

157 Lechner, C. C. & Becker, C. F. W. Exploring the effect of native and artificial peptide modifications on silaffin induced silica precipitation. *Chemical Science* **3**, 3500-3504 (2012).

158 Dreher, M. R. *et al.* Evaluation of an elastin-like polypeptide–doxorubicin conjugate for cancer therapy. *Journal of Controlled Release* **91**, 31-43 (2003).

159 Zhang, J. *et al.* Protein-binding aptamer assisted signal amplification for the detection of influenza A (H1N1) DNA sequences based on quantum dot fluorescence polarization analysis. *Analyst* **138**, 4722-4727 (2013).

160 Yamaoka, T. *et al.* Mechanism for the phase transition of a genetically engineered elastin model peptide (VPGIG) 40 in aqueous solution. *Biomacromolecules* **4**, 1680-1685 (2003).

161 Shields, C. W. *et al.* Nucleation and Growth Synthesis of Siloxane Gels to Form Functional, Monodisperse, and Acoustically Programmable Particles. *Angewandte Chemie International Edition* **53**, 8070-8073 (2014).

162 Rosenberg, S. A., Yang, J. C. & Restifo, N. P. Cancer immunotherapy: moving beyond current vaccines. *Nature medicine* **10**, 909-915 (2004).

163 Gu, F. X. *et al.* Targeted nanoparticles for cancer therapy. *Nano today* **2**, 14-21 (2007).

164 Corti, A., Curnis, F., Arap, W. & Pasqualini, R. The neovasculature homing motif NGR: more than meets the eye. *Blood* **112**, 2628-2635 (2008).

165 Arap, W., Pasqualini, R. & Ruoslahti, E. Cancer treatment by targeted drug delivery to tumor vasculature in a mouse model. *Science* **279**, 377-380 (1998).

166 Buehler, A. *et al.* cNGR: a novel homing sequence for CD13/APN targeted molecular imaging of murine cardiac angiogenesis in vivo. *Arteriosclerosis, thrombosis, and vascular biology* **26**, 2681-2687 (2006).

167 Simnick, A. J., Valencia, C. A., Liu, R. & Chilkoti, A. Morphing low-affinity ligands into high-avidity nanoparticles by thermally triggered self-assembly of a genetically encoded polymer. *ACS nano* **4**, 2217-2227 (2010).

Biography

A Wei Han was born on January 27, 1988 in Lanzhou, Gansu Province, China. His family immigrated to the United States in 1995, and he grew up in Minneapolis and Eden Prairie Minnesota. He graduated from Eden Prairie High school in 2006 and subsequently enrolled at Duke University, where he earned a B.S.E. in Biomedical Engineering and a B.S. in Economics in 2010. While an undergraduate student, he gained his first research experience in the lab of Prof. Ashutosh Chilkoti as a Pratt Undergraduate Research Fellow under the guidance of Drs. Weiping Gao and Miriam Amiram.

After graduation, Wei remained at Duke University and joined the graduate program in the department of Biomedical Engineering to pursue his Ph.D. under the guidance of Prof. Gabriel P. López in 2010. During his time as a graduate student, Wei was supported by fellowships from the Duke Center for Biomolecular and Tissue Engineering (CBTE) and the NSF Research Triangle Materials and Science Engineering Center (MRSEC). He was a member of the Duke CBTE Certificate program and won the 2012 CBTE Kewaunee Student Service Award. Wei was active in extracurricular and service activities during his time in graduate school, serving as president of the Engineering Graduate Student Council (EGSC), Biomedical Engineering departmental representative to the Graduate and Professional Student Council (GPSC), chair of the Duke Graduate Young Trustee Screening Committee and a member of the Duke

University Board of Trustees Business and Finance Committee. He also helped found and was a workshop chair for the Ph.D. Plus Enhancement Program, a program developed towards assisting Ph.D. students identify and prepare for career opportunities after graduate school.

Wei has contributed to the following publications:

W. Han, L. Tang, S. Zauscher, A. Chilkoti, G.P. López. "Selective Silica Application from Silica-promoting Elastin-like Polypeptide Micelle Nanoparticles" (In preparation)

W. Han, A. Chilkoti, G.P. López.. "Self-Assembled Hybrid Elastin-like Polypeptide / Silica Nanoparticles Enable Triggered Drug Release" (In preparation)

W. Han, S.R. MacEwan, A. Chilkoti, G.P. López.. "Bio-inspired Synthesis of Hybrid Silica Nanoparticles Templated from Elastin-like Polypeptide Micelles" *Nanoscale*, 2015, 7: 12038-12044.

W. Han, L.K. Ista, G. Gupta, L. Li, J.M. Harris, G.P. López.. "Siliceous Nanobiomaterials" in *Handbook of Nanomaterial Properties*. Springer, 2014

A. Thapa, **W. Han**, R.H. Simons, A. Chilkoti, G.P. López.. "Effect of Detergents on the Thermal Behavior of Elastin-Like Polypeptides" *Biopolymers,* 2013, 99: 55-62.

A. Ghoorchian, J.R. Simon, B. Bharti, **W. Han**, X. Zhao, A. Chilkoti, G.P. López.. "Bioinspired Reversibly Cross-linked Hydrogels Comprising Polypeptide Micelles Exhibit Enhanced Mechanical Properties" *Advanced Functional Materials*, 2015, 25: 3122-3130.